Joint Multiuser Power Allocation and Iterative Multi-Antenna Receiver Design

Valtteri Tervo

The dissertation is made based on a curriculum that is organized by the Collaborative Education Program of Japan Advanced Institute of Science and Technology and University of Oulu

Abstract

This thesis concentrates on joint optimization of transmit power allocation and receive filtering in multiuser, multi-antenna communications. Due to the increasing number of wireless devices, the design of energy-efficient communication links is becoming increasingly important. In cellular mobile communications, reducing the average power consumption in uplink transmission is beneficial for users in order to extend battery life and, hence, energy efficiency in general. However, the power consumption of the high power amplifier (HPA) at the transmitter depends on the peak power of the transmission. This thesis focuses on power allocation problems for single-carrier (SC) frequency division multiple access (FDMA) and orthogonal FDMA (OFDMA) transmission assuming iterative reception.

The goal in the first scheme presented in this thesis is to reduce the average power consumption by designing a power allocation method that takes into account the convergence properties of an iterative receiver in multiuser uplink communications. The proposed scheme can guarantee that the desired quality of service (QoS) is achieved after a sufficient number of iterations.

Reducing the peak-to-average power ratio (PAPR) in any transmission system is beneficial because it allows the use of inexpensive, energy-efficient power amplifiers. The goal in the second scheme presented in this thesis is to control the PAPR of the transmitted signal. Hence, in addition to the QoS constraint, the instantaneous PAPR constraint is derived for SC-FDMA and OFDMA transmission. Moreover, a statistical approach is considered in which the power variance of the transmitted waveform is controlled. The QoS and PAPR constraints are considered jointly and, therefore, the proposed power allocation strategy jointly takes into account the channel quality and the PAPR characteristics of the power amplifier. However, the PAPR constraint can be adopted to any SC-FDMA or OFDMA framework and it is not restricted to the scheme presented in this thesis. The objective of the optimization problems considered throughout the thesis is to minimize the sum power. The majority of the derived constraints are non-convex and therefore, two alternative successive convex approximations (SCAs) are derived for all the non-convex constraints considered.

The numerical results show that the proposed power allocation strategies can significantly reduce the average transmission power of users while allowing flexible PAPR

control. Hence, the proposed methods can be used to extend battery life for users and especially improve the QoS at the cell edges.

Keywords: Power minimization, soft interference cancellation, MMSE receiver, multiuser detection, single carrier, OFDMA, EXIT chart, convergence constraint

To my family

Preface

The research work related to this thesis is a result of the dual degree doctoral programme between the University of Oulu, Finland, and the Japan Advanced Institute of Science and Technology (JAIST), Japan. At the University of Oulu, the work has been carried out at the Centre for Wireless Communications (CWC) and the Department of Communications Engineering (DCE). At JAIST, the research was conducted at the Information Theory and Signal Processing Laboratory of the School of Information Science. Under the dual degree programme, I have been able to work in two different cultural environments. Although this has provided scientific diversity, it has also increased my level of maturity in general.

I would like to thank my supervisors, Docent Antti Tölli, Professor Tadashi Matsumoto and Professor Markku Juntti for their invaluable technical, financial and administrative guidance and support. Docent Tölli's extremely high technical expertise has been a crucial part of the research work. Professor Matsumoto's enthusiasm and technical knowledge has been motivating and encouraging. Professor Juntti's technical and academic guidance also played a crucial role in my graduation.

I wish to express my gratitude to the reviewers of the thesis, Professor Ping Li from City University of Hong Kong, Professor Henk Wymeersch from Chalmers University of Technology, Sweden, and Professor Hidekazu Murata from Kyoto University, Japan. Furthermore, I would like to thank the internal evaluators at JAIST, Professor Brian Kurkoski and Professor Mineo Kaneko, for their valuable comments and suggestions regarding the thesis.

I wish to thank all my past and present co-workers at CWC and JAIST. I would especially like to thank Dr Juha Karjalainen, who was the key person in the choice of research topic for the thesis. Furthermore, I am deeply grateful for the technical discussions I have had with Jarkko Kaleva, Harri Pennanen, Dr Petri Komulainen and my former roommate Qiang Xue. You have helped me to clarify many things in my mind. I would also like to thank my colleague Pen-Shun Lu for joint papers and fruitful cooperation. I have also had the pleasure to guide the master's thesis of Kushal Tiwari, and that experience was extremely valuable for me.

While conducting the research, I have been able to work on several projects, such as Distributed Decision Making for Future Wireless Communication Systems (DIDES),

Slepian-Wolf Cooperation Wireless Networks (SWOCNET), Interference Management for Wireless Networks Beyond Present Horizon+ (IMANET+) and Network Compression Based Wireless Cooperative Communication Systems (NETCOBRA). The main funders of the projects were the Finnish Funding Agency for Technology and Innovation (TEKES) and the Academy of Finland (AoF). I have also received personal funding from the Nokia Foundation, Finnish Foundation for Technology Promotion, Riitta and Jorma J. Takanen Foundation, Walther Ahlström Foundation, Ulla Tuominen Foundation, KAUTE-Foundation and Tauno Tönning Foundation.

I am grateful to my parents, Heljä and Ahti, for their support and encouragement towards education. I am also grateful for my siblings Sakari, Elina, Samuli, and Inkeri for making my life much richer and to Kalevi, Oskari and Nuutti also for the technical discussions we have had.

Finally, I would like to express my deepest gratitude to my family: my wife Kirsi for her invaluable love, support and understanding, and my son Frans, for being there and enriching my life.

Symbols and abbreviations

a_{qnm}	a complex phase shift at the m^{th} time instant associated with the combination of the q^{th} and n^{th} phase shifts on the Fourier precoders at the SC-FDMA transmitter
b_i	a complex symbol belonging to a modulation alphabet $\mathfrak{B}$
b_l^u	transmitted symbol of user u at time instant l
$\hat{b}_l^u$	estimate of the l^{th} transmitted symbol of the u^{th} user
$\tilde{b}_l^u$	soft estimate of the u^{th} user's l^{th} symbol
$\boldsymbol{b}$	transmitted multiuser symbol vector ($UN_F \times 1$)
$\tilde{\boldsymbol{b}}$	soft estimate vector of the multiuser symbols ($UN_F \times 1$)
$\tilde{\boldsymbol{b}}^u$	soft estimate vector of the u^{th} user's symbol vector ($N_F \times 1$)
$\boldsymbol{b}^u$	transmitted symbol vector of user u
$\ddot{\boldsymbol{b}}^u$	vector for the detected data stream of the u^{th} user with elements $\lvert\tilde{b}_l^u\rvert^2$ ($N_F \times 1$)
$\grave{\boldsymbol{b}}^u$	the output time domain symbol vector of the ZF filter for the u^{th} user
$\mathbb{B}$	binary number field
$\mathfrak{B}$	modulation symbol alphabet
c_l^u	transmitted bit for the u^{th} user associated with the l^{th} bit position
c'^u_l	interleaved encoded bit for the u^{th} user associated with the l^{th} bit position
$c'_{i,q}$	transmitted bit associated with the q^{th} position of a symbol b_i
$\bar{c}'_{i,q}$	antipodally modulated transmitted bit associated with the q^{th} position of a symbol b_i
$\boldsymbol{c}'_i$	transmitted bit vector associated with a symbol b_i
$\boldsymbol{c}^u$	encoded bit vector of user u
$\boldsymbol{c}'^u$	interleaved encoded bit vector of user u
$\mathbb{C}$	complex number field
$\mathscr{C}_u$	forward error correction code of user u
d_l^u	a parameter depending on the transmitted symbol sequence of user u at the l^{th} frequency bin
$\tilde{d}^u_{mn_2n_1}$	a parameter depending on the transmitted symbol sequence of user u at the m^{th} time instant associated with the combination of the symbols

	from frequency bins n_1 and n_2
$\mathbb{E}\{\cdot\}$	the expectation operator
$\hat{f}_u(\cdot)$	the EXIT function of the equalizer of user u
$\hat{f}_u^{\mathrm{2D}}(\cdot)$	the EXIT function of the equalizer of user u having equal *a priori* inputs from all the decoders
$\mathring{f}_u(\cdot)$	the EXIT function of the decoder of user u
$f_{m,l}$	an element of the DFT matrix for the m^{th} row and the l^{th} column
$\boldsymbol{F}$	DFT matrix ($N_F \times N_F$)
$\boldsymbol{F}_N$	block diagonal DFT matrix having DFT matrices on the diagonal ($N_F N \times N_F N$)
$g_{k,m}^u$	an element (k,m) of the SC-FDMA precoder
$h_{u,l}^r$	fading gain for the l^{th} multipath component in the channel between the u^{th} user and the r^{th} receive antenna
$\boldsymbol{H}_u$	block circulant channel matrix of user u ($N_R N_F \times U N_F$)
$\boldsymbol{H}_u^r$	circulant channel matrix of user u associated with receive antenna r ($N_F \times N_F$)
$\hat{I}_u^{\mathrm{E}}$	the average MI between the transmitted interleaved coded bits $\boldsymbol{c}'^u$ and the LLRs $\hat{\boldsymbol{L}}_u'$ at the output of the equalizer
$\hat{I}_{u,k}^{\mathrm{E}}$	the average MI between the transmitted interleaved coded bits $\boldsymbol{c}'^u$ and the LLRs $\hat{\boldsymbol{L}}_u'$ at the output of the equalizer of the u^{th} user at the k^{th} MI index
$\hat{I}_u^{\mathrm{A}}$	the average MI between the transmitted interleaved coded bits $\boldsymbol{c}'^u$ and the LLRs $\mathring{\boldsymbol{L}}_u$ at the input of the equalizer
$\hat{I}_u^{\mathrm{A}} / \mathring{I}_l^{\mathrm{E}}$	the *a priori* MI for the equalizer of user u provided by the decoder of user l
$\mathring{I}_u^{\mathrm{A}}$	the average MI between the transmitted coded bits $\boldsymbol{c}^u$ and the LLRs $\hat{\boldsymbol{L}}_u$ at the input of the decoder
$\mathring{I}_u^{\mathrm{E}}$	the average MI between the transmitted coded bits $\boldsymbol{c}^u$ and the LLRs $\mathring{\boldsymbol{L}}_u$ at the output of the decoder
$\mathring{I}_k^u$	the average MI at the output of the decoder of the u^{th} user at the k^{th} MI index
$\mathring{I}_k$	the average MI at the output of the decoder at the k^{th} MI index
$\mathring{I}_u^{\mathrm{E,target}}$	target for the equalizer's *a priori* mutual information
$\boldsymbol{I}_N$	an identity matrix ($N \times N$)
$\mathrm{J}(\cdot)$	function which maps its argument value to mutual information

$\mathrm{J}_{N_Q}(\cdot)$	function which maps its argument value to mutual information assuming N_Q-ary quadrature amplitude modulation
K	number of MI indices
$\hat{L}'_{u,l}$	a log-likelihood ratio at the output of the equalizer associated with the interleaved encoded bit c'^{u}_{l}
$\mathring{L}'_{u,l}$	a log-likelihood ratio at the input of the equalizer associated with the interleaved encoded bit c'^{u}_{l}
$\hat{\boldsymbol{L}}'_{u}$	a vector of log-likelihood ratios at the output of the equalizer associated with the interleaved encoded bit vector $\boldsymbol{c}'^{u}$
$\mathring{\mathbf{L}}_{u}$	a vector of log-likelihood ratios at the output of the decoder associated with the encoded bit vector $\boldsymbol{c}^{u}$
$\hat{\boldsymbol{L}}_{u}$	a vector of log-likelihood ratios at the input of the decoder associated with the encoded bit vector $\boldsymbol{c}^{u}$
$\mathscr{M}_u(\cdot)$	modulation mapping function of user u
n^u_m	a complex noise sample of the equivalent AWGN channel at the output of the MMSE filter for the u^{th} user associated with the m^{th} frequency bin
N_F	number of bins in discrete Fourier transform
N_L	length of the channel impulse response
N_Q	number of bits per modulation symbol
N_R	number of receive antennas
N^u_F	number of frequency bins allocated to user u
$\mathscr{N}_F$	a set of all frequency bins
$\mathscr{N}^u_F$	a set of frequency bins allocated to user u
$\mathscr{N}^{\mathbb{C}}(\mu,\sigma^2)$	Circularly symmetric complex normal distribution with mean μ and variance σ^2
$P_{u,l}$	l^{th} diagonal element of the transmission power matrix $\boldsymbol{P}_u$ associated with the u^{th} user
$P_{\max}$	the maximum value of transmission power
P^u_{avg}	the average value of transmission power of user u
$\boldsymbol{P}$	diagonal power allocation matrix $(UN_F \times UN_F)$
$\boldsymbol{P}_u$	diagonal power allocation matrix for the u^{th} user $(N_F \times N_F)$
$\tilde{\boldsymbol{P}}_m$	power allocation matrix for the m^{th} frequency bin $(U \times U)$
$\boldsymbol{r}$	received time domain signal vector $(N_R N_F \times 1)$
$\tilde{\boldsymbol{r}}$	received frequency domain signal vector $(N_R N_F \times 1)$

$\tilde{\boldsymbol{r}}^{u,\mathrm{ZF}}$	the input signal vector for the MMSE filter after ZF equalization
$\tilde{\boldsymbol{r}}_m$	received frequency domain signal vector associated with the m^{th} frequency bin ($N_R \times 1$)
$\hat{\boldsymbol{r}}$	the output vector of soft cancelation ($N_R N_F \times 1$)
$\hat{\boldsymbol{r}}^{u,\mathrm{ZF}}$	the output vector of soft cancelation for the u^{th} user after ZF equalization
$\hat{\boldsymbol{r}}_m$	the output vector of soft cancelation associated with the m^{th} frequency bin ($N_R \times 1$)
$\breve{\boldsymbol{r}}^u$	combination of the residual and the desired signal associated with the u^{th} user ($N_R N_F \times 1$)
$\breve{\boldsymbol{r}}^{u,m}$	combination of the residual and the desired signal associated with the u^{th} user's m^{th} frequency bin ($N_R \times 1$)
$\mathbb{R}$	real number field
R_c^u	forward error correction code rate of user u
s_l^u	transmitted symbol of user u at time instant l after IDFT
$\boldsymbol{s}^u$	transmitted symbol vector of user u after IDFT
$t_{u,n}^k$	an auxiliary variable bounding the per subcarrier SINR for the u^{th} user's n^{th} frequency bin at the k^{th} MI index
$\hat{t}_{u,n}^k$	a point for the local approximation
$\boldsymbol{t}$	a set of auxiliary variables bounding the per subcarrier SINR
U	number of users
$\boldsymbol{v}$	vector of noise samples ($N_R N_F \times 1$)
$\boldsymbol{v}_m$	vector of noise samples at the m^{th} frequency bin ($N_R \times 1$)
$\boldsymbol{w}_{u,m}$	zero forcing vector for the u^{th} user associated with the m^{th} frequency bin
$\boldsymbol{W}_m$	zero forcing matrix for the m^{th} frequency bin ($U \times N_R$)
$\boldsymbol{W}^u$	zero forcing matrix for the u^{th} user ($N_F \times N_R N_F$)
$\ddot{\boldsymbol{W}}_u$	a diagonal matrix with elements $\|\|w_{u,m}\|\|^2$
$\mathscr{W}$	a set containing all the receive beamformers in SC-FDMA
$\tilde{\mathscr{W}}$	a set containing all the receive beamformers in OFDMA
$\boldsymbol{x}_u$	information bit vector of user u
$\alpha_{u,m}$	a variable related to the power as $P_{u,m} = e^{\alpha_{u,m}}$
$\boldsymbol{\alpha}$	a set of variables related to the power as $P_{u,m} = e^{\alpha_{u,m}}$, $u = 1,2,\ldots,U$, $m = 1,2,\ldots,N_F$
$\beta_{mn_1n_2}^u$	a parameter depending on the transmitted symbol sequence of user u at the m^{th} time instant associated with the combination of the symbol power from frequency bins n_1 and n_2

$\boldsymbol{\gamma}_{u,m}$	channel vector for the m^{th} frequency bin of user u ($N_R \times 1$)
$\boldsymbol{\Gamma}$	frequency domain channel matrix ($N_R N_F \times U N_F$)
$\boldsymbol{\Gamma}_u$	frequency domain channel matrix for the u^{th} user ($N_R N_F \times N_F$)
$\boldsymbol{\Gamma}_{u,m}$	frequency domain channel matrix for the u^{th} user's m^{th} frequency bin ($N_R \times N_R$)
$\tilde{\boldsymbol{\Gamma}}_m$	frequency domain channel matrix composed of U channel vectors in the m^{th} frequency bin ($N_R \times U$)
δ_u	a user-specific parameter controlling the PAPR
Δ^u	average residual interference of the soft symbol estimates of the u^{th} user
Δ_k	average residual interference of the soft symbol estimates at the k^{th} MI index
$\varepsilon_u(\cdot)$	a function controlling the minimum gap between the EXIT function of the equalizer of user u and the inverse of the decoder's EXIT function of user u
ε_u	a gap between the EXIT function of the equalizer of user u and the inverse of the decoder's EXIT function of user u
$\varepsilon_{u,k}$	a gap between the EXIT function of the equalizer of user u and the inverse of the decoder's EXIT function of user u at the k^{th} MI index
ζ_u	the effective SINR for the u^{th} user in SC-FDMA
ζ_u^k	the effective SINR for the u^{th} user at the k^{th} MI index in SC-FDMA
$\zeta_u^{k,\text{ZF}}$	the effective SINR for the u^{th} user at the k^{th} MI index in SC-FDMA with ZF equalization
$\tilde{\zeta}_u$	the effective SINR for the u^{th} user in OFDMA
$\tilde{\zeta}_{u,m}$	the effective SINR for the u^{th} user's m^{th} frequency bin in OFDMA
$\tilde{\zeta}_{u,m}^k$	the effective SINR for the u^{th} user's m^{th} frequency bin at the k^{th} MI index in OFDMA
η_u^k	a scaling factor of the MMSE filter for the u^{th} user at the k^{th} MI index in SC-FDMA
$\tilde{\eta}_u^k$	a scaling factor of the MMSE filter for the u^{th} user at the k^{th} MI index in OFDMA
$\eta_{mn_1n_2}^u$	a parameter depending on the transmitted symbol sequence of user u at the m^{th} time instant associated with the combination of the symbols from frequency bins n_1 and n_2
κ	normalization factor
κ_u	a parameter depending on the transmitted symbol sequence of user u

μ_u	the average power of the transmitted signal of user u
ν_m	a noise sample in frequency domain at the m^{th} frequency bin
$\boldsymbol{\nu}$	a vector of noise samples in frequency domain
$\xi_{u,k}$	auxiliary constant for the CCPA in SC-FDMA
$\tilde{\xi}_{u,k}$	auxiliary constant for the CCPA in OFDMA
$\boldsymbol{\pi}_u$	random permutation matrix associated with user u
σ_v^2	variance of noise
σ_Z^2	variance of the LLRs
$\hat{\sigma}_{u,k}^2$	the variance of the LLRs at the output of the equalizer of the u^{th} user at the k^{th} MI index
$(\hat{\sigma}_{u,m}^k)^2$	the variance of the LLRs at the output of the equalizer of the u^{th} user's m^{th} frequency bin at the k^{th} MI index
$\mathring{\sigma}_{u,k}^2$	the variance of the LLRs at the input of the decoder of the u^{th} user at the k^{th} MI index
$\tilde{\sigma}_u^2$	a parameter controlling the variance of the power of the transmitted signal of the u^{th} user
$\boldsymbol{\Sigma}_{\hat{\boldsymbol{r}},m}$	interference covariance matrix of the m^{th} frequency bin in SC-FDMA ($N_R \times N_R$)
$\boldsymbol{\Sigma}_{\hat{\boldsymbol{r}},m}^k$	interference covariance matrix of the m^{th} frequency bin at the k^{th} MI index in SC-FDMA ($N_R \times N_R$)
$\tilde{\boldsymbol{\Sigma}}_{\hat{\boldsymbol{r}},m}^k$	interference covariance matrix of the m^{th} frequency bin at the k^{th} MI index in OFDMA ($N_R \times N_R$)
$\tilde{\boldsymbol{\Sigma}}_{\hat{\boldsymbol{r}},m}$	interference covariance matrix of the m^{th} frequency bin of the u^{th} user in OFDMA ($N_R \times N_R$)
$\phi_{u,m}$	channel gain of the equivalent AWGN channel at the output of the MMSE filter for the u^{th} user associated with the m^{th} frequency bin
$\hat{\Psi}_m^u$	the output frequency domain symbol of the ZF filter for the u^{th} user at the m^{th} frequency bin
Ψ_m^u	data symbol in frequency domain for the u^{th} user at the m^{th} frequency bin
$\boldsymbol{\Psi}$	data symbol vector in frequency domain
$\boldsymbol{\Psi}^u$	data symbol vector in frequency domain for the u^{th} user
$\boldsymbol{\Psi}_m$	data symbol vector in frequency domain at the m^{th} frequency bin
$\hat{\boldsymbol{\Psi}}_m$	the output frequency domain symbol vector of the ZF filter at the m^{th} frequency bin

$\boldsymbol{\omega}_{u,m}$	receive beamforming vector for the m^{th} frequency bin of user u in SC-FDMA ($N_R \times 1$)
$\boldsymbol{\omega}_{u,m}^{k}$	receive beamforming vector for the m^{th} frequency bin of user u at the k^{th} MI index in SC-FDMA ($N_R \times 1$)
$\tilde{\boldsymbol{\omega}}_{u,m}$	receive beamforming vector for the m^{th} frequency bin of user u in OFDMA ($N_R \times 1$)
$\tilde{\boldsymbol{\omega}}_{u,m}^{k}$	receive beamforming vector for the m^{th} frequency bin of user u at the k^{th} MI index in OFDMA ($N_R \times 1$)
$\check{\boldsymbol{\Omega}}_u$	filtering matrix for the u^{th} user in SC-FDMA ($N_R N_F \times N_F$)
$\check{\boldsymbol{\Omega}}_u^{r}$	filtering matrix for the u^{th} user associated with the r^{th} receive antenna in SC-FDMA ($N_F \times N_F$)
$\otimes$	the Kronecker product
$\exists$	there exists
$\|\|\cdot\|\|$	Euclidean norm
$(\cdot)^{\text{T}}$	transpose of the argument
$(\cdot)^{\text{H}}$	complex conjugate transpose (Hermitian) of the argument
$(\cdot)^{\dagger}$	Moore-Penrose pseudo-inverse
$(\cdot)^{(*)}$	values for arguments obtained through optimization
$(\cdot)^{*}$	complex conjugate of the argument
$[\,\cdot\,]_{m,n}$	takes the element (m,n) of the argument matrix
$[\,\cdot\,]_{m:n}$	takes the elements from m to n, $n \geq m$ of the argument vector
avg$\{\cdot\}$	calculates the arithmetic mean of the elements of the argument vector
bdiag$\{\cdot\}$	generates a block diagonal matrix that has the argument matrices on the diagonal
circ$\{\cdot\}$	circulant operation, in which each column of the matrix is a cyclically shifted version of the successive column
diag$(\cdot)$	generates a diagonal matrix that has the argument values on the diagonal
BEP	bit error probability
BER	bit error rate
BPSK	binary phase-shift keying
CC	convergence constraint
CCDF	complementary cumulative distribution function
CCPA	convergence constrained power allocation
CDMA	code division multiple access
COV	change of variables

CP	cyclic prefix
CSI	channel state information
DFT	discrete Fourier transform
DL	downlink
EDGE	Enhanced Data Rates for GSM Evolution
EP	equal power allocation
EXIT	extrinsic information transfer
FD	frequency domain
FDE	frequency domain equalization
FDMA	frequency division multiple access
FEC	forward error correction
GP	geometric program
GPRS	General Packet Radio Service
GSM	Global System for Mobile Communications
HPA	high-power amplifier
IBI	inter block interference
IDFT	inverse discrete Fourier transform
IMT-A	International Mobile Telecommunications-Advanced
IRC	interference rejection combining
ISI	inter-symbol-interference
IS95	Interim Standard 95
ITU	International Telecommunication Union
ITU-R	International Telecommunication Union - Radio Communications Sector
LHS	left-hand side
LLR	log-likelihood ratio
LMMSE	linear minimum mean square error
LTE	Long Term Evolution
LTE-A	Long Term Evolution-Advanced
MAP	maximum *a posteriori*
MCS	modulation coding scheme
MI	mutual information
MIMO	multiple-input multiple-output
MMSE	minimum mean square error
MRC	maximal ratio combining

MSE	mean square error
MU	multiuser
MUI	multiuser interference
NMT	Nordic mobile telephone
OES	orthogonal allocation via exhaustive search
OFDM	orthogonal frequency division multiplexing
OFDMA	orthogonal frequency division multiple access
OFDMA-ZF	OFDMA with ZF equalization
PAPR	peak-to-average power ratio
PAP	power allocation problem
PSK	phase-shift keying
PTS	partial transmit sequences
QAM	quadrature amplitude modulation
QoS	quality of service
QPSK	quadrature phase-shift keying
RHS	right-hand side
RX	receiver
SC	single carrier
SC-ZF	SC-FDMA with ZF equalization
SCA	successive convex approximation
SCACOV	successive convex approximation via change of variables
SCAGP	successive convex approximation via geometric programming
SC-FDMA	single carrier frequency division multiple access
SDMA	spatial division multiple access
SftI/SftO	soft-in / soft-out
SIMO	single-input multiple-output
SINR	signal-to-interference-plus-noise-ratio
SISO	single-input single-output
SLM	selected mapping
SNR	signal-to-noise ratio
TDMA	time division multiple access
TM	transmission mode
TX	transmitter
UL	uplink
UMTS	Universal Mobile Telecommunications System

WCDMA	wideband code division multiple access
WiMAX	Worldwide Interoperability for Microwave Access
ZF	zero forcing
1G	first generation
2G	second generation
3G	third generation
3GPP	3rd Generation Partnership Project
3GPP2	3rd Generation Partnership Project 2
4G	fourth generation
5G	fifth generation
16-QAM	16-ary quadrature amplitude modulation

Contents

1 Introduction

Due to the increasing number of mobile devices, energy efficiency has become one of the main design criteria in future wireless networks. Reducing the power consumption of transmission devices is a straightforward and effective approach to achieving more energy-efficient wireless communications systems. This thesis deals with power allocation methods aiming to decrease both, the average power consumption and the peak power of the transmission. This joint approach inevitably results in improved energy efficiency for users and, therefore, extends the battery life of mobile devices.

This introductory chapter starts with a brief historical overview of mobile cellular networks, from the first generation system up to current technology and requirements. Furthermore, the key technical concepts used in this thesis are briefly introduced. The scope and objectives of the thesis are then stated, followed by an overview of the contributions.

1.1 Motivation and history

Economic and competitive mobile wireless services require efficient sharing of channel resources. All sharing methods in practice introduce interference of one sort or another which is proportional to the transmitter (TX) power. Therefore, TX power control is a key technique to obtain better balance between the received signal and the interference, which in turn enables more efficient sharing of channel resources [1]. Power control is an intelligent mechanism to select TX power output such that the system achieves a good performance. In this section, a historical overview of mobile cellular networks is given from the power control perspective .

A new mobile generation has appeared approximately every ten years since the first 1G system, Nordic Mobile Telephone (NMT), was introduced in 1981. 1G systems were based on analogue cellular technology and were capable of handling very limited data or no data at all [2]. The cell sizes in an NMT network range from 2 km to 30 km. The smaller cells were usually located in city areas to maintain better service for the larger number of users. Car-phone versions of NMT used a transmission power of up to 15 watts (NMT-450) and 6 watts (NMT-900), and handsets up to 1 watt. The NMT system was based on frequency division multiple access (FDMA) [3], i.e. the total bandwidth of the system is divided into narrow frequency channels using bandpass filters. These

channels are then allocated to users. No TX power control was employed in 1G systems, i.e. the transmit power was designed to be large enough to cover the majority of a cell [4]. However, the theoretical gains in power control were already known [5, 6].

The 1G system was followed by 2G in 1991. The difference to 1G was that the data transmission technique migrated from analogue to digital, bringing the advantage of simpler signal processing. The widely used standard was called the Global System for Mobile Communications (GSM) [7, 8]. Later on, the General Packet Radio Service (GPRS) [9] and Enhanced Data Rates for GSM Evolution (EDGE) [10] were also introduced. In the current GSM standard, the transmission power in the handset is limited to a maximum of 2 watts in GSM 850/900 and 1 watt in GSM 1800/1900. The cell sizes vary according to the implementation environment; there are five different cell sizes: macro, micro, pico, femto, and umbrella cells. The multiple access technologies used in GSM are time division multiple access (TDMA) [11] and FDMA, such that the users are still assigned to distinct subcarriers but these are further divided into several time slots. In GSM, the transmission power of the mobile station was controlled by a power control message sent by the base station [12]. In the 1990s, power control was also an active research area in academia [13–16]. The 2G standard used in the United States (US) is referred as cdmaOne/IS95 [17, 18].

The first 3G [19] system, the Universal Mobile Telecommunications System (UMTS) [20] was introduced in 2001 and it was based on wideband code division multiple access (WCDMA) [21]. The objective in 3G networks was naturally to solve the problems faced in earlier networks. One of the major goals was to achieve a 3G standard that would work over European, North American, and Asian wireless air interfaces. CDMA was already being used in 2G in the US, and therefore separate standards bodies were required to achieve backwards compatibility: the 3rd Generation Partnership Project (3GPP) in Europe and Asia and 3GPP2 in North America. In 2002, CDMA2000 [22] was standardized by 3GPP2 and it was used especially in North America and South Korea, sharing infrastructure with IS95. In CDMA systems, users transmit their signals simultaneously in the same frequency band. User separation is achieved by a user-specific spreading code and hence, the time-frequency resources can be utilized efficiently. The correlation between the spreading codes is, ideally, zero. However, this is not the case in practice due to multi-path propagation and the limited number of orthogonal codes [23]. Therefore, CDMA is interference limited and adaptive power control is necessary to maintain the ability to serve the increasing number of users. While there have been numerous articles considering power control in CDMA systems (see e.g. [24–26])

the focus during the last decade has been towards multi-carrier techniques where full orthogonality between subcarriers can be achieved. Such a technique is called orthogonal frequency division multiplexing (OFDM) [27], where orthogonality among users is maintained by allocating different subcarriers to different users. Resource management for multiuser (MU) OFDM systems has been investigated in numerous articles (see e.g. [28–33]). A comprehensive article on power allocation in wireless cellular networks is found in [34].

The most recent wireless communication systems, i.e. 4G systems [35] were standardized in 2008. The standard is called Long Term Evolution (LTE) and it was not considered to be a 4G standard before 2010, when International Telecommunications Union-Radio Communications Sector (ITU-R) declared that LTE and Mobile WiMAX could nevertheless be considered 4G, providing a substantial level of improvement in performance and capabilities with respect to the initial 3G systems [36]. However, LTE and WiMAX do not completely satisfy the International Mobile Telecommunications-Advanced (IMT-A) requirements for cellular systems. The key features of IMT-A cellular systems are [37, 38]:

– All-IP packet-switched network
– Peak data rates of up to approximately 100 Mbit/s for high mobility such as mobile access and up to approximately 1 Gbit/s for low mobility such as nomadic/local wireless access
– Able to dynamically share and use network resources to support more simultaneous users per cell
– Use of scalable channel bandwidths of 5-20 MHz, optionally up to 40 MHz
– Peak link spectral efficiency of 15 bit/s/Hz in the downlink (DL), and 6.75 bit/s/Hz in the uplink (UL) (meaning that 1 Gbit/s in the DL should be possible over less than 67 MHz bandwidth)
– System spectral efficiency is, in indoor cases, 3 bit/s/Hz/cell in DL and 2.25 bit/s/Hz/cell in UL,
– Smooth handovers across heterogeneous networks
– The ability to offer high quality of service for next generation multimedia support.

LTE Advanced (LTE-A) was released in 2012 [39], and it was to provide higher bitrates in a cost-efficient way and, at the same time, completely fulfil the requirements set by the International Telecommunication Union (ITU) for IMT-A. The key performance improvements in LTE-A are [40]:

– Increased peak data rate: DL 3 Gbit/s, UL 1.5 Gbit/s
– Higher spectral efficiency, from a maximum of 16 bit/s/Hz in LTE to 30 bit/s/Hz in LTE-A
– Increased number of simultaneously active subscribers
– Improved performance at cell edges, e.g. at least 2.40 bit/s/Hz/cell for DL 2x2 multiple-input multiple-output (MIMO).

The main objective of this thesis is to improve performance at cell edges by introducing a novel power allocation method, taking into account the properties of an iterative receiver (RX) and the characteristics of a transmit power amplifier. The iterative RX and the impact of the transmit power amplifier will be in focus in the following two sections, respectively.

After 1G, the development of each of the systems mentioned above took about ten years, measured from the start of the research to the first standardization. One of the key concepts in 4G systems is multi-antenna transmission and reception, i.e. MIMO technology. In MU MIMO, user separation is performed in the spatial domain and hence, the same frequency and time resources can be used by distinct users. The concept of spatial division multiple access (SDMA) and its theoretical gains was already known in the early 90s [41, 42]. However, the problem was that even though significant power gains can be achieved with directed beams, the control information needs to be broadcasted. The technology used at that time was not able to handle adaptive transmit beamforming efficiently. However, interference rejection combining (IRC) was used on the RX side to decrease multiuser interference (MUI) by noise whitening and to coherently combine the different signal components using the matched filter [43]. IRC is actually a scaled version of minimum mean square error (MMSE) RX and it can be viewed as a receive beamforming technology. In the LTE-A standard, transmit beamforming is based on code books, i.e. transmit beamformers are selected based on information about the channel state [44]. However, it should be noted that, in practice, MIMO is beneficial only for high-quality radio channels because the channel state information (CSI) is not available or imperfect. For situations with a low signal-to-noise ratio (SNR), it is better to use other types of multi-antenna techniques to instead improve the SNR, e.g. by means of TX diversity. In this thesis, the focus is on single antenna transmission with multi-antenna MU detection. However, the extension to multi-antenna transmission is straightforward.

4G systems are based on frequency division duplex (FDD), i.e. the DL and UL

signals are transmitted in different frequency bands. 5G systems are likely to be based on time division duplex (TDD) where the DL and UL signals are transmitted in different time slots. This allows the use of the channel reciprocity, which makes CSI available at the TX. Therefore, it will be possible to utilize more advanced TX precoding schemes in 5G systems.

1.2 Frequency domain multiple access and iterative equalization

Frequency domain equalization (FDE) for single-carrier (SC) transmission [45] and multi-carrier schemes based on OFDM are known as efficient techniques for tackling the inter-symbol-interference (ISI) problem in frequency-selective fading channels. Both of the aforementioned techniques can be extended to MU communications yielding SC frequency division multiple access (FDMA) [46] and orthogonal frequency division multiple access (OFDMA) [47], respectively. In OFDMA all available subcarriers are grouped into different subchannels[1] that are assigned to distinct users. User separation at the RX side is straightforward due to the orthogonality of the subchannels. OFDMA has been selected as the DL transmission scheme of the 3GPP 4G mobile broadband standard [44].

SC-FDMA [46] has been selected as the UL transmission scheme for the 3GPP LTE-A standard [44], due to its good peak-to-average power ratio (PAPR) properties. SC-FDMA can be viewed as a form of OFDMA [47] in which an additional discrete Fourier transform (DFT) and an inverse DFT (IDFT) are added at the TX and RX ends, respectively. A DFT precoder spreads all the symbols across the whole frequency band, forming a virtual SC structure which is known to lead to a reduced PAPR. The derivation of the physical layer quality of service (QoS) constraints, such as SINR or rate constraints, differ in these two schemes: In OFDMA, the frequency domain (FD) channel matrix is block diagonal and, therefore, subcarriers' signal-to-interference-plus-noise ratio (SINR) values decouple. The DFT spreading in SC-FDMA leads to the average SINR constraint where the average is taken over the subcarriers. Hence, the SINR constraint is convex for OFDMA and non-convex for SC-FDMA.

[1] The bandwidth of each subchannel is less than the coherence bandwidth of the channel which results in flat fading subchannels.

1.2.1 Turbo equalization

Optimal MU detection in SC-FDMA in the presence of a frequency-selective channel results in prohibitively high computational complexity. A linear minimum mean square error (LMMSE) detector provides an attractive low-complexity scheme for the detection of FDMA signal in the presence of ISI and MUI utilizing the circulant structure of channel matrices [48, 49].

Iterative FDE techniques can achieve a significant performance gain over linear FDE in ISI channels [49]. In iterative FDE, the key idea is to utilize the feedback from a soft-output forward error correction (FEC) decoder that is updated according to the "turbo" principle. To exploit the full merit of an iterative RX, the convergence properties of the RX need to be taken into account jointly at the TX and the RX. In [50], extrinsic information transfer (EXIT) analysis [51] is utilized to determine the optimal power allocation in an MU turbo-coded CDMA system. In [52], convergence analysis for iterative minimum mean square error (MMSE) equalizer is performed using SNR variance charts [49]. Furthermore, the authors in [52] use convergence analysis to formulate the TX power allocation problem in frequency-selective single-input single-output (SISO) channels with the iterative RX mentioned above, assuming the availability of perfect CSI at both the TX and the RX. In [53, 54], the impact of precoder design on convergence properties of the soft cancelation FD MMSE equalizer is demonstrated. In [55], precoder design for MU MIMO ISI channels based on iterative LMMSE detection is considered. The design criterion of the precoder in [55] is to maximize the SINR at the end of the iterative process. In [56], in-depth analysis of the power allocation problem in SC MIMO systems with iterative MMSE equalization has been presented.

1.2.2 Extrinsic information transfer chart

The advantages of soft information processing were truly realized after the foundation of turbo codes [57] in 1993. However, the convergence properties of this type of iterative process were not yet fully understood. The EXIT chart is one of the most powerful tools for analysing and optimizing parameters in iterative processing [58–60]. The convergence of an iterative process can be predicted by investigating the exchange of extrinsic information of soft-in/soft-out (SftI/SftO) blocks in the form of mutual information (MI) between transmitted bits and the corresponding log-likelihood ratios (LLRs). The analysis can be performed independently for each block, which eliminates the neces-

sity of time-consuming chain simulations. When applied to joint equalizer and FEC decoder design, the objective is to guarantee an open convergence tunnel between the EXIT functions of the equalizer and the decoder. To be more specific, the EXIT function of the equalizer has to be above the inverse EXIT function of the decoder until the 'MI convergence point', which determines the communication reliability achieved by the iterative equalizer, represented by bit error probability (BEP). Therefore, the width of the tunnel and the MI convergence point are the key parameters when optimizing an iterative process using EXIT charts [61, 62].

1.3 PAPR problem in multi-carrier transmission

It is well known that power allocation in multi-carrier transmission provides significant improvement in terms of total power consumption [43]. In [56, 63], a power allocation technique taking into account the convergence properties of an iterative RX was derived for SC-FDMA showing substantial improvement in terms of reducing the SNR requirements for the desired QoS target. However, the use of FD power allocation leads to an increased value of the PAPR. Motivated by this fact, a framework is constructed in this thesis by which the PAPR can be controlled via FD power allocation. The proposed PAPR constraints are applied to the optimization framework introduced in [63]. However, the PAPR constraints themselves are general and can be applied to any SC-FDMA or OFDMA framework.

In addition to the average power of the transmitted signal, the power consumption of the power amplifier also depends on the peak power of the transmission. Hence, the wasted supply power can be reduced by decreasing the PAPR of the input signal [64]. Furthermore, since the peak power in cellular systems is limited by local authority, the average uplink power has to be limited to take into account the high peaks. Hence, the proposed method is especially beneficial for power-limited cell edge users. In this section, the PAPR problem is described starting with the fundamentals followed by a literature review of PAPR reduction techniques. Since SC-FDMA can be viewed as DFT precoded OFDMA, the PAPR problem described for OFDMA applies equivalently to SC-FDMA.

1.3.1 Fundamentals

An OFDM signal consists of independently modulated subcarriers. The high peak power occurs when the subcarriers add up coherently. E.g., when N subcarriers are added with the same phase and amplitude, the peak power is N times the average power of the signal [65]. The relation between the peak power and the average power is called the PAPR. From the mobile user's perspective, the PAPR problem is characterized into two main categories:

1. The energy consumed by the high-power amplifier (HPA) is related to the peak power values. Therefore, transmitting the signal with a high PAPR is inefficient, because the peaks of the wave do not transport any more information than the average power of the signal over time.
2. Distortion-free transmission of such a signal requires linear operation of HPA over a range N times the average power.

In practice, the high peak values are not tolerable because the wasted supply power has a harmful impact on either battery life in mobile applications (UL) or the energy cost of network operation (DL). Furthermore, from a technology viewpoint, it is challenging to provide such a large linear range of HPAs. Therefore, the HPA output signal is cut off or *clipped* at some point relative to the average power [64], resulting in a distorted signal due to intermodulation among the subcarriers. Furthermore, the clipping introduces out-of-band radiation, resulting in the necessity to increase a spectral guard band between adjacent services, zero-input subcarriers, or some kind of out-of-band reduction method [66]. The PAPR problem raises several challenges that system designers need to consider: one challenge is to adjust HPA parameters, i.e. HPA backoff and digital predistortion, in some specific way, taking into account the trade-off between power efficiency and nonlinear distortion, which has an impact on data transmission at a global scale [64]. The high PAPR has also an incremental impact on the complexity of analogue-to-digital and digital-to-analogue converters. Another approach to the PAPR problem is to process the baseband signal using some kind of PAPR reduction algorithm. Thus, it is obvious that the PAPR problem involves joint optimization of HPA, predistortion, and a signal processing unit. However, the joint optimization approach that is also considered in this thesis has only been marginally addressed so far.

From the network design perspective, a high PAPR is a limiting factor when the coverage of a base station is considered. The coverage of a base station is determined

by the average uplink power. On the other hand, the peak power of the transmission is limited by the local authority and the peaks exceeding this threshold are clipped, resulting in a distorted signal. Therefore, the average uplink power is restricted to take into account the high peaks. Hence, if the peak power can be reduced, the average power can be increased, which results in improved QoS for cell edge users.

1.3.2 Existing PAPR reduction techniques

Reducing the PAPR in any transmission system is always desirable, as it allows the use of more efficient and inexpensive power amplifiers at the TX. Selected mapping (SLM) [67] and partial transmit sequences (PTS) [68, 69] are classic methods for reducing the PAPR in multi-carrier transmission. The idea is to generate multiple redundant candidate frames and select the best for transmission. By using suitable transforms or mappings, the main goal is to achieve statistical independence between candidates' metrics [64]. Many transforms have been proposed and efficient algorithms have been derived for SLM and PTS (see e.g. [70]). The main drawback in SLM and PTS is that side information is required to decode the transformed sequence at the RX. Another method for PAPR reduction is constellation shaping [71–73], where the objective is to find a constellation in the N-dimensional FD, such that the resulting shaping region in the time domain has a low PAPR. Even though the simulation results look promising, the drawback in constellation shaping is the high implementation complexity.

One of the popular solutions for PAPR reduction is clipping the amplitude of the OFDM signal. The drawback is that the clipping increases the noise level by inducing a clipping noise. Recent work [74, 75] on practical schemes indicates that the main source of the loss is not the distortions or errors introduced, but simply reduced output power. Compressed sensing has been considered for cancelling the clipping noise in [76, 77]. The problem in these approaches is that the performance is restricted due to the weakness of the compressed sensing against noise. In the past, the PAPR problem has been addressed in many papers and overview articles, e.g. [78, 79]. The existing techniques achieve a reduced PAPR at the expense of a transmit signal power increase, bit error rate (BER) increase, data rate loss, computational complexity increase, etc. Recent work on minimizing the PAPR in SC-FDMA transmission can be found in [80–82], where the authors propose different precoding methods for PAPR reduction. However, these methods do not take into account the FD transmit power allocation, the channel or the RX.

1.4 Optimization methods

In this section, the optimization tools used in this thesis are briefly discussed.

1.4.1 Alternating optimization

If some sets or blocks of optimization variables are not coupled through the objective function of the optimization problem, the optimization may be performed independently along these blocks of coordinate vectors; the algorithm updates the coordinates iteratively such that one block of coordinates is considered at a time, while the other ones are fixed. The convergence of this method is guaranteed if the solution obtained in each optimization step is unique. This method is called the block coordinate descent (BCD) method [83].

In this thesis, a similar concept is applied to joint TX-RX optimization where the algorithm alternates between the TX and RX optimization problems. In the optimization problem presented in this thesis, the sub-problems in the iterative algorithm are not convex and thus, the solution is not necessarily unique. However, the convergence of the objective value can be justified by showing that each step improves the objective. In this thesis, the iterative TX-RX optimization algorithm is referred as *alternating optimization*.

1.4.2 Successive convex approximation

Some of the constraints in the optimization problems considered in this thesis are non-convex, even for a fixed RX filter. Therefore, the successive convex approximation (SCA) [84] method is used for those constraints. The idea is to transform a non-convex optimization problem into a convex form such that the solution of the transformed problem always satisfies the constraints of the original problem. An example of SCA is a local linear approximation of a concave function. Updating the approximation point iteratively, a local solution of the original problem can be obtained. A more detailed description of SCA and its convergence properties can be found in [84, 85]. In this thesis, two different SCA methods are applied: successive convex approximation via change of variables (SCACOV) and successive convex approximation via geometric programming (SCAGP).

SCACOV is based on the idea presented in [86] where a change of variables (COV)

is performed to create a log-concave objective function. In this thesis, the technique is used to approximate non-convex constraints as convex ones. SCAGP utilizes the concept derived in [87] where the denominator of the objective is approximated as a monomial such that the problem can be approximated as a geometric program (GP) [88]. A comprehensive article on GP and its applications is found in [89]. As SCACOV and SCAGP most likely end up with the same result, the decision of which method to choose has to be made case by case. For instance, the number of approximated constraints can be different depending on the approximation method.

1.5 Scope and objectives of the thesis

This thesis concentrates on the design of FD UL power allocation for FDMA[2] transmission. The thesis can be divided into two parts: in the first part, the aim is to jointly optimize the multiuser TX power allocation and the complex weights at the RX filter such that the convergence properties of an iterative equalizer are taken into account. More specifically, the gap between the EXIT curves of the decoder and the equalizer is, at minimum, the desired value until the predetermined convergence point. The convergence point is the MI after the detection determining the QoS of each user. In the latter part of the thesis, the characteristics of a transmit power amplifier are also taken into account. In other words, the instantaneous and statistical PAPR are controlled via FD power allocation. As depicted in Fig. 1, the optimization algorithms can be executed at the base station or on the mobile user side depending on the available information. If global CSI is needed for optimization, the optimization is performed at the base station and the power allocation obtained is reported to the users. If all the parameter values needed in the optimization are available on the mobile user side, the algorithm can be executed by users themselves resulting in reduced signalling.

The concept of convergence-constrained power allocation (CCPA) was originally derived in [56] for single-user MIMO systems with SC-FDMA transmission. The authors show that the convergence constraints (CCs) transfer to multiple SINR constraints. In a single-user MIMO, the subcarriers can be perfectly decoupled using singular value decomposition leading to convex SINR constraints. The objective of the optimization problem is to minimize the sum power over the subcarriers. Therefore, the optimization problem derived in [56] is a convex problem. This thesis extends the concept of CCPA to MU single-input multiple-output (SIMO) systems, showing that substantial gains in

[2]Here FDMA includes SC-FDMA and OFDMA.

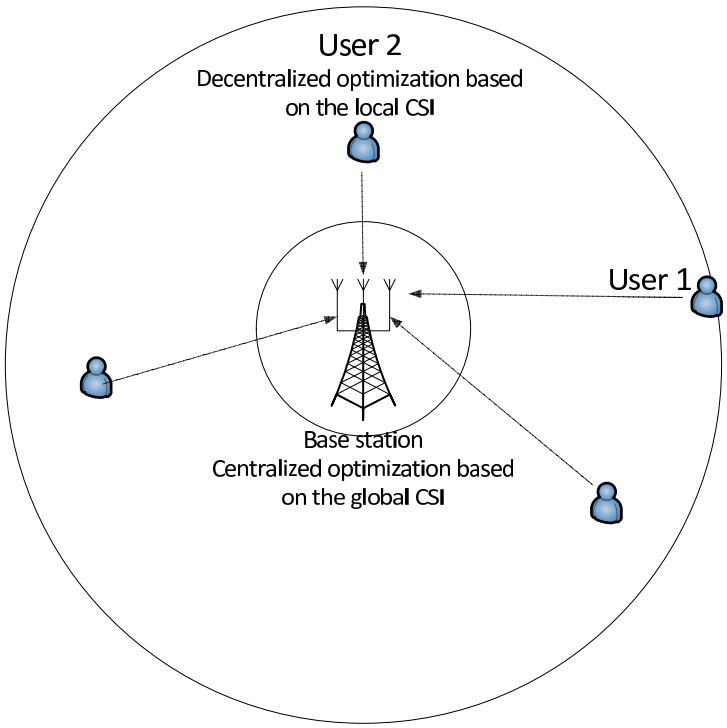

Fig. 1. Single cell system with multiple users and a base station with multiple antennas.

terms of total power consumption can also be achieved in MU systems. Furthermore, the objective is also to extend the concept from binary phase-shift keying (BPSK) and quadrature phase-shift keying (QPSK) to 16-ary quadrature amplitude modulation (16-QAM) providing a concept for the generalization towards higher-order modulations. Moreover, in addition to SC-FDMA, OFDMA is also considered. Since the power allocation strategy is novel, only a single-cell system is considered in this phase of the research; the multi-cell scenario is left for future work. The extension to a multi-cell scenario is rather straightforward, i.e. the interference from the other cells is taken into account in the SINR constraints. The majority of the derived power allocation strategies presented in this thesis require full CSI, although suboptimal alternatives can be derived where only the local CSI is required.

The motivation for using SC-FDMA is that it has better PAPR characteristics than OFDMA. However, it was observed that CCPA increases the PAPR. The objective in the latter part of the thesis is to find out a way to flexibly control the PAPR in multi-carrier transmission.

1.6 Contributions and outline

The system model assumed throughout the thesis is presented in Chapter 2. UL transmission with multiple single-antenna users and a base station with multiple antennas is considered. Iterative equalizers are derived for SC-FDMA and OFDMA systems in Sections 2.2.1 and 2.2.2, respectively.

Chapter 3 is mainly based on [63, 90] although the CC for OFDMA was introduced in [91]. The novel aspect of Chapter 3 is the derivation of the CC for MU communications. The presence of multiple users leads to multidimensional EXIT functions, which makes the optimization very complex as such. A suboptimal solution referred as *diagonal sampling* is presented in Section 3.1.2. The CC is applied for MU SIMO UL communications in Sections 3.1.3 and 3.1.4, where BPSK, QPSK, and 16-QAM are considered. The constraints are derived for both SC-FDMA and OFDMA. In [56], only QPSK is considered. In this thesis, a heuristic approach for 16-QAM is also derived. Unlike in [56], the joint optimization of the multiple TXs and the RX is not convex. Thus, the non-convex joint optimization problem is split into separate TX and RX optimization problems. Section 3.3.3 demonstrates that the MMSE RX is a power minimizing RX and, therefore, the objective value in this type of alternating optimization converges towards a local solution.

Unlike the power minimization problem with the classic per-subcarrier SINR constraint [92], the problem considered in this thesis cannot be formulated as a convex problem even for a fixed RX filter. Therefore, two efficient algorithms, SCACOV and SCAGP, are proposed for solving the TX optimization problem for fixed receive beamformers. The SCAs are presented in a general form in Section 3.2 and then applied to CCPA considered in this thesis in Section 3.3.

Chapter 4 is based on [91, 93, 94]. Two approaches for PAPR-aware power allocation in multi-carrier transmission are presented. The first approach, presented in Section 4.1, optimally restricts the PAPR to below a preset threshold value while guaranteeing the preset QoS target. The second approach, presented in Section 4.2, controls the PAPR by statistically controlling the variance of the power of the transmitted signal. The instantaneous PAPR and the variance are derived for SC-FDMA and OFDMA. The PAPR and power variance derivations presented in this thesis apply to any normalized data modulation technique. The PAPR constraints are applied to the optimization framework presented in Chapter 3 and SCACOV and SCAGP are derived for each of the constraints.

Finally, conclusions are drawn in Chapter 5 with a discussion about the future research directions.

1.7 Author's contribution

This thesis is written as a monograph based on five original publications [63, 90, 91, 93, 94], including one accepted [63] and one submitted [91] journal paper and three conference papers [90, 93, 94]. The author of this thesis had the main role in developing the ideas, deriving the equations, writing the MATLAB code and writing the papers. The role of the co-authors was to provide guidance, ideas and criticism during the research and writing process.

In addition to publications [63, 90, 91, 93, 94], which comprise the main content of the thesis, publications [95–97] by the author and the co-authored publication [98] are not included in the thesis.

In summary, the main contributions of the thesis include:

- The derivation of a convergence constraint (CC) for MU systems
- Diagonal sampling for discretization of CC
- The derivation of CC in MU SIMO uplink SC-FDMA and OFDMA communications with BPSK, QPSK and 16-QAM
- Two suboptimal approaches for convergence-constrained power allocation
- The joint optimization of a transmit power allocation and receive filter in SC-FDMA and OFDMA
- The derivation of an instantaneous PAPR constraint for SC-FDMA and OFDMA transmission
- The derivation of a transmission power variance constraint for SC-FDMA and OFDMA transmission
- The derivation of two successive convex approximations for all the non-convex constraints considered.

2 Multicarrier transmission and iterative equalization

In this chapter, the system model of UL transmission in a single cell system with U single antenna users and a base station with N_R antennas is presented. Furthermore, the RX with iterative FD turbo equalization is derived.

2.1 Multi-carrier transmission

The TX side of the system model is depicted in Fig. 2. Each user's data stream $\mathbf{x}_u \in \mathbb{B}^{R_c^u N_Q N_F}$, $u = 1,2,\ldots,U$, is encoded by a FEC code $\mathscr{C}_u$ with a code rate $R_c^u \leq 1$. N_Q denotes the number of bits per modulation symbol and N_F is the number of frequency bins in DFT. The encoded bits

$$\mathbf{c}^u = [c_1^u, c_2^u, \ldots, c_{N_Q N_F}]^{\mathrm{T}} \in \mathbb{B}^{N_Q N_F} \tag{1}$$

are bit-interleaved by multiplying $\mathbf{c}^u$ by pseudo-random permutation matrix

$$\mathbf{\Pi}_u \in \mathbb{B}^{N_Q N_F \times N_Q N_F}$$

resulting in a bit sequence $\mathbf{c}'^u = \mathbf{\Pi}_u \mathbf{c}^u$. After the interleaving, the sequence $\mathbf{c}'^u$ is mapped with a mapping function $\mathscr{M}_u(\cdot)$ onto a 2^{N_Q}-ary complex symbol $b_l^u \in \mathbb{C}$, $l = 1,2,\ldots,N_F$, resulting in a complex data vector

$$\mathbf{b}^u = [b_1^u, b_2^u, \ldots, b_{N_F}^u]^{\mathrm{T}} \in \mathbb{C}^{N_F}. \tag{2}$$

After the modulation, in SC-FDMA each user's data stream is spread across the sub-channels by multiplying $\mathbf{b}^u$ by a DFT matrix $\mathbf{F} \in \mathbb{C}^{N_F \times N_F}$, $\forall u = 1,2,\ldots,U$, where the elements of $\mathbf{F}$ are given by

$$f_{m,l} = \frac{1}{\sqrt{N_F}} e^{(i2\pi(m-1)(l-1)/N_F)}, \tag{3}$$

$m,l = 1,2,\ldots,N_F$. In OFDMA, this spreading is omitted. Each user's data stream is multiplied with its associated power allocation matrix $\mathbf{P}_u^{\frac{1}{2}}$, where

$$\mathbf{P}_u = \mathrm{diag}([P_{u,1}, P_{u,2}, \ldots, P_{u,N_F}]^{\mathrm{T}}) \in \mathbb{R}^{N_F \times N_F}, \tag{4}$$

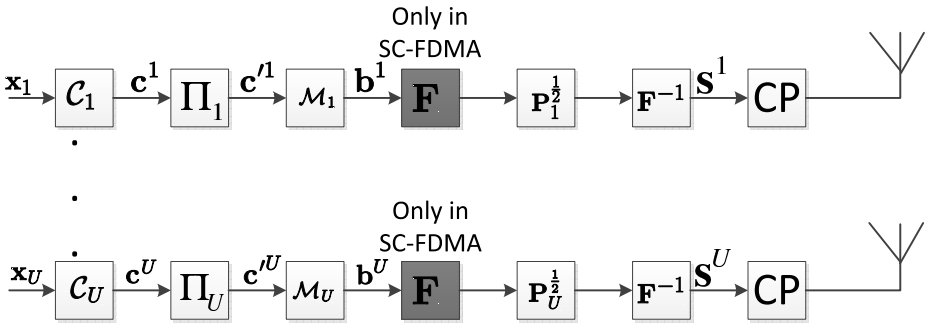

Fig. 2. Block diagram of the transmitter side of the system model.

with $P_{u,l}$ being the power allocated to the lth frequency bin. Finally, before transmission, each user's data stream is transformed into the time domain by the IDFT matrix $\mathbf{F}^{-1}$ resulting in

$$\mathbf{s}^u = [s_1^u, s_2^u, \ldots, s_{N_F}^u]^{\mathrm{T}}, \ \forall u. \tag{5}$$

A cyclic prefix (CP) is added to mitigate inter-block interference (IBI) in SC-FDMA and ISI in OFDMA.

2.2 Receiver

In this section, an iterative RX is presented for SC-FDMA and OFDMA.

2.2.1 SC-FDMA

The RX side of the system model is depicted in Fig. 3. After the CP removal, the signal can be expressed as[3]

$$\mathbf{r} = \mathbf{H}_u \mathbf{F}^{-1} \mathbf{P}_u^{\frac{1}{2}} \mathbf{F} \mathbf{b}^u + \sum_{y \neq u}^{U} \mathbf{H}_y \mathbf{F}^{-1} \mathbf{P}_y^{\frac{1}{2}} \mathbf{F} \mathbf{b}^y + \mathbf{v}, \tag{6}$$

where

$$\mathbf{H}_u = [\mathbf{H}_u^1, \mathbf{H}_u^2, \ldots, \mathbf{H}_u^{N_R}]^{\mathrm{T}} \in \mathbb{C}^{N_R N_F \times N_F} \tag{7}$$

is the space-time channel matrix for user u and

$$\mathbf{H}_u^r = \mathrm{circ}\{[h_{u,1}^r, h_{u,2}^r, \ldots, h_{u,N_L}^r, \mathbf{0}_{1\times N_F - N_L}]^{\mathrm{T}}\} \in \mathbb{C}^{N_F \times N_F} \tag{8}$$

[3] In this thesis, single cell scenario is considered and the impact of inter-cell-interference is omitted.

is the time domain circulant channel matrix for user u at the receive antenna r. The operator circ$\{\}$ generates a matrix that has a circulant structure of its argument vector, N_L denotes the length of the channel impulse response, and $h_{u,l}^{r}$, $l = 1,2,\ldots,N_L$, $r = 1,2,\ldots,N_R$, is the fading factor of multi-path channel. A vector $\mathbf{v} \in \mathbb{C}^{N_R N_F}$ in (6) denotes white additive independent and identically distributed (i.i.d.) Gaussian noise vector with variance σ_v^2. The signal $\mathbf{r}$ is transformed into the FD by using DFT matrix

$$\mathbf{F}_{N_R} = \mathbf{I}_{N_R} \otimes \mathbf{F} \in \mathbb{C}^{N_R N_F \times N_R N_F}, \tag{9}$$

resulting in

$$\tilde{\mathbf{r}} = \mathbf{\Gamma} \mathbf{P}^{\frac{1}{2}} \mathbf{F}_U \mathbf{b} + \mathbf{F}_{N_R} \mathbf{v}, \tag{10}$$

where

$$\mathbf{\Gamma} = [\mathbf{\Gamma}_1, \mathbf{\Gamma}_2, \ldots, \mathbf{\Gamma}_U] \in \mathbb{C}^{N_R N_F \times U N_F} \tag{11}$$

with

$$\mathbf{\Gamma}_u = \text{bdiag}\{\mathbf{\Gamma}_{u,1}, \mathbf{\Gamma}_{u,2}, \ldots, \mathbf{\Gamma}_{u,N_F}\} \in \mathbb{C}^{N_R N_F \times N_F} \tag{12}$$

being the space-frequency channel matrix for user u expressed as

$$\mathbf{\Gamma}_u = \mathbf{F}_{N_R} \mathbf{H}_u \mathbf{F}^{-1}. \tag{13}$$

$\mathbf{\Gamma}_{u,m} \in \mathbb{C}^{N_R \times N_R}$ is the diagonal channel matrix for the m^{th} frequency bin of the u^{th} user,

$$\mathbf{F}_U = \mathbf{I}_U \otimes \mathbf{F} \in \mathbb{C}^{U N_F \times U N_F}, \tag{14}$$

and

$$\mathbf{b} = [\mathbf{b}^{1\mathrm{T}}, \mathbf{b}^{2\mathrm{T}}, \ldots, \mathbf{b}^{U\mathrm{T}}]^{\mathrm{T}} \in \mathbb{C}^{U N_F}. \tag{15}$$

The power allocation matrix is composed by

$$\mathbf{P} = \text{diag}(\mathbf{P}_1, \mathbf{P}_2, \ldots, \mathbf{P}_U) \in \mathbb{R}^{U N_F \times U N_F}. \tag{16}$$

The block diagram of the FD turbo equalizer is depicted in Fig. 4. The FD signal after the soft cancelation can be written as

$$\hat{\mathbf{r}} = \tilde{\mathbf{r}} - \mathbf{\Gamma} \mathbf{P}^{\frac{1}{2}} \mathbf{F}_U \tilde{\mathbf{b}}, \tag{17}$$

where

$$\tilde{\mathbf{b}} = [\tilde{\mathbf{b}^1}^{\mathrm{T}}, \tilde{\mathbf{b}^2}^{\mathrm{T}}, \ldots, \tilde{\mathbf{b}^U}^{\mathrm{T}}]^{\mathrm{T}} \in \mathbb{C}^{U N_F} \tag{18}$$

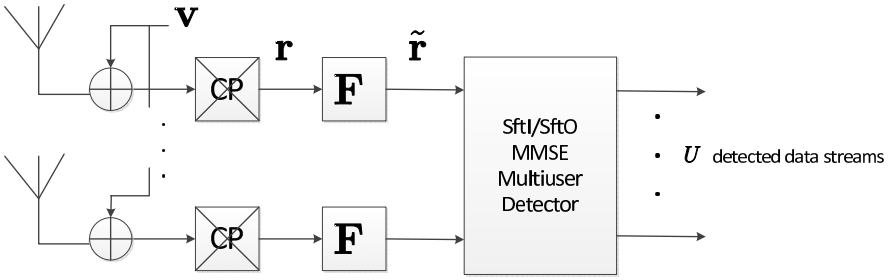

Fig. 3. Block diagram of the receiver side of the system model.

is composed by

$$\tilde{\mathbf{b}}^u = [\tilde{b}^u_1, \tilde{b}^u_2, \ldots, \tilde{b}^u_{N_F}]^{\mathrm{T}} \in \mathbb{C}^{N_F}. \tag{19}$$

The soft symbol estimate $\tilde{b}^u_n$ is calculated as [56]

$$\tilde{b}^u_n = \mathbb{E}\{b^u_n\} = \sum_{b_i \in \mathfrak{B}} b_i \Pr(b^u_n = b_i), \tag{20}$$

where $\mathfrak{B}$ is the modulation symbol alphabet, and the symbol *a priori* probability can be calculated by [99]

$$\begin{aligned} \Pr(b^u_n = b_i) &= \prod_{q=1}^{N_Q} \Pr(c'^u_{N_Q(n-1)+q} = c'_{i,q}) \\ &= \left(\frac{1}{2}\right)^{N_Q} \prod_{q=1}^{N_Q} (1 - \bar{c}'_{i,q} \tanh(\mathring{L}'_{u,(n-1)N_Q+q}/2)), \end{aligned} \tag{21}$$

with

$$\bar{c}'_{i,q} = 2c_{i,q} - 1 \tag{22}$$

and

$$\mathbf{c}'_i = [c'_{i,1}, c'_{i,2}, \ldots, c'_{i,N_Q}]^{\mathrm{T}} \tag{23}$$

is the binary representation of the symbol b_i, depending on the mapping rule for modulation. $\mathring{L}'_{u,(n-1)N_Q+q}$ is the *a priori* LLR of the bit $c'^u_{N_Q(n-1)+q}$, provided by the decoder of user u. After the soft cancelation, the residual and estimated received signal of user u are summed, yielding $\check{\mathbf{r}}_u \in \mathbb{C}^{N_R N_F}$ as [100]

$$\check{\mathbf{r}}_u = \hat{\mathbf{r}} + \mathbf{\Gamma}_u \mathbf{P}_u^{\frac{1}{2}} \mathbf{F} \tilde{\mathbf{b}}^u. \tag{24}$$

The time domain output of the receive filter for the u^{th} user can be written as

$$\hat{\mathbf{b}}^u = \mathbf{F}^{-1} \check{\mathbf{\Omega}}_u^{\mathrm{H}} \check{\mathbf{r}}_u, \tag{25}$$

where

$$\breve{\mathbf{\Omega}}_u = [\breve{\mathbf{\Omega}}_u^1, \breve{\mathbf{\Omega}}_u^2, \ldots, \breve{\mathbf{\Omega}}_u^{N_R}]^{\mathrm{T}} \in \mathbb{C}^{N_R N_F \times N_F} \tag{26}$$

is the filtering matrix for the u^{th} user and $\breve{\mathbf{\Omega}}_u^r \in \mathbb{C}^{N_F \times N_F}$ is the filtering matrix for the r^{th} receive antenna of the u^{th} user. The effective SINR of the prior symbol estimates for the u^{th} user can be expressed as

$$\zeta_u = \frac{1}{N_F} \sum_{m=1}^{N_F} \frac{P_{u,m} \boldsymbol{\omega}_{u,m}^{\mathrm{H}} \boldsymbol{\gamma}_{u,m} \boldsymbol{\gamma}_{u,m}^{\mathrm{H}} \boldsymbol{\omega}_{u,m}}{\boldsymbol{\omega}_{u,m}^{\mathrm{H}} \mathbf{\Sigma}_{\hat{\mathbf{r}},m} \boldsymbol{\omega}_{u,m}}, \tag{27}$$

where $\boldsymbol{\gamma}_{u,m} \in \mathbb{C}^{N_R}$ consists of the diagonal elements of $\mathbf{\Gamma}_{u,m}$, i.e., $\boldsymbol{\gamma}_{u,m}$ is the channel vector for the m^{th} frequency bin of user u.

$$\boldsymbol{\omega}_{u,m} = \left[[\breve{\mathbf{\Omega}}_u^1]_{m,m}, [\breve{\mathbf{\Omega}}_u^2]_{m,m} \ldots, [\breve{\mathbf{\Omega}}_u^{N_R}]_{m,m} \right]^{\mathrm{T}} \in \mathbb{C}^{N_R} \tag{28}$$

is the receive beamforming vector for the m^{th} frequency bin of user u. Using the MMSE criterion, the receive beamforming vector is shown to be [101]

$$\boldsymbol{\omega}_{u,m} = \frac{1}{\mathrm{avg}\{\ddot{\mathbf{b}}^u\} \zeta_u + 1} \mathbf{\Sigma}_{\hat{\mathbf{r}},m}^{-1} \boldsymbol{\gamma}_{u,m} \sqrt{P_{u,m}}, \tag{29}$$

where $\mathbf{\Sigma}_{\hat{\mathbf{r}},m} \in \mathbb{C}^{N_R \times N_R}$ is the interference covariance matrix of the m^{th} frequency bin given by

$$\mathbf{\Sigma}_{\hat{\mathbf{r}},m} = \sum_{l=1}^{U} P_{l,m} \boldsymbol{\gamma}_{l,m} \boldsymbol{\gamma}_{l,m}^{\mathrm{H}} \Delta^l + \sigma_v^2 \mathbf{I}_{N_R}. \tag{30}$$

$$\Delta^l = \mathrm{avg}\{\mathbf{1}_{N_F} - \ddot{\mathbf{b}}^l\} \tag{31}$$

is the average residual interference of the soft symbol estimates and

$$\ddot{\mathbf{b}}^l = [|\tilde{b}_1^l|^2, |\tilde{b}_2^l|^2, \ldots, |\tilde{b}_{N_F}^l|^2]^{\mathrm{T}} \in \mathbb{C}^{N_F}. \tag{32}$$

The scalar Δ^l is an approximation which is reasonably accurate for normalized 2^{N_Q}-ary phase-shift keying (PSK) as well as for rectangular 2^{N_Q}-ary quadrature amplitude modulation (QAM) with an appropriate normalization [56]. For QAM, both the transmitted symbol vector $\mathbf{b}^u$ and soft-symbol vector $\tilde{\mathbf{b}}^u$ have to be multiplied by the normalization factor $\kappa = \sqrt{\frac{3}{2(2^{N_Q}-1)}}$. Note that Δ^l is the average taken over the whole symbol sequence. With the appropriate normalization, $\Delta^l = 1$ when no *a priori* information is available and $\Delta^l = 0$ when perfect *a priori* information is available. In fact, Δ^l is an essential approximation in order to use higher order modulations where the power of a symbol is not equal to one. In order to use the approximation Δ^l, the expectation of symbol power has to be one and the length of a block needs to be large enough.

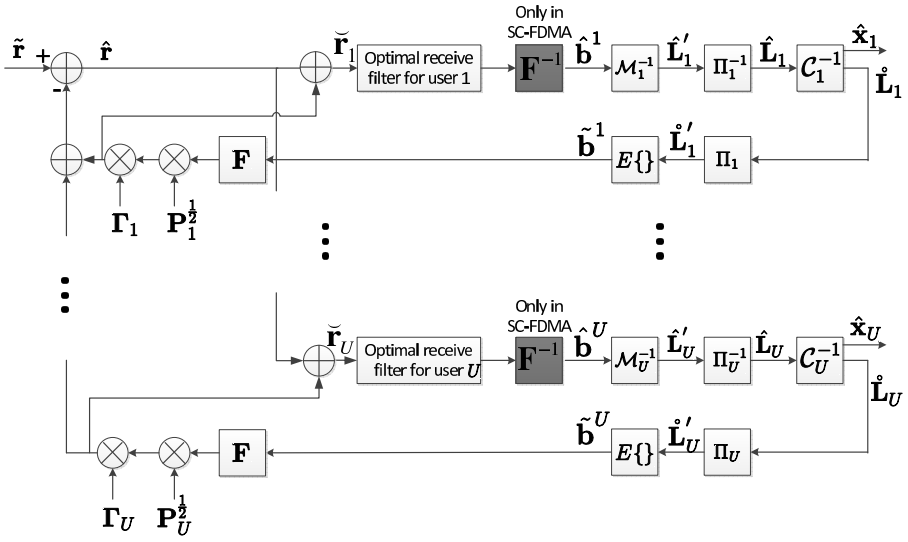

Fig. 4. Block diagram of frequency domain turbo equalizer.

2.2.2 OFDMA

The received signal at the m^{th} subcarrier is

$$\tilde{\mathbf{r}}_m = \sum_{u=1}^{U} \boldsymbol{\gamma}_{u,m} \sqrt{P_{u,m}} b_m^u + \mathbf{v}_m \in \mathbb{C}^{N_R}, \tag{33}$$

where $\mathbf{v}_m \in \mathbb{C}^{N_R}$ consists of noise samples associated with the m^{th} subcarrier. The FD signal after soft cancelation is expressed as

$$\hat{\mathbf{r}}_m = \tilde{\mathbf{r}}_m - \sum_{u=1}^{U} \boldsymbol{\gamma}_{u,m} \sqrt{P_{u,m}} \tilde{b}_m^u. \tag{34}$$

The component which is to be filtered is the summation of the residual and the received signal:

$$\breve{\mathbf{r}}_{u,m} = \hat{\mathbf{r}} + \boldsymbol{\gamma}_{u,m} \sqrt{P_{u,m}} \tilde{b}_m^u. \tag{35}$$

The filtered signal can be expressed as

$$\hat{b}_m^u = \tilde{\boldsymbol{\omega}}_{u,m}^{\text{H}} \breve{\mathbf{r}}_{u,m}, \tag{36}$$

where $\tilde{\boldsymbol{\omega}}_{u,m} \in \mathbb{C}^{N_R}$ is the receive filter of the u^{th} user at the m^{th} subcarrier which can be found by solving

$$\underset{\tilde{\boldsymbol{\omega}}_{u,m}}{\text{minimize}} \; E_{u,m}, \tag{37}$$

where

$$E_{u,m} = \mathbb{E}_{b_m^u, \tilde{\mathbf{v}}_m}\{(b_m^u - \hat{b}_m^u)(b_m^u - \hat{b}_m^u)^{\mathrm{H}}\}. \tag{38}$$

Assuming normalized PSK or rectangular QAM modulation, the mean square error (MSE) given by (38) can be rewritten as

$$\begin{aligned} E_{u,m} = &-2\tilde{\boldsymbol{\omega}}_{u,m}^{\mathrm{H}} \boldsymbol{\gamma}_{u,m}\sqrt{P_{u,m}} + \\ &\tilde{\boldsymbol{\omega}}_{u,m}^{\mathrm{H}}(\boldsymbol{\gamma}_{u,m}\boldsymbol{\gamma}_{u,m}^{\mathrm{H}}P_{u,m} + \sum_{\substack{l=1 \\ l\neq u}}^{U} \boldsymbol{\gamma}_{l,m}\boldsymbol{\gamma}_{l,m}^{\mathrm{H}}P_{l,m}(1-|\tilde{b}_{l,m}|^2) + \sigma_v^2\mathbf{I}_{N_R})\tilde{\boldsymbol{\omega}}_{u,m}, \end{aligned} \tag{39}$$

Similarly to the SC-FDMA case in Section 2.2.1, the interference cancelation term $1-|\tilde{b}_{l,m}|^2$ can be approximated $\forall m$ as $\bar{\Delta}^l = \mathrm{avg}\{\mathbf{1}_{N_F} - \ddot{\mathbf{b}}^l\}$. Taking the derivative of (39) with respect to $\tilde{\boldsymbol{\omega}}_{u,m}^{\mathrm{H}}$ and equating to zero yields

$$\tilde{\boldsymbol{\omega}}_{u,m} = (\boldsymbol{\gamma}_{u,m}\boldsymbol{\gamma}_{u,m}^{\mathrm{H}}P_{u,m} + \tilde{\boldsymbol{\Sigma}}_{\hat{\mathbf{r}},m}^{u})^{-1}\boldsymbol{\gamma}_{u,m}\sqrt{P_{u,m}}, \tag{40}$$

where

$$\tilde{\boldsymbol{\Sigma}}_{\hat{\mathbf{r}},m}^{u} = \sum_{\substack{l=1 \\ l\neq u}}^{U} \boldsymbol{\gamma}_{l,m}\boldsymbol{\gamma}_{l,m}^{\mathrm{H}}P_{l,m}\Delta^l + \sigma_v^2\mathbf{I}_{N_R}. \tag{41}$$

Substituting the solution of (37) to (36) gives the MMSE estimate of the transmitted symbol as

$$\hat{b}_m^u = [(\boldsymbol{\gamma}_{u,m}\boldsymbol{\gamma}_{u,m}^{\mathrm{H}}P_{u,m} + \tilde{\boldsymbol{\Sigma}}_{\hat{\mathbf{r}},m}^{u})^{-1}\boldsymbol{\gamma}_{u,m}\sqrt{P_{u,m}}]^{\mathrm{H}}\breve{\mathbf{r}}_{u,m}, \tag{42}$$

The SINR after the MMSE filter is given by

$$\tilde{\zeta}_{u,m} = \frac{P_{u,m}|\boldsymbol{\gamma}_{u,m}^{\mathrm{H}}\tilde{\boldsymbol{\omega}}_{u,m}|^2}{\sum_{\substack{l=1 \\ l\neq u}}^{U}|\boldsymbol{\gamma}_{l,m}^{\mathrm{H}}\tilde{\boldsymbol{\omega}}_{u,m}|^2P_{l,m}\Delta^l + \sigma_v^2||\tilde{\boldsymbol{\omega}}_{u,m}||^2}. \tag{43}$$

3 Transmitter-receiver optimization

In this chapter, a general description of the CC in MU communications is provided. Then the CC is applied for the system model presented in Chapter 2. General descriptions of two different SCA methods are given in Section 3.2. In Sections 3.3.1 and 3.3.2, suboptimal alternatives for the CC are derived based on orthogonal allocation and spatial zero-forcing (ZF) [43], respectively. The alternating optimization method is proposed for solving the joint TX-RX optimization problem in Section 3.3.3 and the convergence of the min power objective value is proven in the case of MMSE RX. After the description of the alternating optimization, the SCAs are applied to non-convex CCs in Sections 3.3.4 and 3.3.5. The numerical results are given in Section 3.4, followed by a summary in Section 3.5.

3.1 Convergence constraints

In this section, the joint power allocation and receive beamforming optimization problem for the iterative RX is formulated. The general problem formulation follows from [56], where CCPA is derived for single-user MIMO systems. However, the major difference compared to [56] is that the EXIT space now has $U+1$ dimensions.

This section is outlined as follows: First of all, the general problem formulation for MU SIMO systems is provided. It is demonstrated that convergence is guaranteed as long as there exists an open tunnel between the $U+1$-dimensional EXIT surfaces until the desired MI point. After that, a *diagonal sampling* approach is introduced which makes the problem solvable without performing an exhaustive search. Furthermore, the mapping of the MI constraints to LLR variance constraints is derived in the cases of BPSK and QPSK. Finally, CCPA is applied to the case of 16-QAM and it is shown that the proposed CC guarantees convergence for 16-QAM as well. Gray mapping is assumed as a modulation mapping throughout the derivation.

3.1.1 General problem formulation

Let $\hat{I}_u^{\mathrm{E}}$ denote the average MI between the transmitted interleaved coded bits $\mathbf{c}'^u$ and the LLRs

$$\hat{\mathbf{L}}'_u = [\hat{L}'_{u,1}, \hat{L}'_{u,2} \ldots, \hat{L}'_{u,N_Q N_F}]^{\mathrm{T}} \tag{44}$$

at the output of the equalizer calculated as [56, Eq. (18)]

$$\hat{I}_u^{\mathrm{E}} = \frac{1}{N_Q N_F} \sum_{j=1}^{N_Q N_F} I(c_j'^u; \hat{L}'_{u,j}). \tag{45}$$

For notational convenience, equalizer refers to the combined block of the receive filter and soft mapper/demapper. Similarly to [56], a maximum *a posteriori* (MAP) soft mapper/demapper is used in this thesis. Moreover, let $\hat{I}_u^{\mathrm{A}}$ denote the *a priori* MI at the input of the equalizer and

$$\hat{f}_u : [0,1]^U \to [0,1] \tag{46}$$

denote a monotonically increasing EXIT function of the equalizer of the u^{th} user. Similarly, let $\mathring{I}_u^{\mathrm{E}}$ denote the average MI between the transmitted coded bits $\mathbf{c}^u$ and the LLRs $\mathring{\mathbf{L}}_u$ at the output of the decoder and

$$\mathring{f}_u : [0,1] \to [0,1] \tag{47}$$

denote a monotonically increasing EXIT function of the decoder of the u^{th} user. A sufficient condition for the convergence of the turbo equalizer can be written as

$$\exists \{\mathring{I}_i^{\mathrm{E}} \in [0,1]\}_{\substack{i=1 \\ i \neq u}}^{U} : \hat{f}_u(\mathring{I}_1^{\mathrm{E}}, \ldots, \mathring{I}_u^{\mathrm{E}}, \ldots, \mathring{I}_U^{\mathrm{E}}) \geq \mathring{f}_u^{-1}(\mathring{I}_u^{\mathrm{E}}) + \varepsilon_u(\mathring{I}_u^{E}), \forall u = 1, 2 \ldots, U, \tag{48}$$

i.e., for all u, there exists a set of outputs from the decoders of all the users except u such that the EXIT function of the equalizer of user u is above the inverse of the EXIT function of the decoder of user u plus $\varepsilon_u(\mathring{I}_u^{E}) : [0,1] \to]0,1]$ which is a function controlling the minimum gap between the $U+1$-dimensional EXIT function of the equalizer of user u and the inverse of the decoder's EXIT function of user u. In other words, convergence is guaranteed as long as for all the users there exists an open tunnel between the two EXIT surfaces until the convergence point. Constraint (48) is much more challenging to deal with than [56], where the EXIT chart is two-dimensional. This is illustrated in the case of two users in Fig. 5, where the impact of the *a priori* information input from the other user's decoder can be clearly obtained.

In the following, it is demonstrated that (48) guarantees convergence: Let $U = 2$ and assume that there exists an open tunnel between the EXIT surfaces until the convergence point as presented in Fig. 5. Let

$$\mathring{I}_u^{\mathrm{E,target}}, \;\; 0 \leq \mathring{I}_u^{\mathrm{E,target}} \leq 1, \tag{49}$$

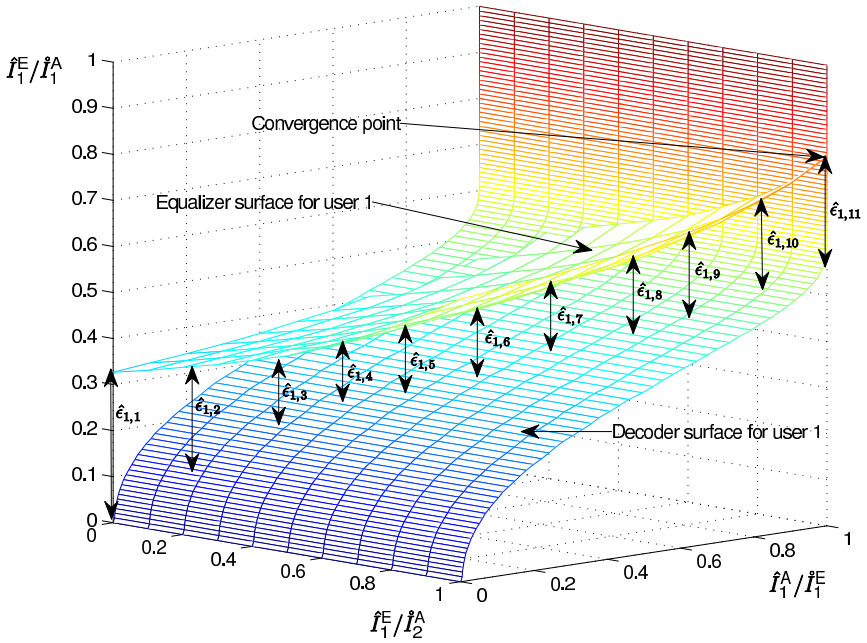

Fig. 5. An example of three-dimensional formulation of the problem for user 1. $U = 2$, $N_F = 8$, $N_R = 1$, $K = 11$, $\mathring{I}_u^{\mathrm{E,target}} = 0.8$, $\mathring{I}_u^{\mathrm{E,target}} = 0.9999$, $\varepsilon_u = 0.1$, $u = 1,2$, $R_c = 1/3$, $N_L = 5$.

be the target MI point of user u after iterations. Furthermore, let $i_u \in \mathbb{N}$ be the index of iteration and $\mathring{I}^{\mathrm{E}}_{u,i_u}$ denote the MI after iteration i_u such that

$$\mathring{I}^{\mathrm{E}}_{u,i_u+1} \geq \mathring{I}^{\mathrm{E}}_{u,i_u}. \tag{50}$$

Focusing on user 1, condition (48) is written

$$\hat{f}_1(\mathring{I}^{\mathrm{E}}_1, \mathring{I}^{\mathrm{E}}_2) \geq \mathring{f}_1^{-1}(\mathring{I}^{\mathrm{E}}_1) + \varepsilon_1(\mathring{I}^{E}_1), \tag{51}$$

such that for each

$$\mathring{I}^{\mathrm{E}}_{1,i_1}, \;\; 0 \leq \mathring{I}^{\mathrm{E}}_{1,i_1} \leq \mathring{I}^{\mathrm{E,target}}_1, \tag{52}$$

there exists at least one

$$\mathring{I}^{\mathrm{E}}_{2,i_2}, \;\; 0 \leq \mathring{I}^{\mathrm{E}}_{2,i_2} \leq \mathring{I}^{\mathrm{E,target}}_2 \tag{53}$$

that satisfies the condition. Let the output value after the first activation of the decoder 1 be $\mathring{I}^{\mathrm{E}}_{1,1}$, such that (51) holds for some $\mathring{I}^{\mathrm{E}}_{2,\tilde{i}_2}$. Due to the monotonicity of the EXIT

function, condition (51) holds for all indices $i_2 \geq \tilde{i}_2$. Activating the decoder of user 1 again, the output of the equalizer is then given by

$$\hat{f}_1(\mathring{I}^{\mathrm{E}}_{1,2}, \mathring{I}^{\mathrm{E}}_{2,\tilde{i}_2}). \tag{54}$$

If condition (51) does not hold at the point

$$(\mathring{I}^{\mathrm{E}}_1, \mathring{I}^{\mathrm{E}}_2, \mathring{I}^{\mathrm{E}}_1) = (\mathring{I}^{\mathrm{E}}_{1,2}, \mathring{I}^{\mathrm{E}}_{2,\tilde{i}_2}, \hat{f}_1(\mathring{I}^{\mathrm{E}}_{1,2}, \mathring{I}^{\mathrm{E}}_{2,\tilde{i}_2})) \tag{55}$$

in the three-dimensional EXIT chart, i.e.,

$$\hat{f}_1(\mathring{I}^{\mathrm{E}}_{1,2}, \mathring{I}^{\mathrm{E}}_{2,\tilde{i}_2})) < \mathring{f}_1^{-1}(\mathring{I}^{\mathrm{E}}_{1,2}) + \varepsilon_1(\mathring{I}^{E}_1), \tag{56}$$

there exists at least one $\mathring{I}^{\mathrm{E}}_{2,i_2}$ that satisfies (51). Hence, $\tilde{i}_2$ can be increased, i.e. decoder 2 can be activated until the condition holds[4]. This process can be repeated until the convergence point is reached.

Let us sample the EXIT functions as

$$\mathring{I}^{u}_{k_u} \in [0, \mathring{I}^{\mathrm{E,target}}_{u}], \;\; k_u = 1, 2, \ldots, K, \tag{57}$$

where $\mathring{I}^{u}_{k_u}$ is the average MI at the output of the decoder of the u^{th} user at the k_u^{th} MI index. To make the problem tractable, the continuous convergence condition (48) is discretized and replaced with

$$\exists \Big\{ \mathring{I}^{i}_{k_i} \in [0,1] : k_i \in \{1, 2, \ldots, K_i\} \Big\}_{\substack{i=1 \\ i \neq u}}^{U} : \hat{f}_u(\mathring{I}^{1}_{k_1}, \ldots, \mathring{I}^{u}_{k_u}, \ldots, \mathring{I}^{U}_{k_U}) \geq \mathring{f}_u^{-1}(\mathring{I}^{u}_{k_u}) + \varepsilon_{u,k_u},$$
$$\forall k_u = 1, 2, \ldots, K_u, \forall u = 1, 2 \ldots, U, \tag{58}$$

with $\varepsilon_{u,k_u} \in]0, 1 - \mathring{f}_u^{-1}(\mathring{I}^{u}_{k_u})]$. Note that the indices k_u, $u = 1, 2, \ldots, U$ in (58) denote the points in the EXIT chart and not the indices of iterations in real chain simulations. This definition is used in the remaining part of the thesis.

3.1.2 Diagonal sampling

In this section, the discussion is restricted to the minimum power problem only, i.e. the objective is to minimize the sum power with constraint (58).

To ease the handling of the problem, let $K_u = K$, $\forall u = 1, 2, \ldots, U$, i.e. the number of discrete points in the EXIT chart is the same for all users. Moreover,

$$\mathring{I}^{u}_{k_u+1} > \mathring{I}^{u}_{k_u}, \;\; \forall k_u = 1, 2, \ldots, K-1, \tag{59}$$

[4] If $U > 2$, all the decoders (excluding the decoder of user 1) can be activated until (51) holds.

i.e. the indexing is ordered such that the MI increases with the index.

A three-dimensional EXIT chart for user 1 is depicted in Fig. 5 for the case of $U = 2$. $\hat{I}_1^{\mathrm{A}}/\mathring{I}_u^{\mathrm{E}}$, $u = 1,2$ denotes the *a priori* information for the equalizer of user 1 provided by the decoder of user u. The double arrows with $\hat{\varepsilon}_{1,k_1}$, $k_1 = 1,2,\ldots,11$, denote the actual gap that is obtained from simulations with constraint (58) and are placed at the diagonal sample points where condition (58) is checked. Since ε_{1,k_1} denotes the minimum gap between the EXIT surfaces, it holds that $\hat{\varepsilon}_{1,k_1} \geq \varepsilon_{1,k_1}$. In this example, we have selected $K = 11$, even though in many cases a smaller K is enough to guarantee convergence. The number of samples and their positions depend on the shape of the decoder EXIT function and must be chosen appropriately case by case [56]. For instance, if the FEC is strong, the inverse of the decoder's EXIT curve is low until it is very close to the convergence point and, therefore, the leftmost part of the EXIT chart is not as crucial as the rightmost part. In other words, the number of sampling points should be larger in that part of the EXIT chart where the gradient of the EXIT function is large. However, the optimal sampling is left for future study.

The number of constraints in (58) is KU. However, to find the minimum power solution with constraint (58), the optimal set of sample points has to be found from

$$\{\mathring{I}_i^{\mathrm{E}} \in [0,1]\}_{\substack{i=1 \\ i\neq u}}^{U} \tag{60}$$

for each $u = 1,2,\ldots,U$. To find the best set of sample points, i.e. the path from origin to the convergence point which leads to a minimum power consumption, one should be able to check all the possible paths in $U+1$-dimensional EXIT space from the origin to the convergence point and choose the one which gives the best result. This leads to a combinatorial optimization problem which is difficult to solve.

If the EXIT surfaces of the decoder and the equalizer do not intersect at any sampled point, the only active constraints are the ones where there is no *a priori* information available from other users. This can be justified by assuming that the EXIT function is monotonically increasing with its arguments, i.e.

$$\hat{f}_u(\mathring{I}_{k_1}^1,\ldots,\mathring{I}_{k_u}^u,\ldots,\mathring{I}_{k_U}^U) \leq \hat{f}_u(\mathring{I}_{\tilde{k}_1}^1,\ldots,\mathring{I}_{\tilde{k}_u}^u,\ldots,\mathring{I}_{\tilde{k}_U}^U) \text{ if } \mathring{I}_{k_u}^u \leq \mathring{I}_{\tilde{k}_u}^u, \ \forall u = 1,2,\ldots,U. \tag{61}$$

In such a case, constraint (58) can be written as

$$\hat{f}_u(0,0,\ldots,0,\mathring{I}_{k_u}^u,0,\ldots,0) \geq \mathring{f}_u^{-1}(\mathring{I}_{k_u}^u) + \varepsilon_{u,k_u}, \forall u = 1,2\ldots,U, \forall k_u = 1,2,\ldots,K. \tag{62}$$

This is the tightest possible constraint and it clearly cannot provide the best solution because with high probability there is another sampling which guarantees convergence

with lower power consumption. However, if the user does not know the modulation coding scheme (MCS), i.e. FEC codes and mapping rules for modulation of other users at the TX, one may consider using constraint (62) to guarantee the reliable communication.

A pragmatic approach is to check only the points in the $U+1$-dimensional EXIT space where all the decoder's outputs are equal, i.e. the K points on the line from the origin to the convergence point is selected. In other words, Δ^l in (30) is equal to Δ_k, $\forall l = 1,2,\ldots,U$, where Δ_k is the average residual interference at the k^{th} MI index. Thus, the $U+1$-dimensional EXIT function of the equalizer is replaced by a two-dimensional function

$$\hat{f}_u(\mathring{I}_k^1,\ldots,\mathring{I}_k^u,\ldots,\mathring{I}_k^U) := \hat{f}_u^{\text{2D}}(\mathring{I}_k^{\text{E}}) \tag{63}$$

and the constraint is written as

$$\hat{f}_u^{\text{2D}}(\mathring{I}_k) \geq \mathring{f}_u^{-1}(\mathring{I}_k) + \varepsilon_{u,k}, \forall k = 1,2,\ldots,K, \forall u = 1,2\ldots,U. \tag{64}$$

This approximation technique is referred to as *diagonal sampling*, which is assumed throughout the remaining part of the thesis.

An example of the impact of diagonal sampling on the resulting equalizer's EXIT surface is depicted in Fig. 6 for a system with two users and one receive antenna. It can be obtained from Fig. 6(a) that there is a path to the convergence point if the *a priori* information coming from the decoder of user 2 is high. Fig. 6(b) demonstrates that the equalizer's EXIT surface is higher compared to Fig. 6(a) because of the diagonal constraints.

An example of the impact of diagonal sampling on the resulting equalizer's EXIT surface is depicted in Fig. 7 for a system with two users and two receive antennas. It can be seen that the EXIT surfaces in exhaustive search and diagonal sampling are identical. This is due to the fact that a user separation can be performed in a spatial domain and the impact of *a priori* information coming from user 2 is no longer as crucial.

3.1.3 BPSK / QPSK

Similarly to [56], the MI constraint of (58) can be transformed to a variance constraint using the approximation of the inverse of the 'J-function' [60]

$$\sigma_Z^2 = J^{-1}(I_Z) \approx \left(-\frac{1}{H_1}\log_2(1-I_Z^{\frac{1}{H_3}}) \right)^{\frac{1}{H_2}}, \tag{65}$$

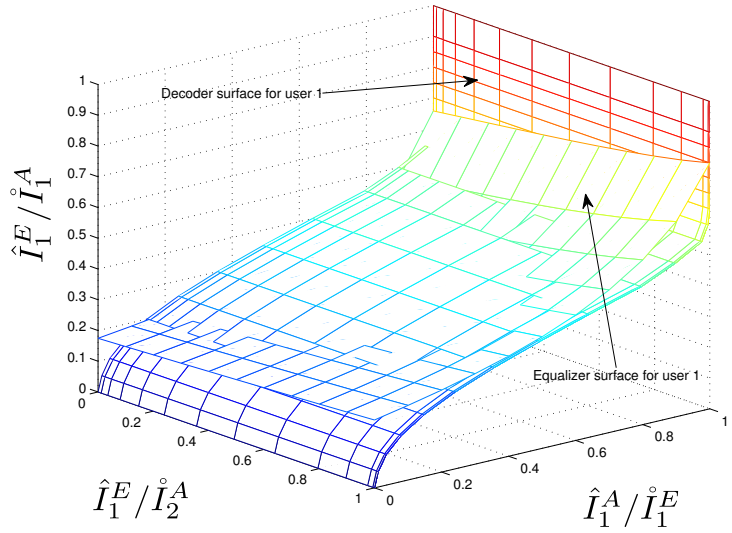

(a)

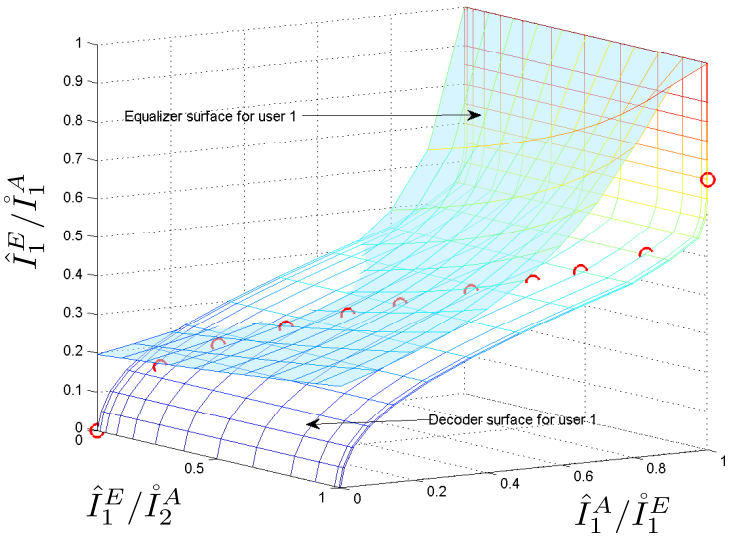

(b)

Fig. 6. An example of a three-dimensional formulation of the problem for user 1 using (a) exhaustive search, (b) diagonal sampling. $U=2$, $N_F=8$, $N_R=1$, $K=11$, $\hat{I}_u^{\mathrm{E,target}}=0.8$, $\tilde{I}_u^{\mathrm{E,target}}=0.9999$, $\varepsilon_u=0.1$, $u=1,2$, $R_c=1/3$, $N_L=5$**. Red circles indicate the points where the convergence constraint is activated.**

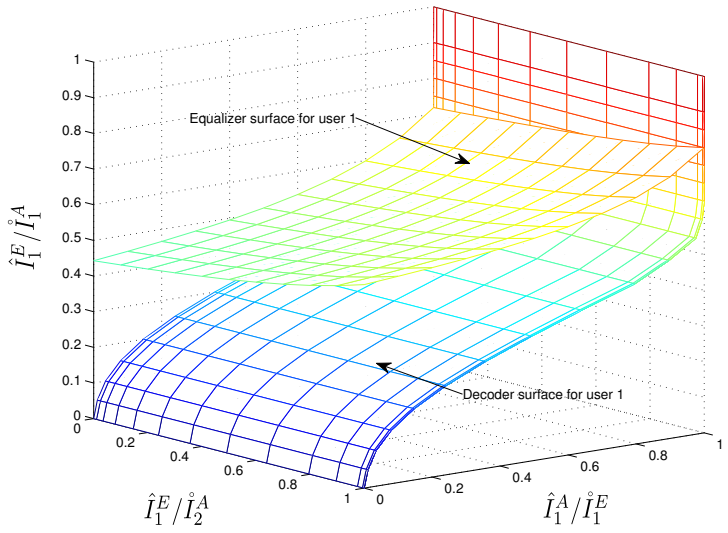

(a)

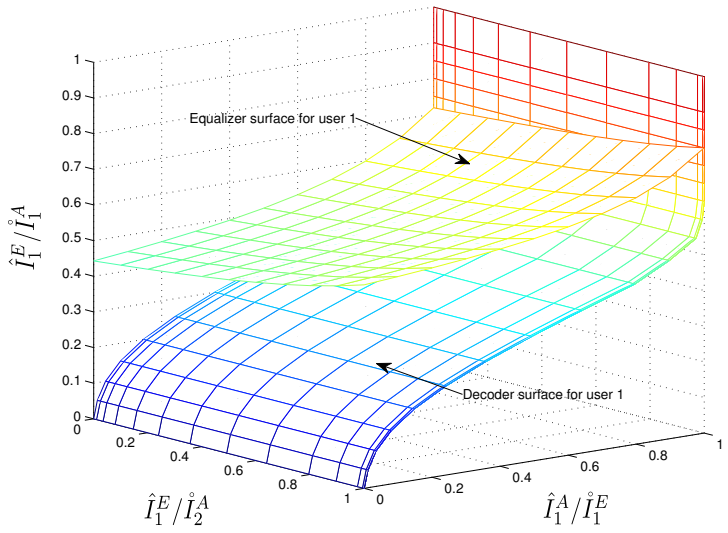

(b)

Fig. 7. An example of a three-dimensional formulation of the problem for user 1 using (a) exhaustive search, (b) diagonal sampling. $U = 2$**,** $N_F = 8$**,** $N_R = 2$**,** $K = 11$**,** $\hat{I}_u^{\mathbf{E,target}} = 0.8$**,** $\mathring{I}_u^{\mathbf{E,target}} = 0.9999$**,** $\varepsilon_u = 0.1$**,** $u = 1, 2$**,** $R_c = 1/3$**,** $N_L = 5$**.**

where σ_Z^2 is the LLR variance, $I_Z \in [0,1]$ is the MI, and the parameters H_1, H_2 and H_3 can be found by the least squares (LS) curve fitting with the constellation constrained capacity (CCC) equation [102]. Now, the MI constraint of (64) can be written as

$$\hat{\sigma}_{u,k}^2 \geq \mathring{\sigma}_{u,k}^2, \forall k = 1,2,\ldots,K, \forall u = 1,2\ldots,U, \tag{66}$$

where

$$\hat{\sigma}_{u,k}^2 = \mathrm{J}^{-1}(\hat{f}_u^{\mathrm{2D}}(\mathring{I}_k^{\mathrm{E}})) \tag{67}$$

is the variance of the conditional LLR distribution at the output of the equalizer of user u depending on the MI at the output of all the decoders and

$$\mathring{\sigma}_{u,k}^2 = \mathrm{J}^{-1}(\mathring{f}_u^{-1}(\mathring{I}_{u,k}^{\mathrm{E}}) + \varepsilon_{u,k}) \tag{68}$$

is the variance of the conditional LLR distribution at the input of the decoder of user u depending on the MI at the output of the decoder of user u.

SC-FDMA

In [56], a result presented in [103] is used to find an analytical expression of the LLR variance at the output of the equalizer in the case of QPSK. The same result can be used by noting that $\Delta^l = \Delta_k$ in (30) when diagonal sampling is used. In the case of SC-FDMA, the LLR variance at the output of the equalizer is calculated as [56, Eq. (17)]

$$\hat{\sigma}_{u,k}^2 = \frac{4\zeta_u^k}{1-\zeta_u^k\Delta_k}, \tag{69}$$

where

$$\zeta_u^k = \frac{1}{N_F}\sum_{m=1}^{N_F} \frac{P_{u,m}\boldsymbol{\omega}_{u,m}^{k\mathrm{H}}\boldsymbol{\gamma}_{u,m}\boldsymbol{\gamma}_{u,m}^{\mathrm{H}}\boldsymbol{\omega}_{u,m}^k}{\boldsymbol{\omega}_{u,m}^{k\mathrm{H}}\boldsymbol{\Sigma}_{\tilde{\mathbf{r}},m}^k\boldsymbol{\omega}_{u,m}^k}, \tag{70}$$

and

$$\boldsymbol{\Sigma}_{\tilde{\mathbf{r}},m}^k = \sum_{l=1}^{U} P_{l,m}\boldsymbol{\gamma}_{l,m}\boldsymbol{\gamma}_{l,m}^{\mathrm{H}}\Delta_k + \sigma^2\mathbf{I}_{N_R}. \tag{71}$$

$\boldsymbol{\omega}_{u,m}^k$ denotes the receive beamforming vector for the u^{th} user's m^{th} frequency bin at the k^{th} MI index. The EXIT curve of the equalizer of the u^{th} user can now be obtained using (69) and (65). Substituting (69) in (66) the CC is written as

$$\zeta_u^k \geq \xi_{u,k}, \forall u = 1,2\ldots,U, \forall k = 1,2,\ldots,K, \tag{72}$$

where

$$\xi_{u,k} = \frac{\mathring{\sigma}^2_{u,k}}{4 + \mathring{\sigma}^2_{u,k}\Delta_k}, \tag{73}$$

is a constant that depends on the FEC code.

OFDMA

Similarly to the case of SC-FDMA [103], the output of the MMSE filter can be approximated as the output of an equivalent AWGN channel having b^u_m as its input

$$\hat{b}^u_m = \phi_{u,m} b^u_m + n^u_m, \tag{74}$$

where $n^u_m \sim \mathscr{N}^{\mathbb{C}}(0, \sigma^2_n)$. The channel gain can be calculated as

$$\phi_{u,m} = \mathbb{E}\{\hat{b}^u_m b^{u*}_m\} = \frac{\tilde{\zeta}_{u,m}}{1 + \tilde{\zeta}_{u,m}}, \tag{75}$$

and the variance is computed as [101]

$$\sigma^2_n = \phi_{u,m} - \phi^2_{u,m}. \tag{76}$$

The SNR of the equivalent channel (74) is given by [101]

$$\frac{\phi_{u,m}}{1 - \phi_{u,m}} = \tilde{\zeta}_{u,m}. \tag{77}$$

Utilizing [56, Eq. (17)] the LLR variance for the u^{th} user at the m^{th} subcarrier at the k^{th} MI index can be calculated as

$$(\hat{\sigma}^k_{u,m})^2 = 4\tilde{\zeta}^k_{u,m}, \tag{78}$$

where

$$\tilde{\zeta}^k_{u,m} = \frac{P_{u,m} |\boldsymbol{\gamma}^{\text{H}}_{u,m} \tilde{\boldsymbol{\omega}}^k_{u,m}|^2}{\sum_{\substack{l=1 \\ l \neq u}}^{U} |\boldsymbol{\gamma}^{\text{H}}_{l,m} \tilde{\boldsymbol{\omega}}^k_{u,m}|^2 P_{l,m}\Delta_k + \sigma^2_v ||\tilde{\boldsymbol{\omega}}^k_{u,m}||^2}, \tag{79}$$

and $\tilde{\boldsymbol{\omega}}^k_{u,m}$ denotes the receive beamforming vector for the u^{th} user's m^{th} frequency bin at the k^{th} MI index. Let $\hat{\sigma}^k_{u,m}$ be the standard deviation of the LLRs of the u^{th} user's m^{th} subcarrier at the k^{th} MI index. The average MI over the subcarriers at the output of the equalizer of the u^{th} user is obtained as

$$\hat{I}^{\text{E}}_{u,k} = \frac{1}{N_F} \sum_{m=1}^{N_F} J\Big(\hat{\sigma}^k_{u,m}\Big), \tag{80}$$

where [60]

$$J\left(\hat{\sigma}_{u,m}^{k}\right) = \left(1 - 2^{-H_1(\hat{\sigma}_{u,m}^{k})^{2H_2}}\right)^{H_3}. \tag{81}$$

In the remaining part of the thesis, the LLR variance is assumed to be the same for all the subcarriers, i.e., $(\hat{\sigma}_{u,m}^{k})^2 = \hat{\sigma}_{u,k}^2$. Hence, the CC is given by

$$\tilde{\zeta}_{u,m}^{k} \geq \tilde{\xi}_{u,k}, \forall u = 1,2\ldots,U, \forall m = 1,2,\ldots,N_F, \forall k = 1,2,\ldots,K, \tag{82}$$

where

$$\tilde{\xi}_{u,k} = \frac{\mathring{\sigma}_{u,k}^2}{4}. \tag{83}$$

3.1.4 A heuristic approach to 16-QAM

Similarly to the QPSK case, the MI at the output of the demapper can be transformed to the variance of the conditional LLR distribution by using (65). However, the parameters H_1, H_2 and H_3 are found by fitting function (65) with the corresponding 16-QAM results [101]. Let J_2 and J_4 denote the J-functions for QPSK and 16-QAM, respectively. With these notations, the MI constraint of (64) for 16-QAM can be written as

$$\mathrm{J}_4^{-1}(\hat{f}_u^{\mathrm{2D}}(\mathring{I}_k^{\mathrm{E}})) \geq \mathrm{J}_4^{-1}(\mathring{f}_u^{-1}(\mathring{I}_{u,k}^{\mathrm{E}}) + \varepsilon_{u,k}), \forall k = 1,2,\ldots,K, \forall u = 1,2\ldots,U. \tag{84}$$

The difference in system models with different modulation schemes arises in the soft demapper. To achieve the final form of the CCs in (72) and (82), expressions (69) and (78) were used, respectively, where Gray-mapped QPSK is assumed. With 16-QAM, the mapping between the SINR and the variance of the LLR distributions used for the derivation of the CCs does not hold anymore. However, by substituting the parameter values from [101, Table I] in (65), it can be easily verified that

$$\mathrm{J}_4^{-1}(I_Z) \geq \mathrm{J}_2^{-1}(I_Z), \ \ \forall I_Z \in [0,1] \tag{85}$$

with equality when $I_Z = 0$ or $I_Z = 1$. Inequality (85) can also be verified from Fig. 8, where the inverse J-functions are plotted for different modulation schemes. It is obtained that when modulation order increases, a larger LLR variance is needed to achieve the same SINR, i.e.

$$\mathrm{J}_4^{-1}(\hat{f}_u^{\mathrm{2D}}(\mathring{I}_k^{\mathrm{E}})) \geq \mathrm{J}_2^{-1}(\hat{f}_u^{\mathrm{2D}}(\mathring{I}_k^{\mathrm{E}})) = \hat{\sigma}_{u,k}^2. \tag{86}$$

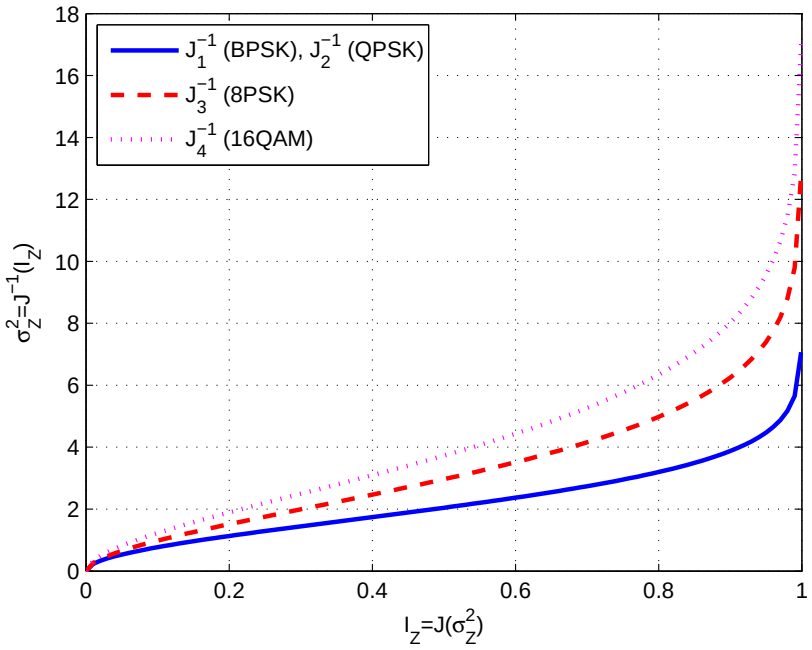

Fig. 8. Inverse J-functions for different modulation schemes. Parameters H_1, H_2 and H_3 are provided in [101].

It can be concluded that for 16-QAM, CC (72) is conservative, i.e. the resulting EXIT curve of the equalizer is never above the true $\hat{I}^{\mathrm{E}}_{u,k}$, $\forall u,k$. Hence, CC (72) guarantees convergence even with 16-QAM. It should be noted that the difference in CCs between the QPSK and 16-QAM arises in (73) where $\mathring{\sigma}^2_{u,k}$ is obtained using either J_2^{-1} or J_4^{-1} depending on the modulation.

3.2 Successive approximation methods

If the transmit power and the RX beamformers are not decoupled in the joint TX-RX optimization problem, the alternating optimization method can be used to find a local optimum. The alternation is between the transmit power and the receive beamformers such that the problem is first solved for fixed RX beamformers and then for fixed TX power allocation using the receive beamformers from the previous iteration and so forth. In many cases, such as in the examples presented in this thesis, alternating optimization is guaranteed to converge to a local optimum [63]. The convergence will be shown in

Section 3.3. In this section, the general power allocation problem for fixed RX filter coefficients is considered.

In this section, the focus is on a power allocation problem that has the form

$$\begin{aligned} \underset{\mathbf{P}}{\text{minimize}} \quad & z_0(\mathbf{P}) \\ \text{subject to} \quad & z_i(\mathbf{P}) \leq 0, i = 1,2,\ldots,N, \end{aligned} \tag{87}$$

where the constraints $z_i(\mathbf{P})$, $i = 1,2,\ldots,N$ are assumed to be in the form of a generalized posynomial:

$$z_i(\mathbf{P}) = \sum_{k=1}^{\hat{K}} y_k^i P_1^{a_{1k}^i} P_2^{a_{2k}^i} \cdots P_{N_F}^{a_{N_F k}^i}, \;\; y_k^i, a_{nk}^i \in \mathbb{R}. \tag{88}$$

which is, in general, a non-convex function. However if $y_k^i \geq 0$, $\forall k$, function (88) is in the form of a posynomial and the constraint $z_i(\mathbf{P}) \leq 0$ can be transformed to an equivalent convex constraint [88]. In order to find an efficient way to solve problem (87), it should be reformulated or approximated as a convex problem. Because the problems that are to be solved in this thesis are non-convex problems, (87) is reformulated and the solution is found iteratively by solving a series of convex problems. In the following, two different approaches for solving (87) are presented: SCACOV and SCAGP. The motivation for introducing two SCAs is to give alternative methods for implementation. The decision of which one to choose depends on the optimization framework and it should be considered case by case. Without loss of generality, the user index can be omitted through the derivation of SCACOV and SCAGP, i.e. P_l, $l = 1,2,\ldots,N_F$ is considered instead of $P_{u,l}$, $u = 1,2,\ldots,U$, $l = 1,2,\ldots,N_F$.

3.2.1 Successive convex approximation via change of variables

The generalized posynomial (88) can be split as

$$z_i(\mathbf{P}) = \sum_{k=1}^{\hat{K}} y_k^{i+} P_1^{a_{1k}^i} P_2^{a_{2k}^i} \cdots P_{N_F}^{a_{N_F k}^i} + \sum_{k=1}^{\hat{K}} y_k^{i-} P_1^{a_{1k}^i} P_2^{a_{2k}^i} \cdots P_{N_F}^{a_{N_F k}^i}, \tag{89}$$

where $y_k^{i+} = \max\{0, y_k^i\}$ and $y_k^{i-} = \min\{0, y_k^i\}$. Using the approach in [88, Chapter 4.5], new variables are defined as $P_k = e^{\alpha_k}$ and the inequality constraint in (87) is rewritten as

$$\ln\Big(\sum_{k=1}^{\hat{K}} e^{\sum_{n=1}^{N_F} a_{nk}^i \alpha_n + \ln y_k^{i+}}\Big) - \ln\Big(\sum_{k=1}^{\hat{K}} e^{\sum_{n=1}^{N_F} a_{nk}^i \alpha_n + \ln(-y_k^{i-})}\Big) \leq 0. \tag{90}$$

The left-hand side (LHS) of (90) is now a difference of convex functions[5]. Similarly to [104], the concave part of (90) can be approximated with its best convex upper bound, i.e. local linear approximation. Let the concave part of (90) be denoted as $T(\boldsymbol{\alpha})$, $\boldsymbol{\alpha} = [\alpha_1, \alpha_2, \ldots, \alpha_{N_F}]^{\mathrm{T}}$. The linear approximation of $T(\boldsymbol{\alpha})$ at a point $\hat{\boldsymbol{\alpha}}$ is given by

$$\hat{T}(\boldsymbol{\alpha}, \hat{\boldsymbol{\alpha}}) = T(\hat{\boldsymbol{\alpha}}) + \sum_{k=1}^{N_F} \frac{\partial T}{\partial \alpha_k}(\hat{\boldsymbol{\alpha}})(\alpha_k - \hat{\alpha}_k). \tag{91}$$

Hence, the SCA for the power allocation problem with constraint (90) can be written as

$$\begin{aligned} \underset{\boldsymbol{\alpha}}{\text{minimize}} \quad & z_0(\boldsymbol{\alpha}) \\ \text{subject to} \quad & \ln\left(\sum_{k=1}^{K} e^{\sum_{n=1}^{N_F} a_{nk}^i \alpha_n + \ln y_k^{i+}}\right) \leq \hat{T}(\boldsymbol{\alpha}, \hat{\boldsymbol{\alpha}}). \end{aligned} \tag{92}$$

The SCA algorithm starts with a feasible initialization $\hat{\alpha}_k = \hat{\alpha}_k^{(0)}, \forall k$. After this, (92) is solved to obtain a solution $\alpha_k^{(*)}$ which is used as a new point for the linear approximation. The procedure is repeated until convergence. The SCA algorithm is summarized in **Algorithm** 1. By projecting the optimal solution from the approximated problem (92) to the original constraint (90), the constraint becomes loose and thus, the objective can always be reduced. Hence, this algorithm guarantees a monotonic convergence of the objective value to a local optimum.

Algorithm 1 Successive convex approximation via change of variables.

1: Set $\hat{\alpha}_k = \hat{\alpha}_k^{(0)}, \forall k$.
2: **repeat**
3: Solve Eq. (92).
4: Update $\hat{\alpha}_k = \alpha_k^{(*)}, \forall k$.
5: **until** Convergence.

3.2.2 Successive convex approximation via geometric programming

Another algorithm for solving (87) can be derived by using the approach introduced in [87] where the SCA is implemented via a series of GPs. The inequality of weighted arithmetic mean and weighted geometric mean states that for any set of $\Phi_m, \alpha_m > 0$,

[5]Note that if $a_{nk}^i \geq 0$, $\forall n, k$, there is no need to take the logarithm.

$m = 1,2,\ldots,N_F$,

$$\frac{\sum_{m=1}^{N_F} \Phi_m \alpha_m}{\Phi} \geq \sqrt[\Phi]{\prod_{m=1}^{N_F} \alpha_m^{\Phi_m}}, \tag{93}$$

where $\Phi = \sum_{m=1}^{N_F} \Phi_m$. Choosing $\Phi_m = \frac{\hat{t}_m}{\sum_{n=1}^{N_F} \hat{t}_n}$, $\hat{t}_m > 0$, $m = 1,2,\ldots,N_F$, and denoting $\alpha_m = \frac{t_m}{\Phi_m}$, yields

$$\sum_{m=1}^{N_F} t_m \geq \prod_{m=1}^{N_F} (\frac{t_m}{\Phi_m})^{\Phi_m}, \tag{94}$$

for all $\Phi_m, t_m > 0$, $m = 1,2,\ldots,N_F$.

Using definition (89), the inequality constraint in (87) can be written as

$$\sum_{k=1}^{\hat{K}} y_k^{i+} P_1^{a_{1k}^i} P_2^{a_{2k}^i} \cdots P_{N_F}^{a_{N_F k}^i} \leq \mathscr{A}(\mathbf{P}), \tag{95}$$

where

$$\mathscr{A}(\mathbf{P}) = \sum_{k=1}^{\hat{K}} (-y_k^{i-}) P_1^{a_{1k}^i} P_2^{a_{2k}^i} \cdots P_{N_F}^{a_{N_F k}^i}. \tag{96}$$

$\mathscr{A}(\mathbf{P})$ can be approximated by its monomial underestimate using inequality (94), yielding

$$\mathscr{A}(\mathbf{P}) \geq \prod_{k=1}^{\hat{K}} \left(\frac{(-y_k^{i-}) P_1^{a_{1k}^i} P_2^{a_{2k}^i} \cdots P_{N_F}^{a_{N_F k}^i}}{\Phi_k^i} \right)^{\Phi_k^i}, \tag{97}$$

where

$$\Phi_k^i = \frac{(-y_k^{i-}) \hat{P}_1^{a_{1k}^i} \hat{P}_2^{a_{2k}^i} \cdots \hat{P}_{N_F}^{a_{N_F k}^i}}{\sum_{k'=1}^{K} (-y_{k'}^{i-}) \hat{P}_1^{a_{1k'}^i} \hat{P}_2^{a_{2k'}^i} \cdots \hat{P}_{N_F}^{a_{N_F k'}^i}}, \tag{98}$$

$\hat{P}_n > 0$, and $P_n > 0$, $n = 1,2,\ldots,N_F$. Hence, constraint (95) can be approximated as

$$\sum_{k=1}^{\hat{K}} y_k^{i+} P_1^{a_{1k}^i} P_2^{a_{2k}^i} \cdots P_{N_F}^{a_{N_F k}^i} \leq \prod_{k=1}^{\hat{K}} \left(\frac{(-y_k^{i-}) P_1^{a_{1k}^i} P_2^{a_{2k}^i} \cdots P_{N_F}^{a_{N_F k}^i}}{\Phi_k^i} \right)^{\Phi_k^i}. \tag{99}$$

Therefore, constraint (99) is a valid GP constraint. The reader should know that GP is not convex as such, but it can be reformulated as a convex problem [88]. Convex transformation is performed by going through the COV procedure presented in the previous section. Changing the variables as $P_k = e^{\alpha_k}$ and taking the logarithms, (99) can be written as

$$\ln \Big(\sum_{k=1}^{\hat{K}} e^{\sum_{n=1}^{N_F} a_{nk}^i \alpha_n + \ln y_k^{i+}} \Big) \leq \sum_{k=1}^{\hat{K}} \big(\sum_{n=1}^{N_F} a_{nk}^i \Phi_k^i \alpha_n + b_k^i \big), \tag{100}$$

where

$$b_k^i = \Phi_k^i \ln\left(\frac{-y_k^{i-}}{\Phi_k^i}\right). \tag{101}$$

The LHS of (100) is a logarithm of a summation of exponentials and the right-hand side (RHS) is a linear function. Hence, (100) is a convex constraint.

The SCA via GP for the power allocation problem with constraint (95) can be written as

$$\begin{aligned} \underset{\mathbf{P}}{\text{minimize}} \quad & z_0(\mathbf{P}) \\ \text{subject to} \quad & \textstyle\sum_{k=1}^{K} y_k^{i+} P_1^{a_{1k}^i} P_2^{a_{2k}^i} \cdots P_{N_F}^{a_{N_F k}^i} \leq \prod_{k=1}^{\hat{K}} \left(\frac{(-y_k^{i-}) P_1^{a_{1k}^i} P_2^{a_{2k}^i} \cdots P_{N_F}^{a_{N_F k}^i}}{\Phi_k^i} \right)^{\Phi_k^i}. \end{aligned} \tag{102}$$

The SCA algorithm is summarized in **Algorithm** 2. Because the monomial approximation is never above the approximated summation (97), the same arguments describing the convergence presented in Sec. 3.2.1 also apply in this case. Hence, it is guaranteed that the objective value in SCA with approximation (102) monotonically converge to a local optimum. It can be seen that both approximations, SCACOV and SCAGP, yield an equivalent constraint where the LHS is a logarithm of a summation of exponentials and the RHS is a linear function. The major difference in these approximations is the form of constraint for which the approximation is performed. In SCACOV, the logarithm is taken first and the logarithmic term is approximated as a linear function. In SCAGP, the constraint is approximated as a monomial before taking the logarithm. This has an impact on the implementation of the solver and it may have an impact on the speed of convergence of the iterative algorithm.

Algorithm 2 Successive convex approximation via geometric programming.

1: Set $\hat{P}_k = \hat{P}_k^{(0)}, \forall k$.
2: **repeat**
3: Calculate Φ_k^i, $\forall k, i$, using (98)
4: Solve Eq. (102).
5: Update $\hat{P}_k = P_k^{(*)}, \forall k$.
6: **until** Convergence.

3.3 Convergence constrained power allocation

In this section, algorithms for solving the TX-RX optimization problem are presented. Sections 3.3.1 and 3.3.2 present suboptimal approaches where the problem reduces to a single-user power loading. In Section 3.3.3, the joint TX-RX optimization problem is split into separate TX and RX optimization problems, which is referred to as *alternating optimization*. The TX optimization for fixed RX is a convex problem for OFDMA but non-convex for SC-FDMA. The non-convex TX optimization problem for a fixed RX is considered in Sections 3.3.4 and 3.3.5.

3.3.1 Orthogonal allocation

In this section, the best possible orthogonal allocation obtained by performing exhaustive search (OES) over all possible subcarrier combinations is considered. Orthogonal in this context indicates that only one user is active in each subcarrier at a time.

SC-FDMA

The CC for OES can be written as

$$\frac{1}{N_F}\sum_{m\in\mathscr{N}_F^u}\frac{P_{u,m}||\boldsymbol{\gamma}_{u,m}||^2}{P_{u,m}||\boldsymbol{\gamma}_{u,m}||^2\Delta_k+\sigma_v^2}\geq\xi_{u,k}, \tag{103}$$

where $\mathscr{N}_F^u$ is the set of frequency bins allocated to user u and $\mathscr{N}_F^l\cap\mathscr{N}_F^u=\varnothing$, $\forall l\neq u$, $\bigcup_{u=1}^{U}\mathscr{N}_F^u=\mathscr{N}_F$. Calculating the Hessian matrix of the LHS of (103) it can be verified that (103) is a convex constraint $\forall k,u$ [56]. Because there is no MUI in OES the optimal RX is the filter matched to the channel.

To find the best possible orthogonal allocation, one needs to check all the possible orthogonal allocations and choose the best. This exhaustive search becomes infeasible when N_F increases. Hence, to reduce the number of combinations, we derive a necessary condition for the minimum number of frequency bins N_F^u to be allocated to user u: Constraint (103) can be written in the form

$$\sum_{m\in\mathscr{N}_F^u}\frac{1}{P_{u,m}||\boldsymbol{\gamma}_{u,m}||^2\Delta_k+\sigma_v^2}\leq\frac{N_F^u-\xi_{u,k}N_F\Delta_k}{\sigma_v^2}, \tag{104}$$

where N_F^u is the cardinality of the set $\mathscr{N}_F^u$. A necessary constraint for the minimum number of frequency bins that has to be allocated to user u is obtained from the non-

negativity of the RHS of Eq. (104) as

$$N_F^u \geq \xi_{u,k} N_F \Delta_k, \quad \forall k = 1,2,\ldots,K. \tag{105}$$

OFDMA

The OES constraint for OFDMA is written as

$$\frac{P_{u,m}|\boldsymbol{\gamma}_{u,m}^{\mathrm{H}} \tilde{\boldsymbol{\omega}}_{u,m}^k|^2}{\sigma_v^2 ||\tilde{\boldsymbol{\omega}}_{u,m}^k||^2} \geq \tilde{\xi}_{u,k} \;\; u = 1,2,\ldots U, \; m \in \mathscr{N}_F^u, k = 1,2,\ldots,K, \tag{106}$$

which reduces to

$$\frac{P_{u,m}||\boldsymbol{\gamma}_{u,m}||^2}{\sigma_v^2} \geq \tilde{\xi}_{u,K} \;\; u = 1,2,\ldots U, \; m \in \mathscr{N}_F^u. \tag{107}$$

However, in orthogonal allocation the symbols b_m^u, $m \notin \mathscr{N}_F^u$, are multiplied by $P_{u,m} = 0$, and therefore, the MI target cannot be satisfied by using OES without increasing the modulation order on the allocated subcarriers. This illustrates the fundamental difference between SC-FDMA and OFDMA. SC-FDMA is more robust to orthogonality in terms of achieving the MI target because all the symbols are spread across the subcarriers by using DFT. Hence, while in OFDMA some of the transmitted symbols are completely erased, in SC-FDMA the loss is distributed through the whole symbol sequence. The loss can then be recovered with the help of a FEC decoder.

3.3.2 Spatial domain zero-forcing equalization

In this method, the aim is to completely remove MUI by spatial domain ZF equalization [43]. Consequently, the users can be decoupled and the problem reduces to multiple single-user problems. However, the noise power increases, which can be a problem in a low-SNR regime. Although this procedure is suboptimal, the problem becomes significantly less complex. After spatial ZF, the ISI still remains and, therefore, MMSE is needed to take care of that.

SC-FDMA

Spatial domain ZF is performed separately for each frequency bin. For that purpose, we use the following notations: let

$$\tilde{\boldsymbol{\Gamma}}_m = [\boldsymbol{\gamma}_{1,m}, \boldsymbol{\gamma}_{2,m}, \ldots, \boldsymbol{\gamma}_{U,m}] \in \mathbb{C}^{N_R \times U} \tag{108}$$

be the FD channel matrix composed of U channel vectors in the m^{th} frequency bin. Similarly, let

$$\tilde{\mathbf{P}}_m = \text{diag}([P_{1,m}, P_{2,m}, \ldots, P_{U,m}]^{\text{T}}) \in \mathbb{R}^{U \times U} \tag{109}$$

be the power allocation matrix for the m^{th} frequency bin. The data symbol vector in FD is denoted as

$$\boldsymbol{\psi} = [\boldsymbol{\psi}^{1\,\text{T}}, \boldsymbol{\psi}^{2\,\text{T}}, \ldots, \boldsymbol{\psi}^{U\,\text{T}}]^{\text{T}} = \mathbf{F}_U \mathbf{b} \in \mathbb{C}^{UN_F}, \tag{110}$$

where

$$\boldsymbol{\psi}^u = [\psi_1^u, \psi_2^u, \ldots, \psi_{N_F}^u]^{\text{T}} \in \mathbb{C}^{N_F}. \tag{111}$$

The received signal, focusing on the m^{th} frequency bin, is derived as

$$\tilde{\mathbf{r}}_m = \tilde{\boldsymbol{\Gamma}}_m \tilde{\mathbf{P}}_m^{\frac{1}{2}} \boldsymbol{\psi}_m + \boldsymbol{\nu}_{[(m-1)N_R+1:mN_R]}, \tag{112}$$

where

$$\boldsymbol{\psi}_m = [\psi_m^1, \psi_m^2, \ldots, \psi_m^U]^{\text{T}} \in \mathbb{C}^U \tag{113}$$

and

$$\boldsymbol{\nu} = [\nu_1, \nu_2, \ldots, \nu_{N_R N_F}]^{\text{T}} = \mathbf{F}_{N_R} \mathbf{v} \in \mathbb{C}^{N_R N_F}. \tag{114}$$

The ZF matrix $\mathbf{W}_m^{\text{H}} \in \mathbb{C}^{U \times N_R}$ is the Moore–Penrose pseudo-inverse [105] of the channel matrix $\tilde{\boldsymbol{\Gamma}}_m$ calculated by

$$\mathbf{W}_m^{\text{H}} = \tilde{\boldsymbol{\Gamma}}_m^{\dagger} = (\tilde{\boldsymbol{\Gamma}}_m^{\text{H}} \tilde{\boldsymbol{\Gamma}}_m)^{-1} \tilde{\boldsymbol{\Gamma}}_m^{\text{H}}. \tag{115}$$

The U symbols can be extracted from the m^{th} frequency bin by

$$\begin{aligned} \hat{\boldsymbol{\psi}}_m &= \mathbf{W}_m^{\text{H}} \tilde{\mathbf{r}}_m \\ &= \tilde{\mathbf{P}}_m^{\frac{1}{2}} \boldsymbol{\psi}_m + \mathbf{W}_m^{\text{H}} \boldsymbol{\nu}_{(m-1)N_R+1:mN_R}, \end{aligned} \tag{116}$$

where

$$\hat{\boldsymbol{\psi}}_m = [\hat{\psi}_m^1, \hat{\psi}_m^2, \ldots, \hat{\psi}_m^U]^{\text{T}} \in \mathbb{C}^U. \tag{117}$$

Finally, the time domain symbol estimate vector for the u^{th} user can be expressed as

$$\grave{\mathbf{b}}^u = \mathbf{F}^{-1} \hat{\boldsymbol{\psi}}^u, \tag{118}$$

where

$$\hat{\boldsymbol{\psi}}^u = [\hat{\psi}_1^u, \hat{\psi}_2^u, \ldots, \hat{\psi}_{N_F}^u]^{\text{T}} \in \mathbb{C}^{N_F}. \tag{119}$$

After ZF, the input for the MMSE is

$$\tilde{\mathbf{r}}^{u,\text{ZF}} = \mathbf{P}_u^{\frac{1}{2}} \mathbf{F} \mathbf{b}^u + \mathbf{W}^{u\text{H}} \mathbf{F}_{N_R} \mathbf{v}, \; \forall u = 1, 2, \ldots, U, \tag{120}$$

where

$$\mathbf{W}^{u\mathrm{H}} = \begin{bmatrix} \mathbf{w}_{u,1}^{\mathrm{H}} & 0 & \cdots & 0 \\ 0 & \mathbf{w}_{u,2}^{\mathrm{H}} & \ddots & 0 \\ \vdots & \ddots & \ddots & \vdots \\ 0 & 0 & \cdots & \mathbf{w}_{u,N_F}^{\mathrm{H}} \end{bmatrix}_{N_F \times N_R N_F},$$

and $\mathbf{w}_{u,m}$ is the u^{th} row of $\mathbf{W}_m^{\mathrm{H}}$. The output of the MMSE filter for u^{th} user at the k^{th} MI index can now be written as

$$\hat{\mathbf{b}}^u = \frac{1}{\zeta_u^{k,\mathrm{ZF}} \mathrm{avg}\{\ddot{\boldsymbol{b}}^u\} + 1} (\mathbf{F}^{-1} \mathbf{P}_u^{\frac{1}{2}} (\mathbf{P}_u^{\frac{1}{2}} \boldsymbol{\Delta}_k \mathbf{P}_u^{\frac{1}{2}} + \sigma_v^2 \ddot{\mathbf{W}}_u)^{-1} \hat{\mathbf{r}}^{u,\mathrm{ZF}} + \zeta_u^{k,\mathrm{ZF}} \tilde{\mathbf{b}}^u), \tag{121}$$

where

$$\hat{\mathbf{r}}^{u,\mathrm{ZF}} = \tilde{\mathbf{r}}^{u,\mathrm{ZF}} - \mathbf{P}_u^{\frac{1}{2}} \mathbf{F} \tilde{\mathbf{b}}^u \tag{122}$$

and

$$\ddot{\mathbf{W}}_u = \mathrm{diag}([||\mathbf{w}_{u,1}||^2, ||\mathbf{w}_{u,2}||^2, \ldots, ||\mathbf{w}_{u,N_F}||^2]^{\mathrm{T}}) \in \mathbb{R}^{N_F \times N_F}. \tag{123}$$

CC (72) reduces to

$$\zeta_u^{k,\mathrm{ZF}} \geq \xi_{u,k}, \tag{124}$$

where

$$\zeta_u^{k,\mathrm{ZF}} = \frac{1}{N_F} \sum_{m=1}^{N_F} \frac{P_{u,m}}{P_{u,m} \Delta_k + \sigma_v^2 ||\mathbf{w}_{u,m}||^2}. \tag{125}$$

Calculating the Hessian of (125), it can be verified that (124) is a convex constraint [88].

OFDMA

Using ZF equalization in OFDMA, constraint (82) reduces to

$$\frac{P_{u,m}}{\sigma_v^2 ||\mathbf{w}_{u,m}||^2} \geq \tilde{\xi}_{u,k}, \tag{126}$$

which is also a convex constraint.

3.3.3 Joint optimization of RX filters and TX powers

SC-FDMA

The block diagram illustrating the optimization flow is depicted in Fig. 9. The idea is to perform joint optimization by alternating between the TX and RX optimizations, where

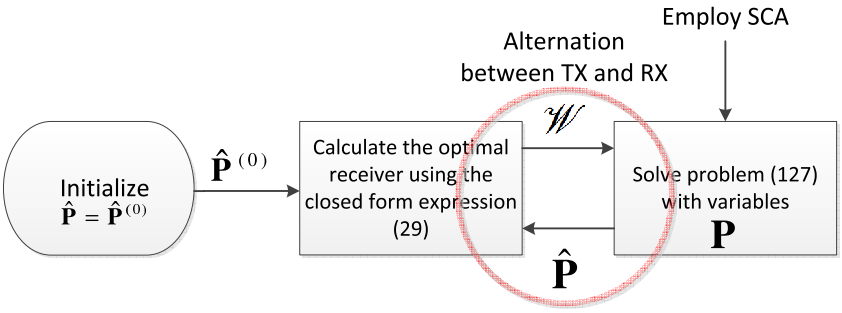

Fig. 9. Block diagram of the optimization flow for SC-FDMA.

SCA is employed for TX optimization.

The power minimization problem for SC-FDMA with the CC derived in Section 3.1 is expressed as

$$\begin{aligned} \underset{\mathbf{P},\mathscr{W}}{\text{minimize}} \quad & \text{tr}\{\mathbf{P}\} \\ \text{subject to} \quad & \zeta_u^k \geq \xi_{u,k}, \quad u = 1,2\ldots,U, k = 1,2,\ldots,K, \\ & P_{u,m} \geq 0, \quad u = 1,2,\ldots,U, m = 1,2,\ldots,N_F, \end{aligned} \tag{127}$$

where

$$\mathscr{W} = \{\boldsymbol{\omega}_{u,m}^k : u = 1,2,\ldots,U, m = 1,2,\ldots,N_F, k = 1,2,\ldots,K\}. \tag{128}$$

Problem (127) is not convex with respect to the optimization variables.

The joint TX-RX optimization problem (127) can be solved by using alternating optimization where the non-convex joint optimization problem is split into separate TX and RX optimization. The algorithm starts with a feasible initial guess[6] $\hat{\mathbf{P}}^{(0)}$ followed by the calculation of the optimal receive filter. After that, problem (127) is solved for a fixed $\mathscr{W}$. The overall algorithm is presented in **Algorithm** 3, where $\mathbf{P}^{(*)}$ represents a solution to problem (127) for fixed $\mathscr{W}$ and $\mathscr{W}^{(*)}$ represents the optimal $\mathscr{W}$ for fixed $\mathbf{P}$.

A monotonic convergence of the objective value in alternating optimization can be justified by the fact that each step improves the objective. In the following, it is shown that the soft cancelation MMSE RX (29) is a power-minimizing RX.

Differentiating the Lagrangian of (127) with respect to the receive beamforming vectors and equating to zero yields

$$\frac{\partial}{\partial \boldsymbol{\omega}_{u,m}^k} \frac{P_{u,m} \boldsymbol{\omega}_{u,m}^{k\text{H}} \boldsymbol{\gamma}_{u,m} \boldsymbol{\gamma}_{u,m}^{\text{H}} \boldsymbol{\omega}_{u,m}^k}{\boldsymbol{\omega}_{u,m}^{k\text{H}} \boldsymbol{\Sigma}_{\hat{\mathbf{r}},m}^k \boldsymbol{\omega}_{u,m}^k} = 0. \tag{129}$$

[6]Can be found by e.g., using ZF algorithm [43].

Algorithm 3 Alternating Optimization for SC-FDMA.

1. Initialize $\hat{\mathbf{P}} = \hat{\mathbf{P}}^{(0)}$
   repeat
      Calculate the optimal $\mathscr{W}$ from (29).
      Set $\mathscr{W} = \mathscr{W}^{(*)}$ and solve problem (127) with variables $\mathbf{P}$.
      Update $\hat{\mathbf{P}} = \mathbf{P}^{(*)}$
   until Convergence

Calculating the derivative in (129) and solving $\boldsymbol{\omega}_{u,m}^{k}$ results in

$$\boldsymbol{\omega}_{u,m}^{k} = \frac{\boldsymbol{\omega}_{u,m}^{k\mathrm{H}} \boldsymbol{\Sigma}_{\hat{\mathbf{r}},m}^{k} \boldsymbol{\omega}_{u,m}^{k}}{P_{u,m} \boldsymbol{\omega}_{u,m}^{k\mathrm{H}} \boldsymbol{\gamma}_{u,m} \boldsymbol{\gamma}_{u,m}^{\mathrm{H}} \boldsymbol{\omega}_{u,m}^{k}} \boldsymbol{\gamma}_{u,m}^{\mathrm{H}} \boldsymbol{\omega}_{u,m}^{k} \sqrt{P_{u,m}} \times (\boldsymbol{\Sigma}_{\hat{\mathbf{r}},m}^{k})^{-1} \boldsymbol{\gamma}_{u,m} \sqrt{P_{u,m}}, \tag{130}$$

where

$$\frac{\boldsymbol{\omega}_{u,m}^{k\mathrm{H}} \boldsymbol{\Sigma}_{\hat{\mathbf{r}},m}^{k} \boldsymbol{\omega}_{u,m}^{k}}{P_{u,m} \boldsymbol{\omega}_{u,m}^{k\mathrm{H}} \boldsymbol{\gamma}_{u,m} \boldsymbol{\gamma}_{u,m}^{\mathrm{H}} \boldsymbol{\omega}_{u,m}^{k}} \in \mathbb{R}^{+}. \tag{131}$$

Further assuming that

$$\boldsymbol{\gamma}_{u,m}^{\mathrm{H}} \boldsymbol{\omega}_{u,m}^{k} \in \mathbb{R}, \tag{132}$$

the optimal receive beamforming vector for the m^{th} frequency bin of the u^{th} user at the k^{th} MI index is given by

$$\boldsymbol{\omega}_{u,m}^{k} = \eta_{u}^{k} (\boldsymbol{\Sigma}_{\hat{\mathbf{r}},m}^{k})^{-1} \boldsymbol{\gamma}_{u,m} \sqrt{P_{u,m}}, \tag{133}$$

where $\boldsymbol{\Sigma}_{\hat{\mathbf{r}},m}^{k}$ denotes the interference covariance matrix for the m^{th} frequency bin at the k^{th} MI index and $\eta_{u}^{k} \in \mathbb{R}$. Assumption (132) is justified by the fact that the RX $\boldsymbol{\omega}_{u,m}^{k}$ can be multiplied by any factor $e^{j\theta}$, $\theta \in [0, 2\pi]$, such that $e^{j\theta} \boldsymbol{\gamma}_{u,m}^{\mathrm{H}} \boldsymbol{\omega}_{u,m}^{k} \in \mathbb{R}$, without changing the SINR. Hence, the optimal RX (29) is actually the MMSE RX used in [100, Chapter 5] up to a scalar multiplier leading to exactly the same SINR. The scaling factor η_{u}^{k} should be chosen such that it matches with the assumptions made in the soft demapper. With the notations given in Chapter 2, the turbo equalizer works properly only if the scaling factor η_{u}^{k} is chosen to be [101]

$$\eta_{u}^{k} = \frac{1}{\mathrm{avg}\{\ddot{\mathbf{b}}^{u}\} \zeta_{u,k} + 1}. \tag{134}$$

OFDMA

The power minimization problem for OFDMA with the CC is expressed as

$$\begin{aligned} \underset{\mathbf{P},\tilde{\mathscr{W}}}{\text{minimize}} \quad & \text{tr}\{\mathbf{P}\} \\ \text{subject to} \quad & \tilde{\zeta}^k_{u,m} \geq \tilde{\xi}_{u,k}, \quad u = 1,2\ldots,U, m = 1,2,\ldots,N_F, k = 1,2,\ldots,K, \\ & P_{u,m} \geq 0, \qquad u = 1,2,\ldots,U, m = 1,2,\ldots,N_F, \end{aligned} \tag{135}$$

where

$$\tilde{\mathscr{W}} = \{\tilde{\boldsymbol{\omega}}^k_{u,m} : u = 1,2,\ldots,U, m = 1,2,\ldots,N_F, k = 1,2,\ldots,K\}. \tag{136}$$

For fixed $\tilde{\mathscr{W}}$, the objective and all the constraints in problem (135) are linear. Hence, (135) is convex for fixed $\tilde{\mathscr{W}}$. Differentiating the Lagrangian of (135) with respect to the receive beamforming vectors and equating to zero yields

$$\frac{\partial}{\partial \tilde{\boldsymbol{\omega}}^k_{u,m}} \frac{P_{u,m}\tilde{\boldsymbol{\omega}}^{k\text{H}}_{u,m}\boldsymbol{\gamma}_{u,m}\boldsymbol{\gamma}^{\text{H}}_{u,m}\tilde{\boldsymbol{\omega}}^k_{u,m}}{\tilde{\boldsymbol{\omega}}^{k\text{H}}_{u,m}\tilde{\boldsymbol{\Sigma}}^{u,k}_{\hat{\mathbf{r}},m}\tilde{\boldsymbol{\omega}}^k_{u,m}} = 0, \tag{137}$$

where

$$\tilde{\boldsymbol{\Sigma}}^{u,k}_{\hat{\mathbf{r}},m} = \sum_{\substack{l=1 \\ l\neq u}}^{U} \boldsymbol{\gamma}_{l,m}\boldsymbol{\gamma}^{\text{H}}_{l,m}P_{l,m}\Delta_k + \sigma_v^2\mathbf{I}_{N_R}. \tag{138}$$

Calculating the derivative in (137) and solving $\tilde{\boldsymbol{\omega}}^k_{u,m}$ results in

$$\tilde{\boldsymbol{\omega}}^k_{u,m} = \frac{\sqrt{P_{u,m}}}{\tilde{\zeta}^k_{u,m}}\boldsymbol{\gamma}^{\text{H}}_{u,m}\tilde{\boldsymbol{\omega}}^k_{u,m}(\tilde{\boldsymbol{\Sigma}}^{u,k}_{\hat{\mathbf{r}},m})^{-1}\sqrt{P_{u,m}}\boldsymbol{\gamma}_{u,m} \tag{139}$$

where $\frac{\sqrt{P_{u,m}}}{\tilde{\zeta}^k_{u,m}} \in \mathbb{R}^+$. Similarly to the SC-FDMA case, it can be assumed that $\boldsymbol{\gamma}^{\text{H}}_{u,m}\boldsymbol{\omega}^k_{u,m} \in \mathbb{R}$. Hence, the optimal receive beamforming vector for the m^{th} frequency bin of the u^{th} user at the k^{th} MI index is given by

$$\tilde{\boldsymbol{\omega}}^k_{u,m} = \tilde{\eta}^k_u(\tilde{\boldsymbol{\Sigma}}^{u,k}_{\hat{\mathbf{r}},m})^{-1}\boldsymbol{\gamma}_{u,m}\sqrt{P_{u,m}}, \tag{140}$$

where $\tilde{\eta}^k_u \in \mathbb{R}$. It remains to show that (40) and (140) lead to the same SINR. Using the matrix inversion lemma [106][7], MMSE filter (40) can be rewritten as

$$\tilde{\boldsymbol{\omega}}^k_{u,m} = \frac{1}{1+\zeta^k_{u,m}}(\tilde{\boldsymbol{\Sigma}}^{u,k}_{\hat{\mathbf{r}},m})^{-1}\boldsymbol{\gamma}_{u,m}\sqrt{P_{u,m}}, \tag{141}$$

where $\frac{1}{1+\zeta^k_{u,m}} \in \mathbb{R}^+$. It can be seen that (140) and (141) are equivalent up to a scalar multiplier and hence, lead to the same SINR. The alternating optimization algorithm for OFDMA is presented in **Algorithm** 4.

[7] $(\mathbf{A}+\mathbf{CBC}^{\text{T}})^{-1} = \mathbf{A}^{-1} - \mathbf{A}^{-1}\mathbf{C}(\mathbf{B}^{-1}+\mathbf{C}^{\text{T}}\mathbf{A}^{-1}\mathbf{C})^{-1}\mathbf{C}^{\text{T}}\mathbf{A}^{-1}$

Algorithm 4 Alternating Optimization for OFDMA.

1. Initialize $\hat{\mathbf{P}} = \hat{\mathbf{P}}^{(0)}$
   repeat
      Calculate the optimal $\tilde{\mathscr{W}}$ from (40).
      Set $\tilde{\mathscr{W}} = \tilde{\mathscr{W}}^{(*)}$ and solve problem (135) with variables $\mathbf{P}$.
      Update $\hat{\mathbf{P}} = \mathbf{P}^{(*)}$
   until Convergence

3.3.4 Successive convex approximation via change of variables

In the following two subsections, the focus is on solving problem (127) for fixed $\mathscr{W}$, denoted as power allocation problem (PAP).

To ease the handling of (127), the problem is written in equivalent form by splitting the CC into *sum SINR* and *per subcarrier SINR* parts as follows:

$$\begin{aligned} &\frac{1}{N_F}\sum_{m=1}^{N_F} t_{u,m}^k \geq \xi_{u,k} \\ &t_{u,n}^k = \frac{P_{u,n}|\boldsymbol{\omega}_{u,n}^{k\mathrm{H}}\boldsymbol{\gamma}_{u,n}|^2}{\sum_{l=1}^{U} P_{l,n}|\boldsymbol{\omega}_{u,n}^{k\mathrm{H}}\boldsymbol{\gamma}_{l,n}|^2\Delta_k + \sigma_v^2||\boldsymbol{\omega}_{u,n}^k||^2}. \end{aligned} \tag{142}$$

At the optimal point, the constraints hold with equality, and hence, the equality in (142) can be relaxed, leading to an equivalent formulation of the PAP as

$$\begin{aligned} \underset{\mathbf{P},\tilde{W},\mathbf{t}}{\text{minimize}} \quad & \textstyle\sum_{u=1}^{U}\sum_{m=1}^{N_F} P_{u,m} \\ \text{subject to} \quad & \tfrac{1}{N_F}\textstyle\sum_{m=1}^{N_F} t_{u,m}^k \geq \xi_{u,k}, \;\; u = 1,2,\ldots,U, k = 1,2,\ldots,K, \\ & P_{u,n}|\boldsymbol{\omega}_{u,n}^{k\mathrm{H}}\boldsymbol{\gamma}_{u,n}|^2 \geq t_{u,n}^k\Big(\textstyle\sum_{l=1}^{U} P_{l,n}|\boldsymbol{\omega}_{u,n}^{k\mathrm{H}}\boldsymbol{\gamma}_{l,n}|^2\Delta_k + \sigma_v^2||\boldsymbol{\omega}_{u,n}^k||^2\Big), k = 1,2,\ldots,K, \\ & u = 1,2,\ldots,U, n = 1,2,\ldots,N_F, \\ & P_{u,n} \geq 0, u = 1,2,\ldots,U, n = 1,2,\ldots,N_F, \end{aligned} \tag{143}$$

where $\mathbf{t} = \{t_{u,m}^k : u = 1,2,\ldots,U, k = 1,2,\ldots,K, m = 1,2,\ldots,N_F\}$. It can be seen that the RHS of the *per subcarrier SINR* constraint is a posynomial and the RHS is a linear function. Hence, it can be transformed to a convex constraint. However, the LHS of the *sum SINR* constraint is a posynomial and, therefore, needs to be approximated as presented in Section 3.2.

Following the procedure presented in Section 3.2.1, new variables $\alpha_{u,m} \in \mathbb{R}$ are introduced such that $P_{u,m} = e^{\alpha_{u,m}}, \forall u = 1,2,\ldots,U, m = 1,2,\ldots,N_F$. The PAP with the new variables can be equivalently written as

$$\begin{aligned} \underset{\boldsymbol{\alpha},\mathbf{t}}{\text{minimize}} \quad & \textstyle\sum_{u=1}^{U}\sum_{m=1}^{N_F} e^{\alpha_{u,m}} \\ \text{subject to} \quad & \tfrac{1}{N_F}\textstyle\sum_{m=1}^{N_F} t_{u,m}^{k} \geq \xi_{u,k}, u = 1,2,\ldots,U, k = 1,2,\ldots,K, \\ & \frac{e^{\alpha_{u,n}}|\boldsymbol{\omega}_{u,n}^{k\,\mathrm{H}}\boldsymbol{\gamma}_{u,n}|^2}{\sum_{l=1}^{U} e^{\alpha_{l,n}}|\boldsymbol{\omega}_{u,n}^{k\,\mathrm{H}}\boldsymbol{\gamma}_{l,n}|^2\Delta_k+\sigma_v^2||\boldsymbol{\omega}_{u,n}^{k}||^2} \geq t_{u,n}^{k}, k = 1,2,\ldots,K, \\ & u = 1,2,\ldots,U, \qquad\qquad n = 1,2,\ldots,N_F, \end{aligned} \tag{144}$$

where $\boldsymbol{\alpha} = \{\alpha_{u,m} : u = 1,2,\ldots,U, m = 1,2,\ldots,N_F\}$. Taking the natural logarithm of the *per subcarrier SINR* constraint yields

$$\alpha_{u,n} + 2\ln(|\boldsymbol{\omega}_{u,n}^{k\mathrm{H}}\boldsymbol{\gamma}_{u,n}|) - \ln(\sum_{l=1}^{U} e^{\alpha_{l,n}}|\boldsymbol{\omega}_{u,n}^{k\mathrm{H}}\boldsymbol{\gamma}_{l,n}|^2\Delta_k + \sigma_v^2||\boldsymbol{\omega}_{u,n}^{k}||^2) \geq \ln t_{u,n}^{k}. \tag{145}$$

It is well known that logarithm of the summation of the exponentials is convex. Hence, the LHS of constraint (145) is concave. The RHS of (145) can be locally approximated with its best convex upper bound, i.e. a linear approximation of $\ln t_{u,n}^{k}$ at a point $\hat{t}_{u,n}^{k}$:

$$Y(t_{u,n}^{k}, \hat{t}_{u,n}^{k}) = \ln \hat{t}_{u,n}^{k} + \frac{(t_{u,n}^{k} - \hat{t}_{u,n}^{k})}{\hat{t}_{u,n}^{k}}. \tag{146}$$

A local convex approximation of (144) can be written as

$$\begin{aligned} \underset{\boldsymbol{\alpha},\mathbf{t}}{\text{minimize}} \quad & \textstyle\sum_{u=1}^{U}\sum_{m=1}^{N_F} e^{\alpha_{u,m}} \\ \text{subject to} \quad & \textstyle\sum_{m=1}^{N_F} t_{u,m}^{k} \geq N_F\xi_{u,k}, u = 1,2,\ldots,U, k = 1,2,\ldots,K, \\ & \alpha_{u,n} + 2\ln(|\boldsymbol{\omega}_{u,n}^{k\mathrm{H}}\boldsymbol{\gamma}_{u,n}|) - \ln(\textstyle\sum_{l=1}^{U} e^{\alpha_{l,n}}|\boldsymbol{\omega}_{u,n}^{k\mathrm{H}}\boldsymbol{\gamma}_{l,n}|^2\Delta_k + \sigma_v^2||\boldsymbol{\omega}_{u,n}^{k}||^2) \geq \\ & Y(t_{u,n}^{k}, \hat{t}_{u,n}^{k}), u = 1,2,\ldots,U, k = 1,2,\ldots,K, n = 1,2,\ldots,N_F, \end{aligned} \tag{147}$$

and it can be solved efficiently by using standard optimization tools, e.g. interior-point methods [88]. The SCA algorithm for PAP is summarized in **Algorithm** 5.

Algorithm 5 Successive convex approximation for PAP via change of variables.

1: Set $\hat{t}_{u,n}^{k} = \hat{t}_{u,n}^{k(0)}, \forall u,k,n.$
2: **repeat**
3: Solve Eq. (147).
4: Update $\hat{t}_{u,n}^{k} = t_{u,n}^{k(*)}, \forall u,k,n.$
5: **until** Convergence.

3.3.5 Successive convex approximation via geometric programming

Another algorithm for solving the PAP can be derived by using the approach presented in Section 3.2.2 where the SCA is implemented via series of GPs [88]. Using (97), the summation constraint can be replaced by its monomial underestimate, with which a local approximation of (127) for a fixed $\mathscr{W}$ can be derived in the form of GP, as

$$\begin{aligned}
\underset{\mathbf{P},\mathbf{t}}{\text{minimize}} \quad & \text{tr}\{\mathbf{P}\} \\
\text{subject to} \quad & \textstyle\prod_{n=1}^{N_F} (\frac{t_{u,n}^k}{\Phi_{u,n}^k})^{\Phi_{u,n}^k} \geq N_F \xi_{u,k}, u = 1,2,\ldots,U, k = 1,2,\ldots,K, \\
& P_{u,m} |\boldsymbol{\omega}_{u,m}^{k\,\mathrm{H}} \boldsymbol{\gamma}_{u,m}|^2 \geq (\textstyle\sum_{l=1}^{U} P_{l,m} |\boldsymbol{\omega}_{u,m}^{k\,\mathrm{H}} \boldsymbol{\gamma}_{l,m}|^2 \Delta_k + \sigma_v^2 |\boldsymbol{\omega}_{u,m}^k|^2) t_{u,m}^k, \\
& u = 1,2,\ldots,U, k = 1,2,\ldots,K, m = 1,2,\ldots,N_F, \\
& P_{u,m} \geq 0, \quad u = 1,2,\ldots,U, m = 1,2,\ldots,N_F,
\end{aligned} \tag{148}$$

where

$$\Phi_{u,m}^k = \frac{\hat{t}_{u,m}^k}{\sum_{n=1}^{N_F} \hat{t}_{u,n}^k}. \tag{149}$$

Now the objective is a posynomial, the LHSs of the inequality constraints are monomials and the RHSs are posynomials. Hence, (148) is in the form of a GP, which can be transformed to a convex optimization problem [88]. The SCA algorithm for PAP is summarized in **Algorithm** 6.

Algorithm 6 Successive convex approximation for PAP via geometric programming.

1: Set $\hat{P}_{u,m} = \hat{P}_{u,m}^{(0)}, \forall u,m$.
2: **repeat**
3: Calculate $\Phi_{u,m}^k$, $\forall u,m,k$, using (149).
4: Solve Eq. (102).
5: Update $\hat{P}_{u,m} = P_{u,m}^{(*)}, \forall k$.
6: **until** Convergence.

The motivation for introducing two different SCAs via COV and via GP is to give alternative approaches for the implementation of the optimization algorithm. The main difference is in the approximated constraints: In (147), the per subcarrier constraint is approximated and the number of the approximated constraints is UN_FK. In (148), the sum SINR constraint is approximated and the number of approximated constraints is UK.

3.4 Numerical results

In this section, the numerical results obtained by simulations are shown to evaluate the performance of the proposed algorithms. The stopping criterion of **Algorithms** 3–6 is that the change in the objective function becomes less than or equal to a small specific value between two successive iterations. In simulations, the stopping threshold value was set at 0.05 for **Algorithms** 3–4 and 0.01 for **Algorithms** 5–6. EP-SC-FDMA and EP-OFDMA denote the SC-FDMA and OFDMA transmission with equal power allocation, respectively. In equal power allocation (EP), equal power is allocated to all users across the frequency band, where the power level satisfying the CCs is found using a bisection algorithm [88]. SC-ZF and OFDMA-ZF denote SC-FDMA and OFDMA transmission with ZF equalization, respectively.

The results were obtained with the following parameters: $N_F = 8$, QPSK ($N_Q = 2$) and 16-QAM ($N_Q = 4$) with Gray mapping, and systematic repeat accumulate (RA) code [107] with a code rate of 1/3 and eight internal iterations. It can be seen from (127) and (135) that the PAPs expand linearly with N_F. The number of EXIT samples is either $K = 1$ or $K = 5$. In the case of $K = 1$, only one of the CCs for each user is taken into account. More specifically, it means that $\hat{I}_u^{\mathrm{A,target}} = 0$, and $\hat{I}_{u,k}^{\mathrm{E}} = \hat{I}_u^{\mathrm{E,target}}$, $u = 1, 2$, $k = K$. The feedback from the decoder is not taken into account, and hence it corresponds to the linear equalizer. In the case of $K = 5$, the points were placed uniformly along the line from the origin to the convergence point, i.e. uniformly over $[0, \hat{I}^{\mathrm{E,target}}]$. Furthermore, $\varepsilon_{u,k_u} = \varepsilon_u$, $\forall k_u < K$ and $\varepsilon_{u,K} = 0$. The SNR per RX antenna averaged over frequency bins is defined by

$$SNR = \mathrm{tr}\{\mathbf{P}\}/(N_R N_F \sigma_v^2). \tag{150}$$

Two different channel conditions were considered, namely, a static five-path channel where path gains were generated randomly, and a quasi-static Rayleigh fading five-path average equal gain channel.

To verify the accuracy of the method, EXIT simulations were carried out in a static channel, and the trajectories were obtained through chain simulations with a random interleaver with a size of 240,000 bits. The EXIT curve of the decoder was obtained by using 200 blocks for each *a priori* value, with the size of a block being 6,000 bits. The EXIT curves of the equalizer for SC-FDMA using SCAGP and the decoder, as well as the trajectories for two and four users with QPSK and 16-QAM, are depicted in Fig. 10(a). It is found that when $U = 2$ and QPSK is used, the gap between the

EXIT curves satisfies the preset condition and the convergence point is very close to the preset value. Furthermore, the trajectory matches closely with the EXIT curves, which indicates that the algorithm works properly. When the modulation order is increased to 16-QAM there exists a slight discrepancy between the EXIT curves and the trajectory. This is because of inequality (86). Due to the conservativeness of the CC in the case of 16-QAM, the real chain simulation provides a larger MI than the approximated EXIT curves, and hence the actual trajectory reaches the convergence point. Therefore, since the constraint in (127) provides an upper bound for the true SINR, convergence is also guaranteed with 16-QAM. Similar results are also obtained for OFDMA, as depicted in Fig. 10(b). However, for OFDMA the gap between the EXIT curves is larger than ε_u, resulting in significantly larger SNR requirements compared to SC-FDMA. This is due to the difference in CCs. In the case of OFDMA, the SINR requirement is the same for all subcarriers, unlike in SC-FDMA where the average of SINRs over the subcarriers is used.

To obtain the impact of a finite-length interleaver between the channel code and the equalizer, the trajectories were simulated using an interleaver with a length of 6,000 bits. The results are depicted in Fig. 11. It is obtained that the trajectories of both SC-FDMA and OFDMA do not match exactly to the EXIT curves. Furthermore, it can be seen from Fig. 11(b) that when $\varepsilon_4 = 0.01$, the trajectory does not reach the convergence point. In practice, this can be avoided by setting ε_u to a large enough value. Hence, the derived algorithms also work with finite block length codes.

To obtain further insight into the trade-off between ε_u and the required SNR to satisfy the constraints, all the algorithms shown in this chapter were simulated in a static channel with various ε_u, and the SNR values and the number of iterations required to achieve the target point were evaluated. The results are shown in Table 1. It can be seen that decreasing ε_u from 0.2 to 0.1 requires only one or two more iterations and the required SNR can be decreased by roughly 1 dB, depending on the algorithm used. The required SNR can be further reduced by about 0.5 dB by decreasing ε_u to 0.01, while the number of iterations increases approximately three times.

For QPSK, the MI target can be converted to BEP using the equation [51]

$$\mathrm{BEP} \approx \frac{1}{2}\mathrm{erfc}\left(\frac{\sqrt{\mathrm{J}_2^{-1}(\hat{I}_1^{\mathrm{A,target}}) + \mathrm{J}_2^{-1}(\hat{I}_1^{\mathrm{E,target}})}}{2\sqrt{2}}\right). \tag{151}$$

In Fig. 12, the required SNR versus BEP is presented, where four different BEP target values are considered for $u = 1,2$, namely 10^{-3}, 10^{-4}, 10^{-5}, 10^{-6} corresponding to

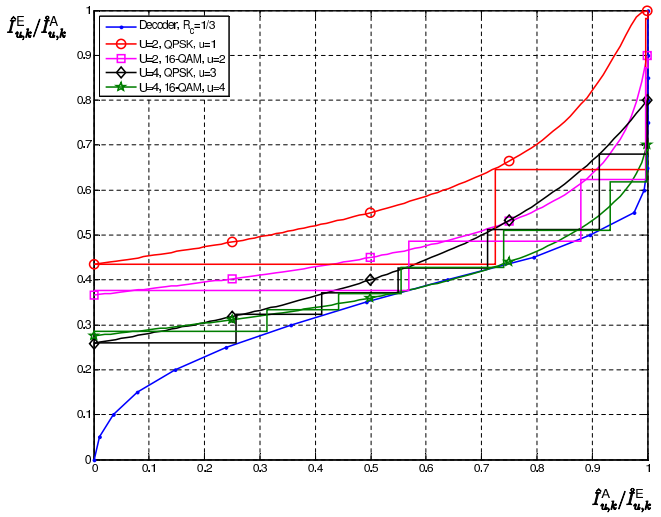

(a)

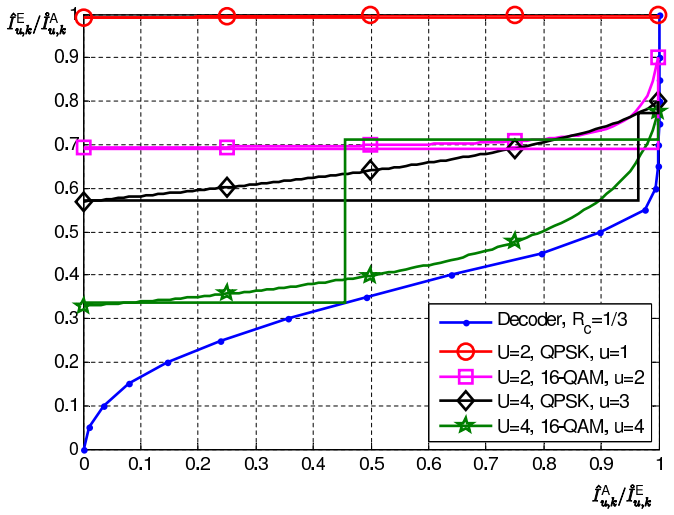

(b)

Fig. 10. Verification EXIT chart in a static channel for (a) SC-FDMA by using SCAGP and (b) OFDMA. System parameter values are $N_F = 8$, $K = 5$, $N_R = U$, $I_u^{E,target} = 0.9999$, $\forall u$, $(I_1^{E,target}, I_2^{E,target}, I_3^{E,target}, I_4^{E,target}) = (0.9999, 0.9, 0.8, 0.7)$ **and** $(\varepsilon_1, \varepsilon_2, \varepsilon_3, \varepsilon_4) = (0.2, 0.1, 0.05, 0.01)$. **When** $U = 2$, **parameters of users 1 and 2 are used.**

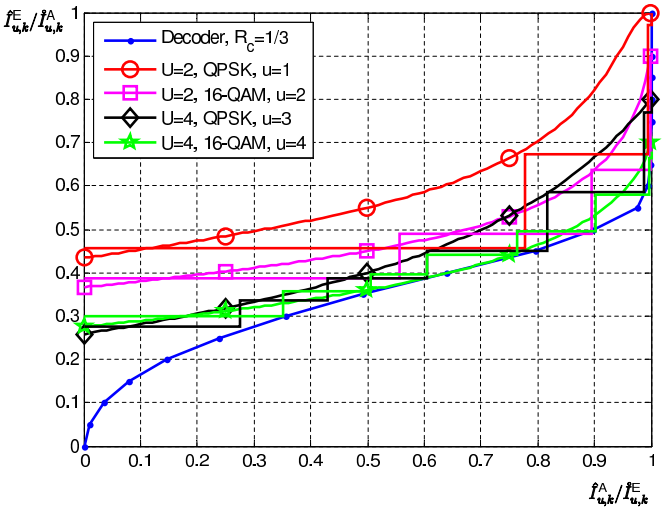

(a)

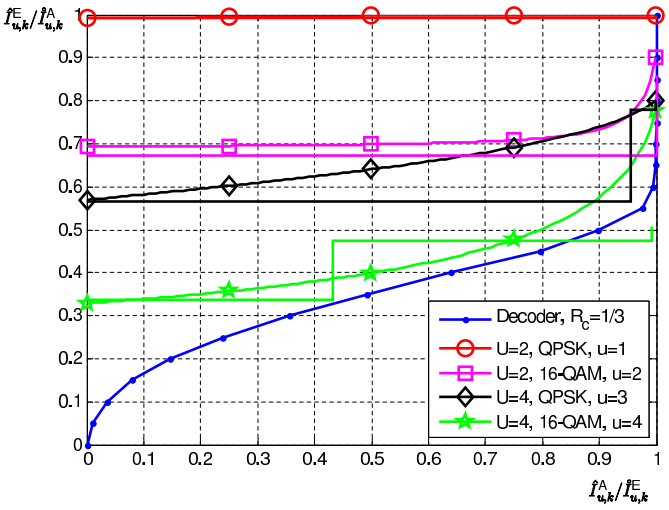

(b)

Fig. 11. Finite block length EXIT chart in a static channel for (a) SC-FDMA by using SCAGP and (b) OFDMA. System parameter values are $N_F = 8$, $K = 5$, $N_R = U$, $I_u^{\mathrm{E,target}} = 0.9999$, $\forall u$, $(I_1^{\mathrm{E,target}}, I_2^{\mathrm{E,target}}, I_3^{\mathrm{E,target}}, I_4^{\mathrm{E,target}}) = (0.9999, 0.9, 0.8, 0.7)$ **and** $(\varepsilon_1, \varepsilon_2, \varepsilon_3, \varepsilon_4) = (0.2, 0.1, 0.05, 0.01)$. **When** $U = 2$**, parameters of users 1 and 2 are used. The length of the interleaver is 6000 bits.**

Table 1. Required SNR and number of iterations with various ε in the case of SC-FDMA. The elements in the table are in the form of SNR(dB) / iterations for user 1 / iterations for user 2. $U = 2$, $N_R = 2$, $N_Q = 2$, $K = 5$, $\hat{I}_u^{\mathrm{A,target}} = 0.9999$, $\forall u$, $\hat{I}_1^{\mathrm{E,target}} = 0.7$, $\hat{I}_1^{\mathrm{E,target}} = 0.9$.

$\varepsilon_1 = \varepsilon_2$	OES	SCAGP	SCACOV	SC-ZF	EP-SC-FDMA
0.01	4.56 / 19 / 18	4.53 / 20 / 18	4.53 / 18 / 17	6.56 / 10 / 10	8.82 / 3 / 3
0.1	5.29 / 6 / 6	5.10 / 6 / 5	5.11 / 6 / 5	7.08 / 5 / 5	8.82 / 3 / 3
0.2	6.89 / 4 / 4	6.12 / 4 / 4	6.13 / 4 / 3	7.96 / 3 / 3	8.82 / 3 / 3

the MI targets $(\hat{I}_u^{\mathrm{E,target}}, \hat{I}_u^{\mathrm{E,target}}) = (0.99, 0.6185)$, $(\hat{I}_u^{\mathrm{E,target}}, \hat{I}_u^{\mathrm{E,target}}) = (0.9987, 0.673)$, $(\hat{I}_u^{\mathrm{E,target}}, \hat{I}_u^{\mathrm{E,target}}) = (0.9998, 0.7892)$, $(\hat{I}_u^{\mathrm{E,target}}, \hat{I}_u^{\mathrm{E,target}}) = (0.9998, 0.9819)$, respectively. It can be seen from Fig. 12(a) that OES, SCAGP and SCACOV achieve the best result when $K = 5$. SC-ZF and EP-SC-FDMA with $K = 5$ are 1.3 dB-3.6 dB worse in terms of SNR, depending on the BEP target and the algorithm used.

It is worth noting that the solution obtained by SCAGP and SCACOV in this particular case is very close to the orthogonal solution (OES). This is due to the fact that when $\Delta^l = 0$, $\forall l = 1, 2, \ldots, U$ in (30), all the interference is cancelled and the optimal RX is the filter matched to the channel. In this case, the optimal allocation strategy to maximize (27) is to allocate power to the strongest bin. However, this would not necessarily satisfy the constraint in (127) if $\Delta_k = 1$. Thus, the power has to be distributed between several bins, which results in higher power consumption. Hence, if the tightest constraint, i.e. $\Delta_k = 1$, can be satisfied using only one frequency bin, it is indeed the best solution. This is the case when the interference level is low, as in the case presented in Fig. 12. When the number of users increases, interference also increases and the orthogonal solution may not be feasible. This can be seen by looking at inequality (105). As was seen in Section 3.1, $\xi_{u,k}$ and Δ_k depend on the channel code used. Thus, it can be concluded that the feasibility of OES algorithm can be controlled by varying the channel code. The following results in this chapter are presented for 16-QAM only with $R_c = 1/3$ where the OES algorithm is not feasible due to (105). Fig. 12(b) illustrates that by using the CC, the desired QoS target can also be achieved with significantly reduced power consumption in OFDMA.

Fig. 13 shows the minimum SNR required to achieve the corresponding MI target for user 1 for each of the proposed algorithms for $U = 2$. It is found that the SNR gain by precoding with $K = 5$ is significant compared to precoding with $K = 1$. In Fig. 13(a), the SNRs with SCAGP and SCACOV are approximately equal and they provide the best results in terms of SNR. As expected, EP with $K = 1$ requires the highest SNR

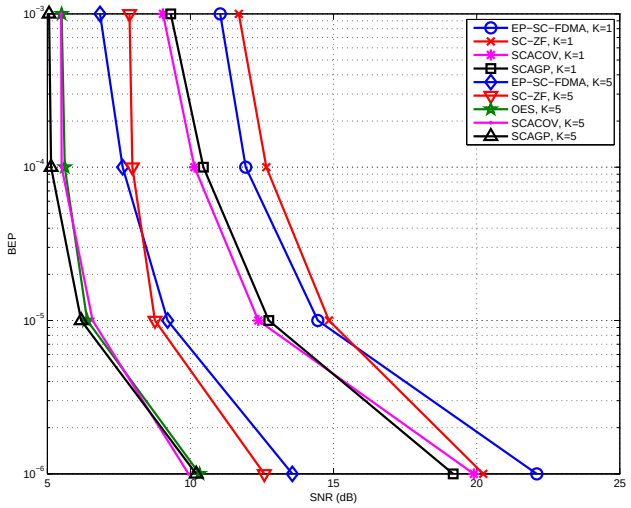

(a)

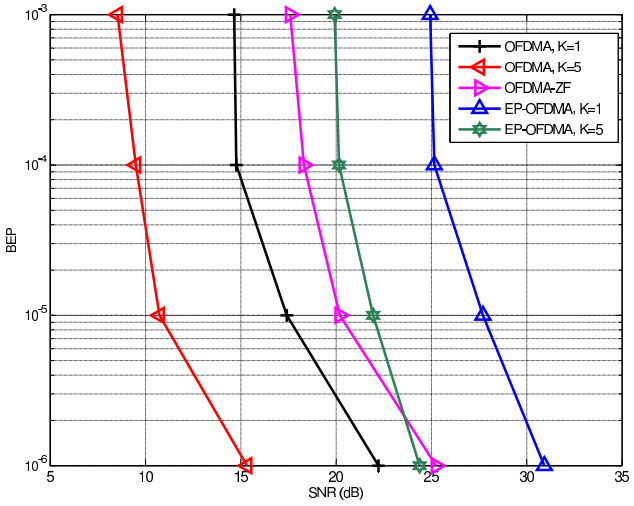

(b)

Fig. 12. The *a posteriori* BEP comparison for (a) SC-FDMA and (b) OFDMA. $U = 2$**,** $N_F = 8$**,** $N_R = 2$**, targets =** $[10^{-3}, 10^{-4}, 10^{-5}, 10^{-6}]$**,** $\varepsilon_u = 0.1$**,** $\forall u$**.**

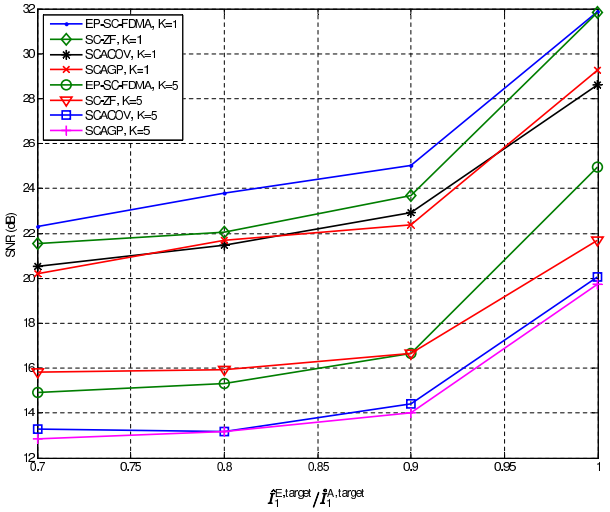

(a)

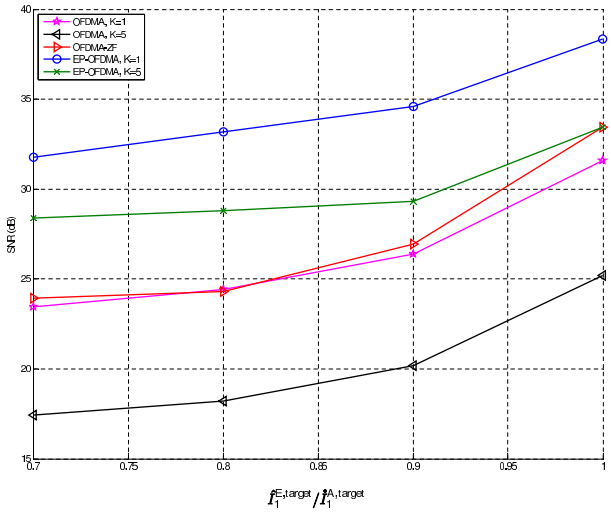

(b)

Fig. 13. SNR required to achieve the corresponding MI targets for user 1 for (a) SC-FDMA and (b) OFDMA. $U = 2$, $N_F = 8$, $N_R = 2$, $N_Q = 4$, $I_2^{E,target} = 0.8$, $I_u^{E,target} = 0.9999$, $u = 1,2$, $\varepsilon_u = 0.1$, $u = 1,2$, $N_L = 5$.

among all the algorithms tested.

Fig. 14 shows the minimum SNR required to achieve the corresponding MI target for user 1 for each of the proposed algorithms for $U = 4$. The results are similar to the case of $U = 2$: SC-ZF with $K = 5$ requires more power than EP-SC-FDMA with $K = 5$ when the MI target is low. However, when MI target increases, SC-ZF performs better than EP-SC-FDMA with $K = 5$. In OFDMA, the iterative equalizer is used to remove the MUI. In OFDMA-ZF, the MUI is already removed by the ZF equalizer and thus, the MMSE equalizer is not needed. Because in the scheme presented in Fig. 14 the noise power is low compared to MUI, the SNR required by OFDMA-ZF is not significantly influenced by the increase of the MI target.

As seen in Section 3.3, both SCAGP and SCACOV are to be solved via series of convex problems. Many efficient tools for solving convex problems are known in the literature [88]. Hence, the complexity analysis boils down to the comparison of how many times the optimization problem needs to be solved for each of the algorithms to achieve convergence according to criteria described at the beginning of this section. The number of solver call times that **Algorithms** 3 and 4 need varies typically between one and nine depending on the simulation setup. The more users, the more iterations are needed. The number of solver call times that **Algorithms** 5 and 6 need in **Algorithm** 3 varies between one and 13.

The motivation for using SC-FDMA is its favourable PAPR properties. The PAPR of the transmitted time domain signal of the u^{th} user is defined as

$$PAPR(\boldsymbol{s}^u) = \frac{\max_m |s_m^u|^2}{\text{avg}[|s_m^u|^2]}. \tag{152}$$

The PAPR of EP-SC-FDMA is only 2.55 dB for 16-QAM due to the equal sizes of DFT and IDFT at the TX and RX. However, the PAPR is increased when power allocation is performed across the frequency band. To demonstrate the trade-off between reduction of the required SNR and increase in PAPR, we measured the PAPR at the output of IDFT in the TX and evaluated the complementary cumulative distribution functions (CCDFs) $\text{Prob}(PAPR(\boldsymbol{s}^u) > \delta)$ for the algorithms investigated in this thesis. The results are shown in Fig. 15. It can be seen from Fig. 15(a) that unequal power allocation increases the PAPR significantly in SC-FDMA. Furthermore, with $K = 5$ the PAPR is higher than with $K = 1$ because with $K = 5$, the power allocation tends to be more orthogonal. However, it can be seen from Fig. 14 that the required SNR is reduced.

The maximum transmission power is defined as

$$P_{\max}(dB) = P_{\text{avg}}^u(dB) + PAPR(\boldsymbol{s}^u)(dB), \tag{153}$$

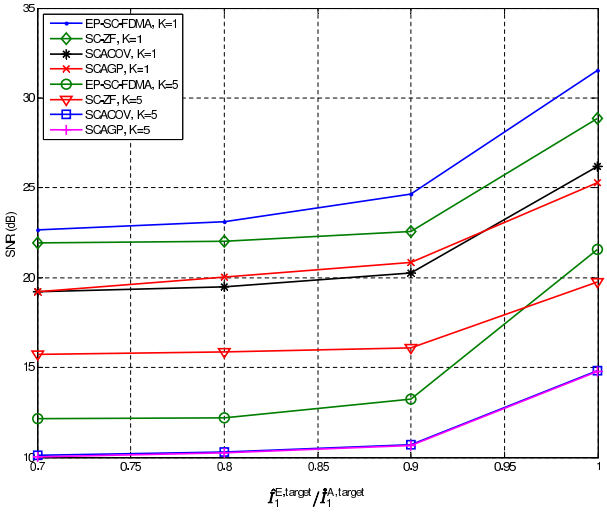

(a)

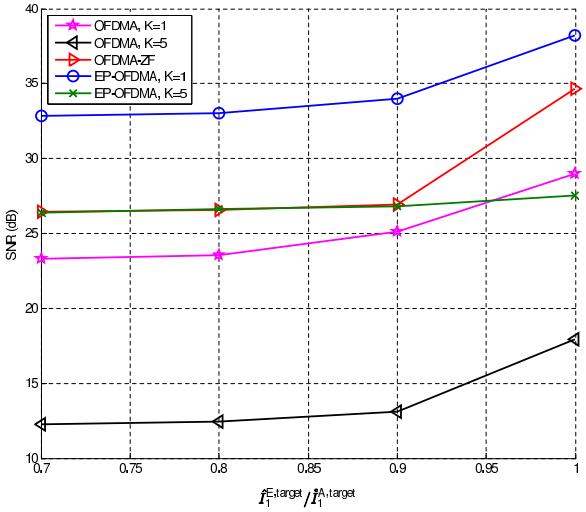

(b)

Fig. 14. SNR require to achieve the corresponding MI targets for user 1 for (a) SC-FDMA and (b) OFDMA. $U = 4$**,** $N_F = 8$**,** $N_R = 4$**,** $N_Q = 4$**,** $\hat{I}_u^{\mathbf{E,target}} = 0.8$**,** $u = 2,3,4$**,** $\hat{I}_u^{\mathbf{E,target}} = 0.9999$**,** $\forall u$**,** $\varepsilon_u = 0.1$**,** $\forall u$**,** $N_L = 5$**.**

where

$$P_{\text{avg}}^{u} = \frac{SNR \times N_R \times \sigma_v^2}{U} \tag{154}$$

denotes the average power per user. Let us consider an example where the maximum transmission power is to be configured according to 8 dB PAPR, which corresponds to the $10^{-2.92}$ value in CCDF for SCAGP and $K = 5$. For that same value of CCDF, the PAPR is 5.14 dB for SCAGP and $K = 1$. Hence, increasing K from one to five, the total power gain is $P_{\max}(dB)^{\text{SCAGP,K=1}} - P_{\max}(dB)^{\text{SCAGP,K=5}} = 15.28dB + 5.14dB - 4.76dB - 8dB = 7.66dB$. Therefore, the increase of K from one to five significantly increases the coverage of precoded transmission. For OFDMA, increasing K from one to five gives a total power gain of 10.58 dB. SCAGP with $K = 5$ requires 6.8 dB lower SNR than EP-SC-FDMA with $K = 5$. Using the same 8 dB example as above, the total power gain is $6.7dB - (8dB - 2.55dB) = 1.25dB$. However, this is only the worst-case comparison, i.e. the DFT and IDFT sizes are not necessarily equal in practice, and the use of different sizes of DFT and IDFT results in an increase in the PAPR of EP-SC-FDMA algorithm [82]. In conclusion, even with the worst-case comparison, SCACOV and SCAGP can achieve significantly larger coverage than EP-SC-FDMA with significantly lower average power consumption.

3.5 Summary and discussion

In this chapter, the CCPA problem for iterative FD MU SIMO detector was derived. Furthermore, with the novel problem derivation, the generalization for higher-order modulations is straightforward. This generalization requires knowledge of the J-functions for different modulation schemes. Then, the derived constraint can be used as an upper bound to guarantee convergence. In the case of a mixture of different modulations, the resulting LLR distribution would be a mixture of Gaussian distributions. One way to perform CCPA for a mixture of different modulation formats is to construct a look-up table where the J-function is defined for the mixtures, e.g. there would be a J-function for the mixture that has 60% 16-QAM and 40% QPSK. Again, the CC would serve as an upper bound and convergence is guaranteed.

Moreover, two SCAs for finding a local solution of the problem were derived. Numerical results indicate that significant gains in terms of average power consumption can be achieved compared to the linear RXs with and without precoding as well as to the iterative RX without precoding. Furthermore, it was shown that the PAPR increase

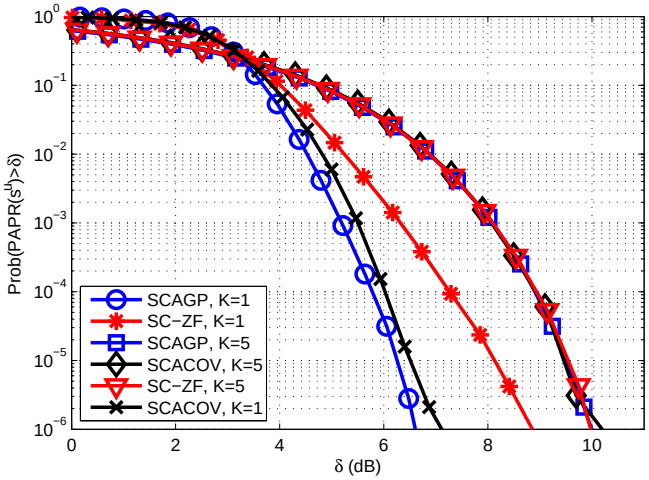

(a)

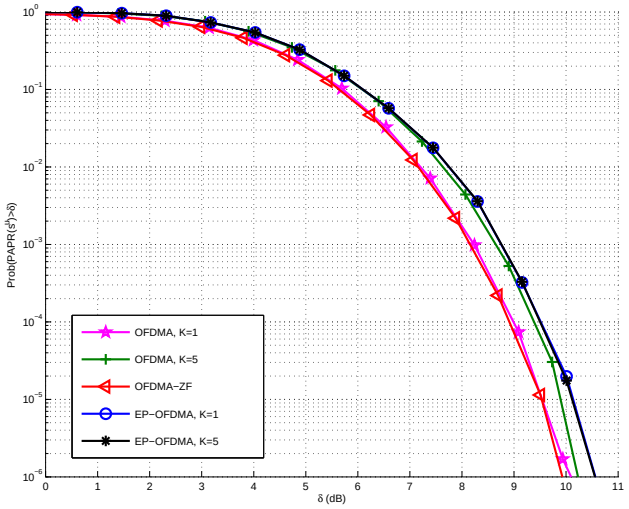

(b)

Fig. 15. CCDF for user 1 for (a) SC-FDMA and (b) OFDMA. $U = 4$, $N_F = 8$, $N_R = 4$, $N_Q = 4$, $\hat{I}_1^{\text{E,target}} = 0.9999$, $\hat{I}_u^{\text{E,target}} = 0.8$, $u = 2,3,4$, $\hat{I}_u^{\text{E,target}} = 0.9999$, $\forall u$, $\varepsilon_u = 0.1$, $\forall u$, $N_L = 5$.

due to precoding is relatively small compared to the gain in the average power consumption. Thus, the maximum cell size is increased by precoding. Algorithms proposed in this work allow the utilization of iterative RX and its convergence properties also on the TX side.

In SC-FDMA, increasing the power in any subcarrier causes self-interference. Therefore, the starting point in the EXIT chart, i.e. the equalization without *a priori* information, is interference-limited. In Section 3.4, it was obtained that when the number of users is low compared to the number of subcarriers, the solution obtained by SCACOV and SCAGP is very close to the orthogonal solution. With no interference, the optimal receiver is a matched filter and the optimal power allocation strategy is to use only the strongest bin. However, in SC-FDMA, increasing the power causes interference and the SINR constraint may not be satisfied by using only one subcarrier. Therefore, the power has to be distributed to several subcarriers, choosing the ones with the highest gains. If two or more users choose the same subcarrier, the interference is further increased. However, if $N_R \geq U$, the user separation can also be performed in the spatial domain using multiple receive antennas.

In OFDMA, the starting point in the EXIT chart is not interference-limited in general. However, in the case presented in the thesis, the same SINR is required for all the users in all subcarriers, and therefore increasing the power of one user causes interference to the others. The optimal strategy would be to use the same average SINR constraint as in the case of SC-FDMA. Then, the optimal solution is likely to be close to the water filling solution (CC may have some impact on the final results). This solution would require some major changes for the system model to be able to support the resulting bit and power loading strategy. Therefore, the impact of CC on the OFDMA with sum SINR constraint is left for future work. In OFDMA, the turbo equalizer is used only for removing the inter-user interference (since there no other type of interference). If $N_R \geq U$, the benefit may be negligible. However, if $N_R < U$, the turbo equalizer may compensate for the loss of degrees of freedom for the power allocation problem.

4 PAPR constrained precoding for iterative multiuser frequency domain MMSE detector

In this chapter, the PAPR constraint is derived for generalized multi-carrier transmission. Moreover, a statistical approach is considered where the power variance of the transmitted waveform is controlled. All the constraints are derived as a function of transmit power allocation, and two successive convex approximations (SCAs) are derived for each of the constraints based on the COV and GP. The proposed power allocation strategy takes jointly into account the channel quality and the PAPR characteristics of the power amplifier. The numerical results show that the proposed power allocation strategy can significantly improve the transmission of power-limited users.

4.1 Instantaneous PAPR constraint

In this section, instantaneous PAPR constraints are derived for SC-FDMA and OFDMA. In addition, SCACOV and SCAGP are derived for each of the constraints.

4.1.1 PAPR constraint for SC-FDMA

Let s_m^u be the m^{th} output of the transmitted waveform for the u^{th} user after the IDFT. The PAPR constraint in general form is expressed as

$$\frac{\max_m |s_m^u|^2}{\text{avg}[|s_m^u|^2]} \leq \delta_u, \tag{155}$$

where $\delta_u \geq 1$ is a user specific parameter controlling the PAPR. The max operator can be eliminated by requiring

$$\frac{|s_m^u|^2}{\text{avg}[|s_m^u|^2]} \leq \delta_u, \ \ \forall m = 1,2,\ldots,N_F. \tag{156}$$

Assuming $\mathbb{E}\{|b_n^u|\} = 1$, $\forall u,n$ and $\mathbb{E}\{b_n^u b_i^{u*}\} = 0$, $\forall n \neq i$, where b_n^{u*} denotes the complex conjugate of b_n^u, the average can be calculated as

$$\text{avg}[|s_m^u|^2] = \frac{1}{N_F}\sum_{m=1}^{N_F} \mathbb{E}\Big\{|s_m^u|^2\Big\} = \frac{1}{N_F}\sum_{m=1}^{N_F} P_{u,m}. \tag{157}$$

The complete derivation of (157) is shown in Appendix 1. The assumption $\mathbb{E}\{|b_n^u|\} = 1$ can be justified for any modulation scheme with a proper normalization factor.

The power of the m^{th} transmitted waveform can be calculated as

$$|s_m^u|^2 = \frac{1}{N_F^2}\sum_{l=1}^{N_F}\left(\kappa^u + 2d_l^u\right)P_{u,l} + \frac{2}{N_F^2}\sum_{\substack{n_1,n_2=1\\ n_2>n_1}}^{N_F}\left(\beta_{mn_1n_2}^u + \eta_{n_1n_2m}^u\right)\sqrt{P_{u,n_1}P_{u,n_2}}, \quad (158)$$

where $\kappa^u \in \mathbb{R}$, $\forall u$, $d_l^u \in \mathbb{R}$, $\forall l,u$, and $\beta_{mn_1n_2}^u, \eta_{n_1n_2m}^u \in \mathbb{R}$, $\forall n_1,n_2,m,u$. It should be noted that the number of summation terms in (158) increases in the order of $N_F^4 - N_F^2(1+2\sum_{n=1}^{N_F-1} n) + N_F + (\sum_{n=1}^{N_F-1} n)^2$. The complete derivation of (158) is given in Appendix 2.

In Appendix 2, it is shown that the factor $\kappa^u + 2d_l^u$ in (158) has to be non-negative. However, the factor $\beta_{mn_1n_2}^u + \eta_{n_1n_2m}^u$ can be negative, depending on the symbol sequence and the power allocation. Let

$$\hat{\eta}_{n_1n_2m}^{u+} = \max\{0, \beta_{mn_1n_2}^u + \eta_{n_1n_2m}^u\} \quad (159)$$

and

$$\hat{\eta}_{n_1n_2m}^{u-} = \min\{\beta_{mn_1n_2}^u + \eta_{n_1n_2m}^u, 0\}. \quad (160)$$

In such a case, the instantaneous PAPR constraint can be written as

$$\begin{aligned}&\frac{1}{N_F}\sum_{l=1}^{N_F}\left(\kappa^u + 2d_l^u\right)P_{u,l} + \frac{2}{N_F}\sum_{\substack{n_1,n_2=1\\ n_2>n_1}}^{N_F}\hat{\eta}_{n_1n_2m}^{u+}\sqrt{P_{u,n_1}P_{u,n_2}}\\ &\leq \delta_u\sum_{l=1}^{N_F}P_{u,l} + \frac{2}{N_F}\sum_{\substack{n_1,n_2=1\\ n_2>n_1}}^{N_F}(-\hat{\eta}_{n_1n_2m}^{u-})\sqrt{P_{u,n_1}P_{u,n_2}}, \forall m = 1,2,\ldots,N_F,\ \forall u = 1,2,\ldots,U,\end{aligned} \quad (161)$$

where all the terms in each summation are nonnegative.

The constraint (161) is a non-convex constraint. The term $\sqrt{P_{u,n_1}P_{u,n_2}}$ existing on both sides of (161) is actually a geometric mean and thus a concave function. While SCA could be directly applied by approximating $\sqrt{P_{u,n_1}P_{u,n_2}}$ on the LHS of (161), two SCAs are presented so that the reformulated constraint can be incorporated to the optimization framework introduced in Chapter 3. In the following, SCACOV and SCAGP are applied for constraint (161).

SCACOV

In SCACOV, constraint (161) is transformed such that it has a convex and concave part. The concave part can be locally approximated by a linear function, i.e. a local underestimator, and applying **Algorithm** 1, a local solution can be found iteratively by updating the approximation point.

Denoting $P_{u,l} = e^{\alpha_{u,l}}$, $u = 1,2,\ldots,U$, $l = 1,2,\ldots,N_F$, constraint (161) becomes

$$\frac{1}{N_F}\sum_{l=1}^{N_F}(\kappa^u + 2d_l^u)e^{\alpha_{u,l}} + \frac{2}{N_F}\sum_{\substack{n_1,n_2=1\\ n_2>n_1}}^{N_F}\hat{\eta}_{n_1n_2m}^{u+}e^{\frac{1}{2}(\alpha_{u,n_1}+\alpha_{u,n_2})} \leq \delta_u\sum_{l=1}^{N_F}e^{\alpha_{u,l}} + \frac{2}{N_F}\sum_{\substack{n_1,n_2=1\\ n_2>n_1}}^{N_F}(-\hat{\eta}_{n_1n_2m}^{u-})e^{\frac{1}{2}(\alpha_{u,n_1}+\alpha_{u,n_2})}. \quad (162)$$

The summation of exponentials is convex, and hence, both sides of (162) are convex functions.

Let

$$T_m(\boldsymbol{\alpha}_u) = \delta_u\sum_{l=1}^{N_F}e^{\alpha_{u,l}} + \frac{2}{N_F}\sum_{\substack{n_1,n_2=1\\ n_2>n_1}}^{N_F}(-\hat{\eta}_{n_1n_2m}^{u-})e^{\frac{1}{2}(\alpha_{u,n_1}+\alpha_{u,n_2})}.$$

The best concave approximation of $T_m(\boldsymbol{\alpha}_u)$ at a point $\hat{\boldsymbol{\alpha}}_u$ is given by

$$\hat{T}_m(\boldsymbol{\alpha}_u,\hat{\boldsymbol{\alpha}}_u) = T_m(\hat{\boldsymbol{\alpha}}_u) + \sum_{k=1}^{N_F}\frac{\partial T_m}{\partial\alpha_{u,k}}(\hat{\boldsymbol{\alpha}}_u)(\alpha_{u,k}-\hat{\alpha}_{u,k}). \quad (163)$$

The partial derivative $\frac{\partial T_m}{\partial\alpha_{u,k}}$ is derived as

$$\frac{\partial T_m}{\partial\alpha_{u,k}} = \delta_u e^{\alpha_{u,k}} + \frac{1}{N_F}\sum_{n=k+1}^{N_F}(-\hat{\eta}_{knm}^{u-})e^{\frac{1}{2}(\alpha_{u,k}+\alpha_{u,n})} + \frac{1}{N_F}\sum_{n=1}^{k-1}(-\hat{\eta}_{nkm}^{u-})e^{\frac{1}{2}(\alpha_{u,n}+\alpha_{u,k})}. \quad (164)$$

The best convex approximation of (162) at a point $\hat{\boldsymbol{\alpha}}_u$ is written as

$$\sum_{l=1}^{N_F}(\kappa^u + 2d_l^u)e^{\alpha_{u,l}} + \frac{2}{N_F}\sum_{\substack{n_1,n_2=1\\ n_2>n_1}}^{N_F}\hat{\eta}_{n_1n_2m}^{u+}e^{\frac{1}{2}(\alpha_{u,n_1}+\alpha_{u,n_2})} \leq \hat{T}_m(\boldsymbol{\alpha}_u,\hat{\boldsymbol{\alpha}}_u), \quad u = 1,2,\ldots,U, m = 1,2,\ldots,N_F. \quad (165)$$

For SCAGP, the constraint needs to be in such a form that it has a posynomial on both sides of the inequality sign. Constraint (161) is directly in that form. Now, the RHS can be successively approximated by a monomial using (97), and a local solution can be found iteratively by updating the parameters in monomial approximation.

Let

$$\mathscr{A}_m(\mathbf{P}_u) = \delta_u \sum_{l=1}^{N_F} P_{u,l} + \frac{2}{N_F} \sum_{\substack{n_1,n_2=1 \\ n_2>n_1}}^{N_F} (-\hat{\eta}_{n_1 n_2 m}^{u-}) \sqrt{P_{u,n_1} P_{u,n_2}} \tag{166}$$

Applying (97) to $\mathscr{A}_m(\mathbf{P}_u)$ yields a lower bound

$$\mathscr{A}_m(\mathbf{P}_u) \geq \left(\frac{\delta_u \prod_{l=1}^{N_F} \left(\frac{P_{u,l}}{\theta_{ul}^{(1)}} \right)^{\theta_{ul}^{(1)}}}{\tau_{um}^{(1)}} \right)^{\tau_{um}^{(1)}} \left(\frac{\frac{2}{N_F} \prod_{\substack{n_1,n_2=1 \\ n_2>n_1}}^{N_F} \left(\frac{(-\hat{\eta}_{n_1 n_2 m}^{u-}) \sqrt{P_{u,n_1} P_{u,n_2}}}{\theta_{n_1 n_2 mu}^{(2)}} \right)^{\theta_{n_1 n_2 mu}^{(2)}}}{\tau_{um}^{(2)}} \right)^{\tau_{um}^{(2)}}, \tag{167}$$

where

$$\begin{aligned} \theta_{ul}^{(1)} &= \frac{P_{u,l}}{\sum_{l'=1}^{N_F} P_{u,l'}}, \\ \theta_{n_1 n_2 mu}^{(2)} &= \frac{-\hat{\eta}_{n_1 n_2 m}^{u-} \sqrt{P_{u,n_1} P_{u,n_2}}}{\sum_{\substack{n_1',n_2'=1 \\ n_2'>n_1'}}^{N_F} -\hat{\eta}_{n_1' n_2' m}^{u-} \sqrt{P_{u,n_1'} P_{u,n_2'}}}, \end{aligned} \tag{168}$$

and weights $\tau_{um}^{(1)}$ and $\tau_{um}^{(2)}$ are given in

$$\begin{aligned} \tau_{um}^{(1)} &= \frac{\delta_u \prod_{l=1}^{N_F} \left(\frac{P_{u,l}}{\theta_{ul}^{(1)}} \right)^{\theta_{ul}^{(1)}}}{\delta_u \prod_{l=1}^{N_F} \left(\frac{P_{u,l}}{\theta_{ul}^{(1)}} \right)^{\theta_{ul}^{(1)}} + \frac{2}{N_F} \prod_{\substack{n_1,n_2=1 \\ n_2>n_1}}^{N_F} \left(\frac{(-\hat{\eta}_{n_1 n_2 m}^{u-}) \sqrt{P_{u,n_1} P_{u,n_2}}}{\theta_{n_1 n_2 mu}^{(2)}} \right)^{\theta_{n_1 n_2 mu}^{(2)}}} \\ \tau_{um}^{(2)} &= \frac{\frac{2}{N_F} \prod_{\substack{n_1,n_2=1 \\ n_2>n_1}}^{N_F} \left(\frac{(-\hat{\eta}_{n_1 n_2 m}^{u-}) \sqrt{P_{u,n_1} P_{u,n_2}}}{\theta_{n_1 n_2 mu}^{(2)}} \right)^{\theta_{n_1 n_2 mu}^{(2)}}}{\delta_u \prod_{l=1}^{N_F} \left(\frac{P_{u,l}}{\theta_{ul}^{(1)}} \right)^{\theta_{ul}^{(1)}} + \frac{2}{N_F} \prod_{\substack{n_1,n_2=1 \\ n_2>n_1}}^{N_F} \left(\frac{(-\hat{\eta}_{n_1 n_2 m}^{u-}) \sqrt{P_{u,n_1} P_{u,n_2}}}{\theta_{n_1 n_2 mu}^{(2)}} \right)^{\theta_{n_1 n_2 mu}^{(2)}}}. \end{aligned} \tag{169}$$

Hence, constraint (161) can be successively approximated $\forall u, m$ as

$$\sum_{l=1}^{N_F}(\kappa^u + 2d_l^u)P_{u,l} + \frac{2}{N_F}\sum_{\substack{n_1,n_2=1\\ n_2>n_1}}^{N_F}\hat{\eta}_{n_1n_2m}^{u+}\sqrt{P_{u,n_1}P_{u,n_2}}$$

$$\leq \left(\frac{\delta_u\prod_{l=1}^{N_F}\left(\frac{P_{u,l}}{\theta_{ul}^{(1)}}\right)^{\theta_{ul}^{(1)}}}{\tau_{um}^{(1)}}\right)^{\tau_{um}^{(1)}}\left(\frac{\frac{2}{N_F}\prod_{\substack{n_1,n_2=1\\ n_2>n_1}}^{N_F}\left(\frac{(-\hat{\eta}_{n_1n_2m}^{u-})\sqrt{P_{u,n_1}P_{u,n_2}}}{\theta_{n_1n_2mu}^{(2)}}\right)^{\theta_{n_1n_2mu}^{(2)}}}{\tau_{um}^{(2)}}\right)^{\tau_{um}^{(2)}}. \quad (170)$$

The LHS is a posynomial and RHS is a monomial and hence, (170) is a valid GP [88] constraint.

4.1.2 PAPR constraint for OFDMA

Going through a similar derivation as in the case of SC-FDMA, the average power in the case of OFDMA is

$$\text{avg}[|s_m^u|^2] = \frac{1}{N_F}\sum_{l=1}^{N_F}P_{u,l}, \quad (171)$$

i.e. the same as in the case of SC-FDMA.

The power of the m^{th} transmitted waveform can be calculated as

$$|s_m^u|^2 = \frac{1}{N_F}\sum_{l=1}^{N_F}|b_l^u|^2P_{u,l} + \frac{1}{N_F}\sum_{\substack{n_1,n_2=1\\ n_2>n_1}}^{N_F}\tilde{d}_{mn_2n_1}^u\sqrt{P_{u,n_1}P_{u,n_2}}, \quad (172)$$

where

$$\tilde{d}_{mn_2n_1}^u = 2\Bigg(\mathscr{R}[a_{mn_2n_1}]\Big(\mathscr{R}[b_{n_2}^u]\mathscr{R}[b_{n_1}^u] + \mathscr{I}[b_{n_2}^u]\mathscr{I}[b_{n_1}^u]\Big) -$$

$$\mathscr{I}[a_{mn_2n_1}]\Big(\mathscr{R}[b_{n_2}^u]\mathscr{I}[b_{n_1}^u] - \mathscr{I}[b_{n_2}^u]\mathscr{R}[b_{n_1}^u]\Big)\Bigg), \quad (173)$$

and

$$a_{mn_2n_1} = e^{\frac{j2\pi(m-1)(n_2-n_1)}{N_F}}. \quad (174)$$

The derivation of (172) is provided in Appendix 3. The number of summation terms in (172) increases in the order or $N_F^2 - \sum_{n=1}^{N_F-1} n$. The PAPR constraint for OFDMA can be

written as

$$\sum_{l=1}^{N_F} |b_l^u|^2 P_{u,l} + \sum_{\substack{n_1,n_2=1 \\ n_2>n_1}}^{N_F} \tilde{d}_{mn_2n_1}^{u+} \sqrt{P_{u,n_1} P_{u,n_2}} \leq \delta_u \sum_{l=1}^{N_F} P_{u,l} + \sum_{\substack{n_1,n_2=1 \\ n_2>n_1}}^{N_F} (-\tilde{d}_{mn_2n_1}^{u-}) \sqrt{P_{u,n_1} P_{u,n_2}}, \tag{175}$$

where

$$\tilde{d}_{mn_2n_1}^{u+} = \max\{0, \tilde{d}_{mn_2n_1}^{u}\} \tag{176}$$

and

$$\tilde{d}_{mn_2n_1}^{u-} = \min\{\tilde{d}_{mn_2n_1}^{u}, 0\}. \tag{177}$$

The major difference between the OFDMA's PAPR constraint and the SC-FDMA's PAPR constraint presented in (161) is in the factors $\hat{\eta}_{n_1n_2m}^{u}$ and $\tilde{d}_{mn_2n_1}^{u}$. Similarly to Section 4.1.1, constraint (175) can be successively approximated as SCACOV or SCAGP or directly approximating $\sqrt{P_{u,n_1} P_{u,n_2}}$ as a linear function.

SCACOV

Changing the variables as $P_{u,m} = e^{\alpha_{u,m}}$, $\forall u,m$, the approximation of (175) is written as

$$\sum_{l=1}^{N_F} |b_l^u|^2 e^{\alpha_{u,l}} + \sum_{\substack{n_1,n_2=1 \\ n_2>n_1}}^{N_F} \tilde{d}_{mn_2n_1}^{u+} e^{\frac{1}{2}(\alpha_{u,n_1}+\alpha_{u,n_2})} \leq \hat{T}_m(\boldsymbol{\alpha}_u, \hat{\boldsymbol{\alpha}}_u), \tag{178}$$

where $\hat{T}_m(\boldsymbol{\alpha}_u, \hat{\boldsymbol{\alpha}}_u)$ is given in (163), $T_m(\boldsymbol{\alpha}_u)$ is the RHS of (175) after COV, and the partial derivatives are given as

$$\frac{\partial T_m}{\partial \alpha_{u,k}} = \delta_u e^{\alpha_{u,k}} + \frac{1}{2} \sum_{n=k+1}^{N_F} (-\tilde{d}_{mkn}^{u-}) e^{\frac{1}{2}(\alpha_{u,k}+\alpha_{u,n})} + \frac{1}{2} \sum_{n=1}^{k-1} (-\tilde{d}_{mnk}^{u-}) e^{\frac{1}{2}(\alpha_{u,n}+\alpha_{u,k})}. \tag{179}$$

SCAGP

Applying (97) to the RHS of (175) yields a constraint

$$\begin{aligned} &\sum_{l=1}^{N_F} |b_l^u|^2 P_{u,l} + \sum_{\substack{n_1,n_2=1 \\ n_2>n_1}}^{N_F} \tilde{d}_{mn_2n_1}^{u+} \sqrt{P_{u,n_1} P_{u,n_2}} \\ &\leq \left(\frac{\delta_u \prod_{l=1}^{N_F} \left(\frac{P_{u,l}}{\theta_{ul}^{(1)}} \right)^{\theta_{ul}^{(1)}}}{\tau_{um}^{(1)}} \right)^{\tau_{um}^{(1)}} \left(\frac{\prod_{\substack{n_1,n_2=1 \\ n_2>n_1}}^{N_F} \left(\frac{(-\tilde{d}_{mn_2n_1}^{u-}) \sqrt{P_{u,n_1} P_{u,n_2}}}{\theta_{mn_2n_1u}^{(2)}} \right)^{\theta_{mn_2n_1u}^{(2)}}}{\tau_{um}^{(2)}} \right)^{\tau_{um}^{(2)}}, \end{aligned} \tag{180}$$

where

$$\theta_{ul}^{(1)} = \frac{P_{u,l}}{\sum_{l'=1}^{N_F} P_{u,l'}},$$
$$\theta_{mn_2n_1u}^{(2)} = \frac{-\tilde{d}_{mn_2n_1}^{u-}\sqrt{P_{u,n_1}P_{u,n_2}}}{\sum_{\substack{n_1',n_2'=1 \\ n_2'>n_1'}}^{N_F} -\tilde{d}_{mn_2'n_1'}^{u-}\sqrt{P_{u,n_1'}P_{u,n_2'}}}, \tag{181}$$

and weights $\tau_{um}^{(1)}$ and $\tau_{um}^{(2)}$ are given in

$$\tau_{um}^{(1)} = \frac{\delta_u \prod_{l=1}^{N_F}\left(\frac{P_{u,l}}{\theta_{ul}^{(1)}}\right)^{\theta_{ul}^{(1)}}}{\delta_u \prod_{l=1}^{N_F}\left(\frac{P_{u,l}}{\theta_{ul}^{(1)}}\right)^{\theta_{ul}^{(1)}} + \prod_{\substack{n_1,n_2=1 \\ n_2>n_1}}^{N_F}\left(\frac{(-\tilde{d}_{mn_2n_1}^{u-})\sqrt{P_{u,n_1}P_{u,n_2}}}{\theta_{mn_2n_1u}^{(2)}}\right)^{\theta_{mn_2n_1u}^{(2)}}}$$
$$\tau_{um}^{(2)} = \frac{\prod_{\substack{n_1,n_2=1 \\ n_2>n_1}}^{N_F}\left(\frac{(-\tilde{d}_{mn_2n_1}^{u-})\sqrt{P_{u,n_1}P_{u,n_2}}}{\theta_{mn_2n_1u}^{(2)}}\right)^{\theta_{mn_2n_1u}^{(2)}}}{\delta_u \prod_{l=1}^{N_F}\left(\frac{P_{u,l}}{\theta_{ul}^{(1)}}\right)^{\theta_{ul}^{(1)}} + \prod_{\substack{n_1,n_2=1 \\ n_2>n_1}}^{N_F}\left(\frac{(-\tilde{d}_{mn_2n_1}^{u-})\sqrt{P_{u,n_1}P_{u,n_2}}}{\theta_{mn_2n_1u}^{(2)}}\right)^{\theta_{mn_2n_1u}^{(2)}}}. \tag{182}$$

Hence, constraint (175) can be successively approximated $\forall u,m$ as (180). The LHS is a posynomial and the RHS is a monomial and hence, (180) is a valid GP constraint.

4.2 Power variance constraint

In this section, the power variance constraint is derived for SC-FDMA and OFDMA together with the SCACOV and SCAGP approximations. In [81, 82], it is shown that decreasing the variance of the power of the transmitted time domain signal decreases the PAPR in SC-FDMA transmission. The difference between the power variance and the instantaneous PAPR constraint is that the power variance constraint does not depend on the transmitted symbol sequence. However, the power variance constraint reduces the PAPR statistically and cannot track the exact PAPR.

4.2.1 Power variance constraint for SC-FDMA

Let the average power of the transmitted signal of the u^{th} user be denoted as $\mu_u = \frac{1}{N_F}\sum_{l=1}^{N_F} P_{u,l}$. Assuming $\mathbb{E}\{|b_n^u|\} = 1$, $\forall u,n$ and $\mathbb{E}\{b_{n_1}^u b_{n_2}^{u*}\} = 0$, $\forall n_1 \neq n_2$, the variance

of the output power is given by

$$\Sigma^2(\mathbf{P}_u) = \frac{1}{N_F}\sum_{k=1}^{N_F}(\mathbb{E}\{|s_k^u|^4\} - \mu_u^2)$$
$$= \frac{1}{N_F}\sum_{k=1}^{N_F}[2(\sum_{m=1}^{N_F}|g_{k,m}^u|^2)^2 - \sum_{m=1}^{N_F}|g_{k,m}^u|^4] - \mu_u^2, \tag{183}$$

where

$$g_{k,m}^u = \frac{1}{N_F}\sum_{q=1}^{N_F}\sqrt{P_{u,q}}a_{qkm}. \tag{184}$$

The first term reduces to

$$\frac{1}{N_F}\sum_{k=1}^{N_F}(\sum_{m=1}^{N_F}|g_{k,m}^u|^2)^2 = \mu_u^2. \tag{185}$$

The second term can be expressed as a function of power allocation as

$$\frac{1}{N_F}\sum_{k=1}^{N_F}\sum_{m=1}^{N_F}|g_{k,m}^u|^4 = \frac{\mu_u^2}{N_F} + \frac{1}{N_F^3}\sum_{n_1,n_2\in\mathscr{S}_1}^{N_F}P_{u,n_1}P_{u,n_2} + \frac{1}{N_F^3}\sum_{n_1,n_2,n_3,n_4\in\mathscr{S}_2}^{N_F}\sqrt{P_{u,n_1}P_{u,n_2}P_{u,n_3}P_{u,n_4}}, \tag{186}$$

where

$$\mathscr{S}_1 = \Big\{n_1,n_2 \in \{1,2,\ldots,N_F\} : n_1 \neq n_2, n_1 - n_2 = \pm N_F/2\Big\} \tag{187}$$

and

$$\mathscr{S}_2 = \Big\{n_1,n_2,n_3,n_4 \in \{1,2,\ldots,N_F\} : n_1 \neq n_2, n_3 \neq n_4, (n_1,n_2) \neq (n_3,n_4),$$
$$n_4 - n_3 \in \{n_1 - n_2, N_F + n_1 - n_2, -N_F + n_1 - n_2\}\Big\}. \tag{188}$$

Substituting (185) and (186) in (183) yields

$$\Sigma^2(\mathbf{P}_u) = \frac{N_F - 1}{N_F^3}(\sum_{l=1}^{N_F}P_{u,l})^2 - \frac{1}{N_F^3}\sum_{n_1,n_2\in\mathscr{S}_1}^{N_F}P_{u,n_1}P_{u,n_2} -$$
$$\frac{1}{N_F^3}\sum_{n_1,n_2,n_3,n_4\in\mathscr{S}_2}^{N_F}\sqrt{P_{u,n_1}P_{u,n_2}P_{u,n_3}P_{u,n_4}}. \tag{189}$$

Computer simulations revealed that the number of summation terms in $\sum_{n_1,n_2,n_3,n_4\in\mathscr{S}_2}^{N_F}$ is $N_F^3 - N_F^2 - N_F$. Hence, the number of summation terms in (189) increases in the order of $N_F^3 - N_F^2 + N_F$. The objective is to control the variance of the normalized power, and

hence $P_{u,l}$ in (189) is divided by $\sum_{n=1}^{N_F} P_{u,n}$, $\forall l$. Hence, the constraint for power variance is written as

$$\Sigma^2(\mathbf{P}_u) \leq \tilde{\sigma}_u^2 (\sum_{l=1}^{N_F} P_{u,l})^2, \tag{190}$$

where $\tilde{\sigma}_u^2 \in \mathbb{R}^+$ is the preset upper bound of the variance of transmitted power for the u^{th} user. Plugging (189) into (190) the constraint can be written as

$$(N_F-1)(\sum_{l=1}^{N_F} P_{u,l})^2 \leq \sum_{n_1,n_2 \in \mathscr{S}_1}^{N_F} P_{u,n_1} P_{u,n_2} + \sum_{n_1,n_2,n_3,n_4 \in \mathscr{S}_2}^{N_F} \sqrt{P_{u,n_1} P_{u,n_2} P_{u,n_3} P_{u,n_4}} + (\sum_{l=1}^{N_F} P_{u,l})^2 \tilde{\sigma}_u^2 N_F^3. \tag{191}$$

Both sides of (191) are posynomials. Thus, SCA is needed for the RHS. Both, SCACOV and SCAGP can be applied for approximating (191).

SCACOV

Changing the variables as $P_{u,m} = e^{\alpha_{u,m}}$, $\forall u,m$, constraint (191) can be approximated as

$$(N_F-1)(\sum_{l=1}^{N_F} e^{\alpha_{u,l}})^2 \leq \hat{T}(\boldsymbol{\alpha}_u, \hat{\boldsymbol{\alpha}}_u), \tag{192}$$

where $\hat{T}(\boldsymbol{\alpha}_u, \hat{\boldsymbol{\alpha}}_u)$ is given in (163), $T(\boldsymbol{\alpha}_u)$ is the RHS of (191) after COV, and the partial derivatives are given as

$$\frac{\partial T}{\partial \alpha_{u,k}} = 2 \sum_{\substack{n=1 \\ n \neq k \\ n-k=\pm N_F/2}}^{N_F} e^{\alpha_{u,n}+\alpha_{u,k}} + 2 \sum_{\substack{n_1,n_2,n_3=1 \\ n_1 \neq n_2, n_3 \neq k \\ (n_1,n_2) \neq (n_3,k) \\ k-n_3 \in \mathscr{S}}}^{N_F} e^{\frac{1}{2}(\alpha_{u,n_1}+\alpha_{u,n_2}+\alpha_{u,n_3}+\alpha_{u,k})} + 2\tilde{\sigma}_u^2 N_F^3 (\sum_{l=1}^{N_F} e^{\alpha_{u,l}+\alpha_{u,k}})^2, \tag{193}$$

where

$$\mathscr{S} = \{n_1 - n_2, N_F + n_1 - n_2, -N_F + n_1 - n_2\}. \tag{194}$$

Similarly to 4.1.2, applying (97) to the RHS of (191) yields a constraint

$$
\begin{aligned}
&(N_F-1)(\sum_{l=1}^{N_F} P_{u,l})^2 \leq \\
&\left(\frac{\prod_{n_1,n_2\in\mathscr{S}_1}\left(\frac{P_{u,n_1}P_{u,n_2}}{\theta^{(1)}_{un_1n_2}}\right)^{\theta^{(1)}_{un_1n_2}}}{\tau_u^{(1)}}\right)^{\tau_u^{(1)}}
\left(\frac{\prod_{n_1,n_2,n_3,n_4\in\mathscr{S}_2}\left(\frac{\sqrt{P_{u,n_1}P_{u,n_2}P_{u,n_3}P_{u,n_4}}}{\theta^{(2)}_{un_1n_2n_3n_4}}\right)^{\theta^{(2)}_{un_1n_2n_3n_4}}}{\tau_u^{(2)}}\right)^{\tau_u^{(2)}} \\
&\times\left(\frac{\tilde{\sigma}_u^2N_F^3\prod_{l=1}^{N_F}\left(\frac{P_{u,l}^2}{\theta^{(3)}_{ul}}\right)^{\theta^{(3)}_{ul}}}{\tau_u^{(3)}}\right)^{\tau_u^{(3)}}
\left(\frac{2\tilde{\sigma}_u^2N_F^3\prod_{\substack{n_1,n_2=1\\n_2>n_1}}^{N_F}\left(\frac{P_{u,n_1}P_{u,n_2}}{\theta^{(4)}_{un_1n_2}}\right)^{\theta^{(4)}_{un_1n_2}}}{\tau_u^{(4)}}\right)^{\tau_u^{(4)}},
\end{aligned}
\tag{195}
$$

where the weights are given in

$$
\begin{aligned}
\tau_u^{(1)} &= \frac{\sum_{n_1,n_2\in\mathscr{S}_1}P_{u,n_1}P_{u,n_2}}{\sum_{n_1,n_2\in\mathscr{S}_1}P_{u,n_1}P_{u,n_2}+\sum_{n_1,n_2,n_3,n_4\in\mathscr{S}_2}\sqrt{P_{u,n_1}P_{u,n_2}P_{u,n_3}P_{u,n_4}}+(\sum_{l=1}^{N_F}P_{u,l})^2\tilde{\sigma}_u^2N_F^3}\\
\tau_u^{(2)} &= \frac{\sum_{n_1,n_2,n_3,n_4\in\mathscr{S}_2}\sqrt{P_{u,n_1}P_{u,n_2}P_{u,n_3}P_{u,n_4}}}{\sum_{n_1,n_2\in\mathscr{S}_1}P_{u,n_1}P_{u,n_2}+\sum_{n_1,n_2,n_3,n_4\in\mathscr{S}_2}\sqrt{P_{u,n_1}P_{u,n_2}P_{u,n_3}P_{u,n_4}}+(\sum_{l=1}^{N_F}P_{u,l})^2\tilde{\sigma}_u^2N_F^3}\\
\tau_u^{(3)} &= \frac{\tilde{\sigma}_u^2N_F^3\sum_{l=1}^{N_F}P_{u,l}^2}{\sum_{n_1,n_2\in\mathscr{S}_1}P_{u,n_1}P_{u,n_2}+\sum_{n_1,n_2,n_3,n_4\in\mathscr{S}_2}\sqrt{P_{u,n_1}P_{u,n_2}P_{u,n_3}P_{u,n_4}}+(\sum_{l=1}^{N_F}P_{u,l})^2\tilde{\sigma}_u^2N_F^3}\\
\tau_u^{(4)} &= \frac{2\tilde{\sigma}_u^2N_F^3\sum_{\substack{n_1,n_2=1\\n_2>n_1}}^{N_F}P_{u,n_1}P_{u,n_2}}{\sum_{n_1,n_2\in\mathscr{S}_1}P_{u,n_1}P_{u,n_2}+\sum_{n_1,n_2,n_3,n_4\in\mathscr{S}_2}\sqrt{P_{u,n_1}P_{u,n_2}P_{u,n_3}P_{u,n_4}}+(\sum_{l=1}^{N_F}P_{u,l})^2\tilde{\sigma}_u^2N_F^3},
\end{aligned}
\tag{196}
$$

and

$$
\begin{aligned}
\theta^{(1)}_{un_1n_2} &= \frac{P_{u,n_1}P_{u,n_2}}{\sum_{n_1',n_2'\in\mathscr{S}_1}P_{u,n_1'}P_{u,n_2'}},\\
\theta^{(2)}_{un_1n_2n_3n_4} &= \frac{\sqrt{P_{u,n_1}P_{u,n_2}P_{u,n_3}P_{u,n_4}}}{\sum_{n_1',n_2',n_3',n_4'\in\mathscr{S}_2}\sqrt{P_{un_1'}P_{u,n_2'}P_{u,n_3'}P_{u,n_4'}}},\\
\theta^{(3)}_{ul} &= \frac{P_{u,l}^2}{\sum_{l'=1}^{N_F}P_{u,l'}^2}, \theta^{(4)}_{un_1n_2} = \frac{P_{u,n_1}P_{u,n_2}}{\sum_{\substack{n_1',n_2'=1\\n_2'>n_1'}}^{N_F}P_{u,n_1'}P_{u,n_2'}}.
\end{aligned}
\tag{197}
$$

4.2.2 Power variance constraint for OFDMA

In the case of OFDMA, the first term of (183) reduces to

$$\frac{1}{N_F}\sum_{k=1}^{N_F}(\sum_{m=1}^{N_F}|g_{k,m}^{u}|^2)^2 = 2\mu_u^2, \tag{198}$$

while the second term is simplified to

$$\frac{1}{N_F}\sum_{k=1}^{N_F}\sum_{m=1}^{N_F}|g_{k,m}^{u}|^4 = \frac{1}{N_F^2}\sum_{m=1}^{N_F}P_{u,m}^2. \tag{199}$$

Substituting (198) and (199) in (183) yields

$$\Sigma^2(\mathbf{P}_u) = \frac{2}{N_F^2}\sum_{\substack{n_1,n_2=1\\ n_2>n_1}}^{N_F}P_{u,n_2}P_{u,n_1}. \tag{200}$$

The summation terms in (200) increases in the order of $N_F(N_F-1)-\sum_{n=1}^{N_F}n$. After normalization, the variance constraint is written as

$$\frac{2}{N_F^2}\sum_{\substack{n_1,n_2=1\\ n_2>n_1}}^{N_F}P_{u,n_2}P_{u,n_1} \leq \tilde{\sigma}_u^2\left(\sum_{m=1}^{N_F}P_{u,m}\right)^2. \tag{201}$$

Both sides of (201) are posynomials. Thus, SCA is needed for the RHS. Both, SCACOV and SCAGP can be applied for approximating (201).

SCACOV

Changing the variables to $P_{u,m} = e^{\alpha_{u,m}}$, $\forall u,m$, constraint (201) can be approximated as

$$\frac{2}{N_F^2}\sum_{\substack{n_1,n_2=1\\ n_2>n_1}}^{N_F}e^{\alpha_{u,n_2}+\alpha_{u,n_1}} \leq \hat{T}(\boldsymbol{\alpha}_u,\hat{\boldsymbol{\alpha}}_u), \tag{202}$$

where $\hat{T}(\boldsymbol{\alpha}_u,\hat{\boldsymbol{\alpha}}_u)$ is given in (163), $T(\boldsymbol{\alpha}_u)$ is the RHS of (191) after COV, and the partial derivatives are given as

$$\frac{\partial T}{\partial \alpha_{u,k}} = 2\tilde{\sigma}_u^2\sum_{m=1}^{N_F}e^{\alpha_{u,m}+\alpha_{u,k}}. \tag{203}$$

Applying (97) to the RHS of (201) yields a constraint

$$\frac{2}{N_F^2}\sum_{\substack{n_1,n_2=1\\ n_2>n_1}}^{N_F} P_{u,n_2}P_{u,n_1} \leq \left(\frac{\prod_{m=1}^{N_F}\left(\frac{P_{u,m}^2}{\theta_{um}^{(1)}}\right)^{\theta_{um}^{(1)}}}{\tau_u^{(1)}}\right)^{\tau_u^{(1)}} \left(\frac{2\prod_{\substack{n_1,n_2=1^N\\ n_2>n_1\ F}}\left(\frac{P_{u,n_1}P_{u,n_2}}{\theta_{un_1n_2}^{(2)}}\right)^{\theta_{un_1n_2}^{(2)}}}{\tau_u^{(2)}}\right)^{\tau_u^{(2)}}, \tag{204}$$

where the weights are given in

$$\begin{aligned}
\tau_u^{(1)} &= \frac{\prod_{m=1}^{N_F}\left(\frac{P_{u,m}^2}{\theta_{um}^{(1)}}\right)^{\theta_{um}^{(1)}}}{\prod_{m=1}^{N_F}\left(\frac{P_{u,m}^2}{\theta_{um}^{(1)}}\right)^{\theta_{um}^{(1)}} + 2\prod_{\substack{n_1,n_2=1^N\\ n_2>n_1\ F}}\left(\frac{P_{u,n_1}P_{u,n_2}}{\theta_{un_1n_2}^{(2)}}\right)^{\theta_{un_1n_2}^{(2)}}} \\
\tau_u^{(2)} &= \frac{2\prod_{\substack{n_1,n_2=1^N\\ n_2>n_1\ F}}\left(\frac{P_{u,n_1}P_{u,n_2}}{\theta_{un_1n_2}^{(2)}}\right)^{\theta_{un_1n_2}^{(2)}}}{\prod_{m=1}^{N_F}\left(\frac{P_{u,m}^2}{\theta_{um}^{(1)}}\right)^{\theta_{um}^{(1)}} + 2\prod_{\substack{n_1,n_2=1^N\\ n_2>n_1\ F}}\left(\frac{P_{u,n_1}P_{u,n_2}}{\theta_{un_1n_2}^{(2)}}\right)^{\theta_{un_1n_2}^{(2)}}},
\end{aligned} \tag{205}$$

and

$$\begin{aligned}
\theta_{un_1}^{(1)} &= \frac{P_{u,n_1}^2}{\sum_{n_1'=1}^{N_F}}, \\
\theta_{un_1n_2}^{(2)} &= \frac{P_{u,n_1}P_{u,n_2}}{\sum_{\substack{n_1',n_2'=1\\ n_2'>n_1'}}^{N_F} P_{u,n_1'}P_{u,n_2'}}.
\end{aligned} \tag{206}$$

4.3 Numerical results

In this section, the results obtained in the simulations are presented. To employ the SCAs considered in this thesis it is necessary to find a feasible starting point for the iterative algorithm. In the case of SC-FDMA, it can be found by setting the power to be equal for all subcarriers. The power level has to be high enough to satisfy the QoS constraints. In equal allocation, the PAPR is 0 dB and 2.55 dB for QPSK and 16-QAM, respectively, which are the modulation schemes considered in the simulations. As long as the target PAPR is above this value, the result obtained by equal allocation satisfies the PAPR constraint for SC-FDMA.

In the case of OFDMA, a feasible starting point for the iterative algorithm can be found with the help of spatial ZF RX. Plugging (171) and (172) into the general PAPR expression $\frac{\max_m |s_m^u|^2}{\text{avg}[|s_m^u|^2]}$, and then increasing $P_{u,n}$ for some n, one can determine that PAPR decreases. Even though this behaviour is not necessarily monotonic, it is straightforward to show[8] that, for OFDMA,

$$\lim_{P_{u,n}\to\infty} \frac{\max_m |s_m^u|^2}{\text{avg}[|s_m^u|^2]} = 1, \text{ for any } n = 1,2,\ldots,N_F. \tag{207}$$

Increasing $P_{u,n}$ does not violate the SINR constraint because ZF RX removes all the interference. The feasible initialization method is summarized as follows:

1. Calculate the ZF matrix.
2. Find the power allocation satisfying the QoS constraint.
3. Increase the power in one subcarrier for all the users until it satisfies the PAPR constraint.

Step 2 can be performed by allocating the same power for all the subcarriers. The power level can be found by using a bisection algorithm [88]. This initialization method presented above applies also with appropriate modifications for a power variance-constrained problem.

The results are obtained with the following parameters: $N_F = 8$, QPSK ($N_Q = 2$) and 16-QAM ($N_Q = 4$) with Gray mapping, and systematic repeat accumulate (RA) code [107] with a code rate of 1/3 and eight internal iterations. Uniform diagonal sampling [63] is used for EXIT sampling in the QoS constraint, and the number of samples is $K = 5$. The SNR per user and per RX antenna averaged over frequency bins is defined by

$$\hat{\text{SNR}} = \text{tr}\{\mathbf{P}\}/(UN_RN_F\sigma_v^2). \tag{208}$$

Two different channel conditions are considered, namely, a static five-path channel (path gains shown in Table 2 for $U = N_R = 2$) and a quasi-static Rayleigh fading five-path average equal gain channel.

Similarly to Chapter 3 the maximum transmission power can be calculated as

$$P_{\max}(dB) = P_{\text{avg}}^u(dB) + PAPR(dB), \tag{209}$$

where

$$P_{\text{avg}}^u = \hat{\text{SNR}} \times N_R \times \sigma_v^2 \tag{210}$$

[8] By applying the L'Hospital's rule.

Table 2. Channel Coefficients.

u,r	$h^r_{u,1}$	$h^r_{u,2}$	$h^r_{u,3}$	$h^r_{u,4}$	$h^r_{u,5}$
1,1	0.1558 - 0.0101i	$-0.2864+$ 0.2518i	$-0.1480+$ 0.1714i	$-0.2826+$ 0.1016i	0.0496 - 0.0455i
1,2	0.0035 + 0.1302i	0.0717 - 0.0431i	0.0165 - 0.0086i	0.2329 - 0.1145i	$-0.0621+$ 0.3623i
2,1	0.1958 + 0.3085i	$-0.2200+$ 0.1349i	0.0376 + 0.0181i	$-0.0072-$ 0.1412i	$-0.1161-$ 0.0344i
2,2	0.1144 + 0.1162i	0.0033 + 0.1916i	0.1799 - 0.3138i	0.2341 - 0.1374i	$-0.0121-$ 0.1128i

denotes the average power per user. Thus, the metric $\hat{\text{SNR}}(dB) + PAPR(dB)$ can be used to compare the algorithms in terms of the range of the transmission.

In order to investigate the impact of different initializations on the convergence of the SCAs, the optimization algorithms were tested assuming a static channel (path gains shown in Table 2). The results can be seen in Table 3, where global iterations refer to TX-RX alternations and local iterations refer to SCA iterations. The stopping threshold of the optimization algorithms are the same as presented in Section 3.4, i.e. 0.05 for TX-RX alternations and 0.01 for SCAs. In Table 3, 'proposed initialization' refers to the methods derived at the beginning of this Section. In the case of SC-FDMA, we compare the proposed initialization with the case where the power level in each subcarrier is selected to be the value shown in the uppermost row. In the case of OFDMA, after performing the ZF initialization, the power in one randomly selected subcarrier is increased by the value shown in the uppermost column. It can be seen that the convergence speed of the SCACOV and SCAGP are approximately equal for OFDMA. In the case of SC-FDMA, there are differences with some initializations. The SNR after convergence is equal for all the initializations. It was obtained that the PAPR for OFDMA after ZF equalization was already below the target value. Therefore, the initialization was feasible for all the cases considered in Table 3. In SC-FDMA a power level of 0.1 is not enough to satisfy the CC, and therefore the initialization is infeasible.

To demonstrate the operational principle of the PAPR constraint, EXIT simulations were carried out in a static channel for a fixed symbol sequence. The EXIT curve of the decoder is obtained by using 200 blocks for each *a priori* value, with the size of a block being 6,000 bits. The EXIT chart of the turbo equalizer when precoding with instantaneous PAPR constraint is presented in Fig. 16. SC-FDMA and OFDMA denote the schemes without the PAPR constraint, i.e. with the QoS constraint only. The

Table 3. Convergence comparison with various initializations. The values are written in the form of global iterations / local iterations / SŃR (dB). $\delta_u = 3$ **dB.** $U = 2$**,** $N_R = 2$**,** $N_Q = 2$**,** $\hat{I}_u^{\mathrm{E,target}} = 0.7892$**,** $u = 1,2$**,** $\mathring{I}_u^{\mathrm{E,target}} = 0.9998$**,** $u = 1,2$**,** $\varepsilon_u = 0.02$**,** $u = 1,2$**,** $\mathbf{b}^1 = 1/\sqrt{2}[-1-i,-1-i,-1-i,1+i,-1-i,1+i,1-i,1+i]^{\mathsf{T}}$**,** $\mathbf{b}^2 = 1/\sqrt{2}[-1+i,-1+i,1-i,-1+i,-1+i,-1-i,-1+i,-1+i]^{\mathsf{T}}$**.**

Initialization	Proposed	0.1	1	10	100
SC-FDMA SCACOV	2/14/1.44	infeasible	3/15/1.44	3/20/1.44	3/36/1.44
SC-FDMA SCAGP	2/16/1.44	infeasible	2/15/1.44	3/19/1.44	3/19/1.44
OFDMA SCACOV	2/12/5.46	2/7/5.46	2/8/5.46	2/9/5.46	2/12/5.46
OFDMA SCAGP	2/12/5.44	2/7/5.44	2/7/5.44	2/9/5.44	2/12/5.44

SC-FDMA result is obtained via SCAGP approximation. Clipping denotes the case where the signal is clipped when the power exceeds the peak value calculated from the PAPR threshold. As seen in Chapter 3, the minimum gap between the EXIT curves of the equalizer and the decoder of user u can be controlled by changing the parameter ε_u. It can be seen from Fig. 16, that with SC-FDMA, the minimum gap between the EXIT curves can be suppressed down to ε_u according to the CC. For OFDMA, the gap is larger than ε_u, which results in significantly larger SNR requirements compared to SC-FDMA. This can be seen in Table 4, where the corresponding SNR and PAPR is listed together with the summation of SNR and PAPR for each algorithm used. The larger SNR requirement of OFDMA compared to SC-FDMA is due to the difference in CCs. In the case of OFDMA, the SINR requirement is the same for all subcarriers, unlike in SC-FDMA where the average of SINRs over the subcarriers is used. On the other hand, there is no intra-user interference in OFDMA, unlike in SC-FDMA for which the starting point in the EXIT chart is interference-limited. Hence, the target point in the case of OFDMA can be achieved even with linear RX by simply increasing the power in all the subcarriers. Clipping reduces the SNR but convergence to the desired MI point is not guaranteed. In the case of SC-FDMA with clipping, the EXIT curves intersect at MI point $(\mathring{I}_u^{\mathrm{E}}, \hat{I}_u^{\mathrm{E}}) = (0.1936, 0.2254)$, which corresponds to BEP value 0.2053. It can be seen from Table 4 that the PAPR threshold is not exceeded with the PAPR constraint. The sum of SNR and PAPR describes the actual power gain achieved by the proposed algorithms, which helps to improving the QoS for cell edge users. It can be seen that in the case of OFDMA the improvement when using the PAPR

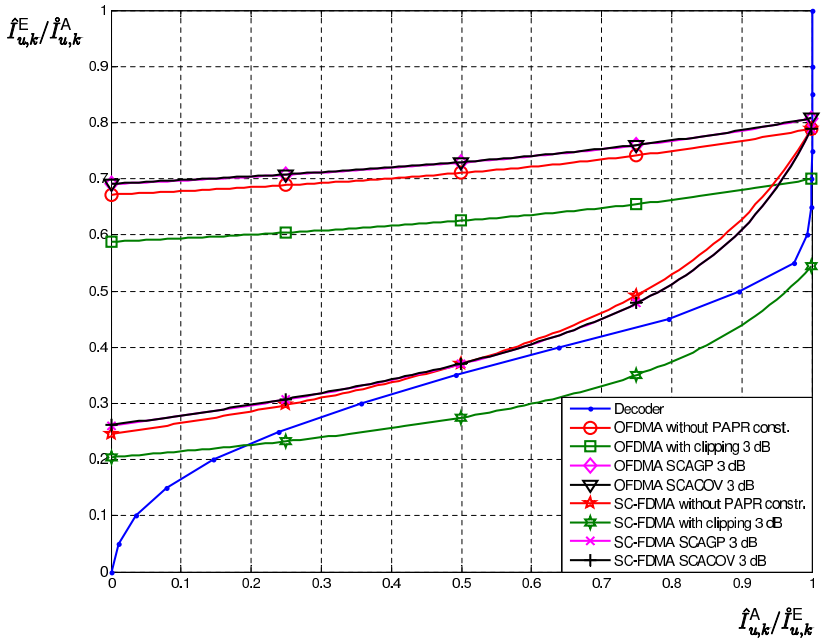

Fig. 16. EXIT chart for $\delta_u = 3$ dB. $U = 2$, $N_R = 2$, $N_Q = 2$, $\mathring{I}_u^{\mathrm{E,target}} = 0.7892$, $u = 1,2$, $\mathring{I}_u^{\mathrm{E,target}} = 0.9998$, $u = 1,2$, $\varepsilon_u = 0.02$, $u = 1,2$, $\mathbf{b}^1 = 1/\sqrt{2}[-1-i,-1-i,-1-i,1+i,-1-i,1+i,1-i,1+i]^{\mathsf{T}}$, $\mathbf{b}^2 = 1/\sqrt{2}[-1+i,-1+i,1-i,-1+i,-1+i,-1-i,-1+i,-1+i]^{\mathsf{T}}$.

constraint is $9.31dB - 8.44dB = 0.87dB$. In the case of SC-FDMA, the improvement is 3.16 dB and 3.17 dB for SCAGP and SCACOV, respectively.

In Fig. 17, the required SNR versus BEP is presented, where the results are obtained by averaging over 200 channel realizations. Four different BEP target values are considered for $u = 1,2$, namely 10^{-3}, 10^{-4}, 10^{-5} and 10^{-6}, corresponding to the MI targets $(\mathring{I}_u^{\mathrm{E,target}}, \hat{I}_u^{\mathrm{E,target}}) = (0.99, 0.6185)$, $(\mathring{I}_u^{\mathrm{E,target}}, \hat{I}_u^{\mathrm{E,target}}) = (0.9987, 0.673)$, $(\mathring{I}_u^{\mathrm{E,target}}, \hat{I}_u^{\mathrm{E,target}}) = (0.9998, 0.7892)$ and $(\mathring{I}_u^{\mathrm{E,target}}, \hat{I}_u^{\mathrm{E,target}}) = (0.9998, 0.9819)$, respectively. It can be seen that for SC-FDMA, the required SNR is roughly the same with and without the PAPR constraint, i.e. the PAPR can be suppressed to 3 dB without a significant increase in transmit power. For OFDMA, the required SNR is increased by 1.19-1.83 dB depending on BEP target and algorithm used.

CCDFs Prob$(PAPR > \delta)$ for SC-FDMA and OFDMA without PAPR constraints and with a BEP target of 10^{-5} are plotted in Fig. 18. CCDFs are calculated such that 10^5 randomly generated symbol sequences of length N_F for each user are sent over 200

Table 4. SNR and PAPR comparison in a static channel. SC-FDMA with clipping did not achieve the MI target.

Algorithm	$\widehat{\text{SNR}}$ (dB)	PAPR (dB)	$\widehat{\text{SNR}}$ + PAPR (dB)
OFDMA	4.97	4.34	9.31
OFDMA with clipping	4.37	3.00	7.37
OFDMA SCAGP	5.44	3.00	8.44
OFDMA SCACOV	5.46	2.98	8.44
SC-FDMA	1.38	6.22	7.60
SC-FDMA with clipping	0.49	3.00	3.49
SC-FDMA SCAGP	1.44	3.00	4.44
SC-FDMA SCACOV	1.44	2.99	4.43

channel realizations. Obviously, for the algorithms with PAPR constraint, the CCDF is 0 when the PAPR is larger than the PAPR threshold. For a CCDF value of 10^{-5}, the corresponding PAPRs are 7.66 dB and 8.52 dB for SC-FDMA and OFDMA, respectively. From Figs. 17 and 18, the $\widehat{\text{SNR}}$+PAPR gains can be calculated for SC-FDMA to be 4.63 dB and 4.29 dB for SCAGP and SCACOV, respectively. Similarly for OFDMA, the gains are 4.29 dB and 4.00 dB, respectively.

CCDFs for the OFDMA scheme when precoding with a variance constraint is shown in Fig. 19. It can be seen that the PAPR can be significantly reduced by decreasing the variance. In fact, the PAPR approaches the theoretical limit, i.e. 2.55 dB for 16-QAM, when the variance target approaches zero. However, because the per-subcarrier SINR constraint is used as a QoS constraint, the SNR increase is high compared to the PAPR reduction.

CCDFs for the SC-FDMA scheme when precoding with a variance constraint are shown in Fig. 20. It can be seen that the PAPR can be significantly reduced with a minor increase in SNR by decreasing the power variance. Similarly to the OFDMA case, the PAPR approaches the theoretical limit when the variance target approaches zero.

4.4 Summary and discussion

In this chapter, the PAPR-constrained power allocation problem for multi-carrier transmission with an iterative MMSE MU multi-antenna RX has been formulated. An analytical expression of PAPR was derived as a function of transmit power allocation for SC-FDMA and OFDMA. The derived PAPR constraints are applicable to any normal-

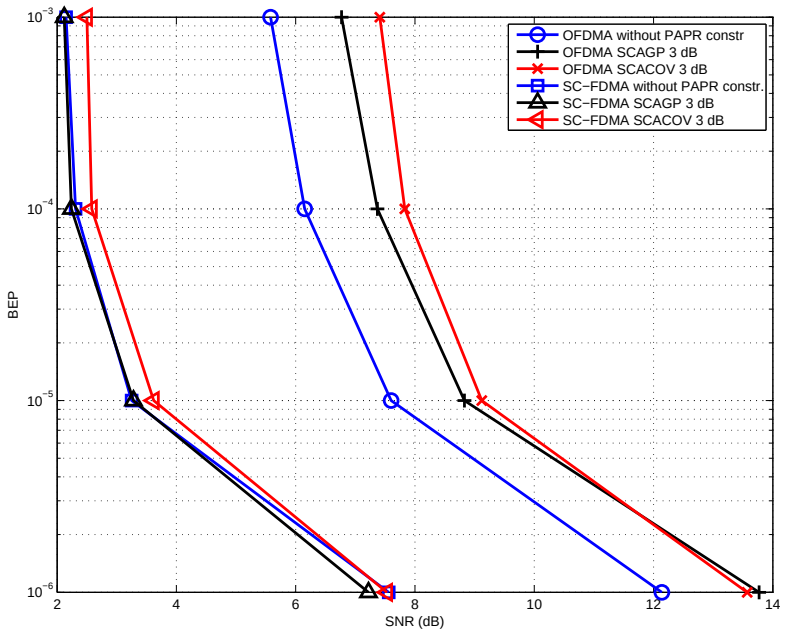

Fig. 17. BEP comparison with $\delta_u = 3$ dB. $U = 2$, $N_R = 2$, $N_Q = 2$, $\varepsilon_u = 0.1$, $u = 1,2$, $N_F = 8$.

ized data modulation format. In addition, a statistical approach considering the transmission power variance-constrained power allocation was derived. It was obtained that, in the case of SC-FDMA, the implementation of PAPR and power variance constraints becomes highly complex with a large N_F. However, in the case of OFDMA, the expansion of the constraints is quadratic, and hence, the number of summation terms in the constraints is feasible.

Two different successive convex approximations were derived for all the proposed constraints. Numerical results indicate that instead of amplitude clipping, the PAPR constraint is of crucial importance to guarantee the convergence of the iterative equalizer. It was also observed that the proposed techniques can significantly improve the power efficiency of the transmission of power-limited users. Hence, the constraints derived in this thesis are especially beneficial for users on the cell edge and, therefore, the physical size of a cell can be increased.

In SC-FDMA, the PAPR and power variance constraint affect such that the power is reduced in the constructive subcarriers and increased in the destructive. 'Constructive

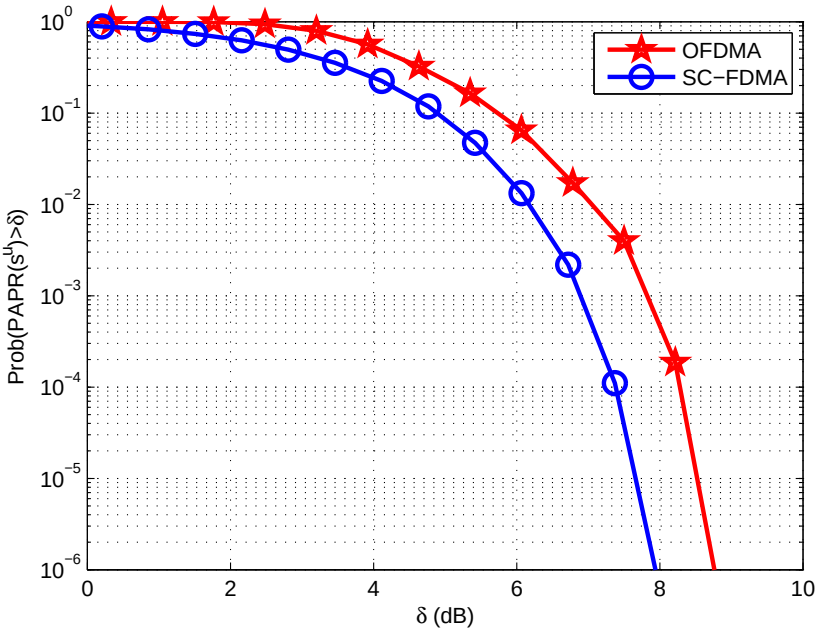

Fig. 18. CCDFs for SC-FDMA and OFDMA without PAPR constraint with BEP target 10^{-5}**.** $U=2$**,** $N_R=2$**,** $N_Q=2$**,** $\hat{I}_u^{\mathrm{E,target}}=0.7892$**,** $u=1,2$**,** $\hat{I}_u^{\mathrm{E,target}}=0.9998$**,** $u=1,2$**,** $\varepsilon_u=0.1$**,** $u=1,2$**.**

subcarriers' means the subcarriers that increase the peak power after the IFFT in the TX ('destructive subcarriers' are the converse).

In OFDMA, since the same SINR is required for all subcarriers, the power can only be increased. Thus, the PAPR and power variance constraints results in an increase in power in destructive subcarriers.

In the PAPR constraint, the constructiveness and destructiveness can be identified based on the transmitted symbol sequence. In the power variance constraint, the constructiveness and destructiveness are based on the statistics: the intuition is that the subcarriers are inherently either constructive or destructive. This can be obtained also from [82], where the spectrum window function is plotted for SC-FDMA after minimizing the power variance.

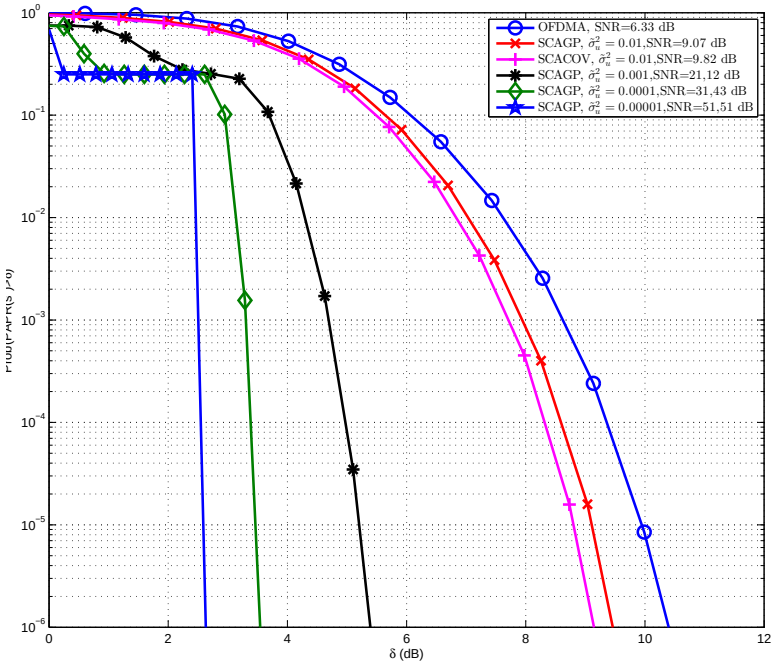

Fig. 19. CCDFs for OFDMA with variance constraint. BEP target=10^{-5}**,** $U = 4$**,** $N_R = 4$**,** $N_Q = 4$**,** $\hat{I}_u^{\text{E,target}} = 0.7892$**,** $\forall u$**,** $I_u^{\text{E,target}} = 0.9998$**,** $\forall u$**,** $\varepsilon_u = 0.1$**,** $\forall u$**.**

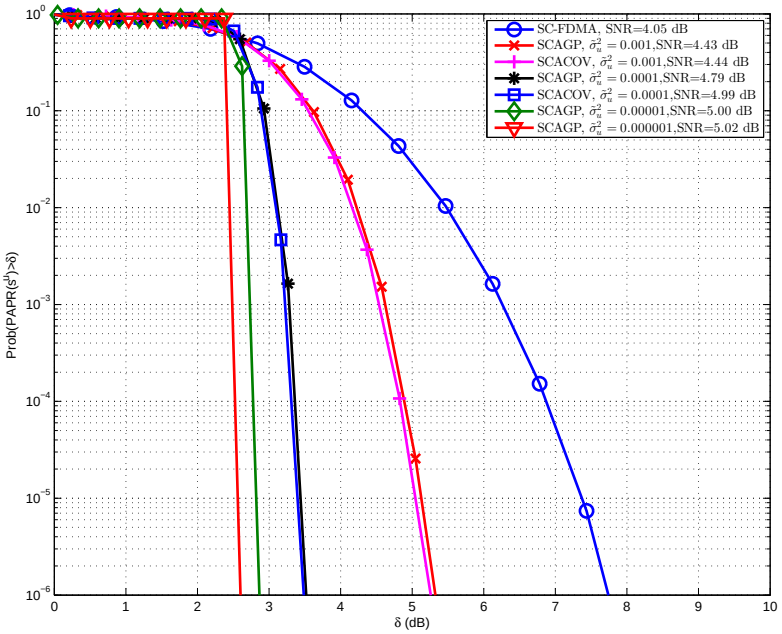

Fig. 20. CCDFs for SC-FDMA with variance constraint. BEP target=10^{-5}**,** $U = 4$**,** $N_R = 4$**,** $N_Q = 4$**,** $\hat{I}_u^{\mathsf{E,target}} = 0.7892$**,** $\forall u$**,** $\hat{I}_u^{\mathsf{E,target}} = 0.9998$**,** $\forall u$**,** $\varepsilon_u = 0.1$**,** $\forall u$**.**

5 Conclusion and future work

Power allocation strategies in multi-carrier MU SIMO UL communications were studied in this thesis. In particular, a power allocation method taking into account the characteristics of an iterative MU detector was derived. Furthermore, two different power allocation methods taking into account the PAPR of the transmitted signal were derived. The first method explicitly restricts the instantaneous PAPR to below the desired threshold with minimum power consumption while guaranteeing the desired QoS. The second method implicitly reduces the PAPR by restricting the power variance of the transmitted signal below the desired value with minimum power consumption while guaranteeing the desired QoS. The first method depends on the transmitted symbol sequence, unlike the second method, for which the variance is taken over all possible symbol sequences. All the power allocation strategies introduced in this thesis were derived for both SC-FDMA and OFDMA.

Chapter 3 studied the CCPA in MU communications. A general formulation for the CC was derived. A novel *diagonal sampling* approach was proposed for sampling the multidimensional EXIT function to guarantee convergence without performing exhaustive searches. The CC was applied to the system model assumed in the thesis, and it was shown that the CC reduces to a set of SINR constraints, where the value of a constraint depends on the sample point and the channel code used. The CC was derived for BPSK and QPSK modulations. Moreover, a heuristic approach for 16-QAM was proposed showing that the CC serves as an upper bound for 16-QAM, and therefore, convergence is guaranteed. This result provides a way to generalize the CCPA for higher-order modulations.

The joint optimization of the transmit power and the receive beamformers was performed via alternating optimization, i.e. the joint optimization problem was split into separate TX and RX optimization problems. A sum power-minimizing solution is found iteratively, alternating between the TX and the RX optimizations. It was shown that the MMSE RX is a power minimizing RX, and hence each step in the iterative algorithm improves the objective. Therefore, the objective value in alternating optimization is guaranteed to converge to a local minimum. The numerical results provided in Chapter 3 indicate that significant improvement in terms of power consumption is achieved with CC compared to the case without CC (i.e., linear RX). The CCPA algorithm derived

in Chapter 3 is one of the few QoS-constrained power allocation methods taking into account the convergence properties of an iterative RX also on the TX side.

Most of the power allocation methods proposed in Chapter 3 require centralized processing, i.e. the base station gathers the required information, performs the calculus and sends the information about the power allocation to each user. In practice, the adjacent subcarriers correlate heavily with each other. Thus, the frequency-selective channel can be divided into resource blocks, where each resource block consists of several subcarriers. Hence, the number of power values that needs to be reported is decreased from the number of subcarriers to the number of resource blocks. If the users are not transmitting simultaneously in the same subcarriers, i.e. orthogonal allocation is used, each of the users is able to calculate its own power allocation based on its own CSI. This can be seen in (103), where the CC is derived for orthogonal allocation. Based on the results presented in Fig. 12, it can be concluded that if the number of users is low, orthogonal allocation becomes an attractive alternative.

In Chapter 4, two PAPR reduction methods were proposed by designing a precoder that takes into account the PAPR characteristics of the HPA while guaranteeing the desired QoS. The first approach restricts the PAPR to below the desired value. For that purpose, the PAPR was derived as a function of the power allocation and the transmitted symbol sequence. A beneficial point in this approach is that the PAPR can be limited to be at most equal to the backoff of the HPA. Hence, the algorithm achieves the minimum power solution while guaranteeing distortion free amplification.

The second approach for PAPR reduction proposed in Chapter 4 was the power variance-constrained power allocation. Hence, the variance of the power of the time domain signal was calculated and the resulting function was restricted to be at most the desired value. The numerical results illustrate that the PAPR can be reduced by reducing the power variance. It was shown that the PAPR approaches the theoretical limit when the variance approaches zero. The beneficial point in the variance-constrained algorithm is that it does not depend on the transmitted symbol sequence. Hence, less information is needed to calculate the power allocation matrix.

Two alternative SCAs were derived for all the non-convex constraints presented in the thesis. SCA is an iterative algorithm where the solution in each iteration satisfies the constraints of the original problem. The beneficial point here is that if there is a latency constraint, the iterative algorithm can be stopped at any iteration and the resulting power allocation and receive filter satisfies the constraints of the original problem.

The PAPR and the variance constraints presented in Chapter 4 depend only on the

local information, i.e. the power allocation and the transmitted symbol sequence in the case of instantaneous PAPR constraint, and the power allocation only in the case of the power variance constraint. If the QoS constraint requires centralized processing, the intuition is that the power variance constraint is a better alternative because it does not require information about the transmitted symbol sequence. However, if the QoS constraint can be handled by using the local information, instantaneous PAPR constraint can be used because the information about the symbol sequence is available.

On the cell edge, the average transmission power is already high. While the average power of the signal is large, the peak values of the signal exceed the power limit set by the local authority with increasing probability. These peaks have to be clipped, causing distortion to the transmitted signal. On the other hand, the operating voltage of HPA has to be as high as the peak values of the output signal. Hence, the power consumption of HPA can be effectively reduced by reducing the peak values of the transmitted signal. In conclusion, the algorithms presented in this thesis are especially beneficial for power-limited cell edge users.

The research presented in this thesis can be further developed in many directions. On one hand, practical implementations of the algorithms should be developed. In Chapter 4, it was demonstrated that, in the case of SC-FDMA, practical implementation requires the reduction of complexity of the constraints. In the case of OFDMA, the expansion of the constraints as a function of N_F is not as in SC-FDMA. Furthermore, because the PAPR is known to be a bigger problem in OFDMA, it may be the transmission scheme for which the proposed PAPR constraints should be considered.

The PAPR constraint can be adopted in various power allocation schemes, and therefore it is an attractive approach for mitigating the impact of nonlinearities of the radio frequency (RF) components. On the other hand, due to the substantial improvement in terms of the average power consumption, CCPA deserves further development. First of all, multi-antenna transmission should be considered. Another problem is transmission in a multi-cell scenario. Probably the most interesting scenario to be investigated is comparison of SC-FDMA and OFDMA with the PAPR constraint in a practical UL scenario. Detection in OFDMA is simple and, therefore, if the PAPR problem can be mitigated, it is also an attractive alternative for UL transmission.

References

1. Rosberg Z & Zander J (1998) Toward a framework for power control in cellular systems. Wireless Networks 4(3): 215–222.
2. Akhtar S (2008) 2G-5G Networks: Evolution of Technologies, Standards, and Deployment. IGI Global, Hershey, Pennsylvania, United States.
3. Gibson J (2002) The Communications Handbook. CRC Press.
4. Lee W (1995) Mobile Cellular Telecommunications : Analog and Digital Systems. McGraw-Hill Professional.
5. Nettleton R & Alavi H (1983) Power control for a spread spectrum cellular mobile radio system. In: Vehicular Technology Conference, 1983. 33rd IEEE, volume 33, pp. 242–246.
6. Fujii T & Sakamoto M (1988) Reduction of cochannel interference in cellular systems by intra-zone channel reassignment and adaptive transmitter power control. In: Vehicular Technology Conference, 1988, IEEE 38th, pp. 668–672.
7. Mouly M, Pautet MB & Foreword By-Haug T (1992) The GSM system for mobile communications. Telecom Publishing.
8. Redl S, Weber M & Oliphant M (1995) An introduction to GSM. Artech House.
9. Bettstetter C, Vogel HJ & Eberspacher J (1999) Gsm phase 2+ general packet radio service gprs: Architecture, protocols, and air interface. Communications Surveys & Tutorials, IEEE 2(3): 2–14.
10. Furuskar A, Mazur S, Muller F & Olofsson H (1999) EDGE: Enhanced data rates for GSM and TDMA/136 evolution. Personal Communications, IEEE 6(3): 56–66.
11. Falconer D, Adachi F & Gudmunson B (1995) Time division multiple access methods for wireless communications. IEEE Communications Magazine .
12. GSM technical specification (1996) Digital cellular telecommunications system (Phase 2+); Radio subsystem link control (GSM 05.08) Version 5.1.0. Technical report, European Telecommunications Standards Institute (ETSI).
13. Zander J (1992) Performance of optimum transmitter power control in cellular radio systems. IEEE Transactions on Vehicular Technology 41(1): 57–62.
14. Knopp R & Humblet PA (1995) Information capacity and power control in single-cell multiuser communications. In: IEEE International Conference on Communications (ICC'95), Seattle,'Gateway to Globalization', volume 1, pp. 331–335. IEEE.
15. Yates RD (1995) A framework for uplink power control in cellular radio systems. IEEE Journal on Selected Areas in Communications 13(7): 1341–1347.
16. Rappaport TS *et al.* (1996) Wireless communications: principles and practice, volume 2. prentice hall PTR New Jersey.
17. Standard MSBSC (1993) for dual-mode wideband spread spectrum cellular system. EIA/TIA IS-95 .
18. Telecommunications Industry Association and Electronic Industries Association *et al.* (1995) Mobile station-base station compatibility standard for dual-mode wideband spread spectrum cellular system. Telecommunications Industry Association.
19. Garg VK & Rappaport TS (2001) Wireless network evolution: 2G to 3G. Prentice Hall PTR.
20. Kaaranen H, Ahtiainen A, Laitinen L, Naghian S & Niemi V (2001) UMTS networks. Ar-

chitecture, Mobility and Services. Wiley .
21. Kohno R, Meidan R & Milstein L (1995) Spread spectrum access methods for wireless personal communications. IEEE Communications Magazine .
22. Garg VK (1999) IS-95 CDMA and cdma2000: cellular/PCS systems implementation. Pearson Education.
23. Rintamäki M (2005) Adaptive power conrol in CDMA cellular communication systems. Ph.D. thesis, Helsinki University of Technology, Espoo, Finland.
24. Gejji RR (1992) Forward-link-power control in CDMA cellular systems. IEEE Transactions on Vehicular Technology 41(4): 532–536.
25. Sampath A, Kumar PS & Holtzman JM (1995) Power control and resource management for a multimedia CDMA wireless system. In: The Sixth IEEE International Symposium on Personal, Indoor and Mobile Radio Communications (PIMRC'95), Wireless: Merging onto the Information Superhighway., volume 1, pp. 21–25. IEEE.
26. Catrein D, Imhof LA & Mathar R (2004) Power control, capacity, and duality of uplink and downlink in cellular CDMA systems. IEEE Transactions on Communications 52(10): 1777–1785.
27. Chang RW (1966) Synthesis of band-limited orthogonal signals for multichannel data transmission. Bell System Technical Journal 45: 1775–1796.
28. Wong CY, Cheng RS, Lataief KB & Murch RD (1999) Multiuser OFDM with adaptive subcarrier, bit, and power allocation. IEEE Journal on Selected Areas in Communications 17(10): 1747–1758.
29. Jang J & Lee KB (2003) Transmit power adaptation for multiuser OFDM systems. IEEE Journal on Selected Areas in Communications 21(2): 171–178.
30. Seong K, Mohseni M & Cioffi JM (2006) Optimal resource allocation for OFDMA downlink systems. In: IEEE International Symposium on Information Theory, pp. 1394–1398. IEEE.
31. Tölli A, Codreanu M & Juntti M (2008) Linear multiuser MIMO transceiver design with quality of service and per-antenna power constraints. IEEE Transactions on Signal Processing 56(7): 3049–3055.
32. Sadr S, Anpalagan A & Raahemifar K (2009) Radio resource allocation algorithms for the downlink of multiuser OFDM communication systems. IEEE Communications Surveys & Tutorials 11(3): 92–106.
33. Chieochan S & Hossain E (2009) Adaptive radio resource allocation in OFDMA systems: a survey of the state-of-the-art approaches. Wireless Communications and Mobile Computing 9(4): 513–527.
34. Chiang M, Hande P, Lan T & Tan CW (2008) Power control in wireless cellular networks. Found. Trends Netw. 2(4): 381–533.
35. Dahlman E, Parkvall S & Skold J (2013) 4G: LTE/LTE-advanced for mobile broadband. Academic Press.
36. Union IT (2010). Itu world radiocommunication seminar highlights future communication technologies.
37. Vilches J (2010). Everything you need to know about 4g wireless technology, techspot.
38. M2134 IR (2008). Requirements related to technical performance for imt-advanced radio interface(s).
39. International Telecommunication Union (ITU) (2012). Press release: IMT-Advanced standards announced for next-generation mobile technology.

40. Wannstrom J (2013). LTE-Advanced.
41. Gerlach D & Paulraj A (1993) Base station transmitter antenna arrays with mobile to base feedback. In: Conference Record of The Twenty-Seventh Asilomar Conference on Signals, Systems and Computers., pp. 1432–1436. IEEE.
42. Naguib AF, Paulraj A & Kailath T (1994) Capacity improvement with base-station antenna arrays in cellular CDMA. IEEE Transactions on Vehicular Technology 43(3): 691–698.
43. Tse D & Viswanath P (2005) Fundamentals of Wireless Communication. Cambridge Univ. Press, Cambridge, U.K.
44. 3rd Generation Partnership Project (3GPP); Technical Specification Group Radio Access Network Evolved Universal Terrestrial Radio Access E-UTRA (2014) Physical channels and modulation 3GPP TS 36.211 Version 12.3.0 (Release 12). Technical report.
45. Falconer D, Ariyavisitakul SL, Benyamin-Seeyar A & Eldson B (2002) Frequency domain equalization for single-carrier broadband wireless systems. IEEE Communications Magazine 40(4): 58–66.
46. Pancaldi F, Vitetta G, Kalbasi R, Al-Dhahir N, Uysal M & Mheidat H (2008) Single-carrier frequency domain equalization. IEEE Signal Processing Magazine 25(5): 37–56.
47. Nee RV & Prasad R (2000) OFDM for Wireless Multimedia Communications. Norwood, MA: Artech House.
48. Kansanen K, Matsumoto T, Schneider C & Thoma R (2005) Frequency-domain MMSE turbo equalization of multilevel coded QAM-convergence in real fields. In: Proceedings of IEEE 16th International Symposium on Personal, Indoor and Mobile Radio Communications, 2005. PIMRC 2005., volume 2, pp. 1019–1023 Vol. 2.
49. Yuan X, Guo Q, Wang X & Ping L (2008) Evolution analysis of low-cost iterative equalization in coded linear systems with cyclic prefix. IEEE Journal on Selected Areas of Communications 26(2): 301–310.
50. Shepherd D, Shi Z, Reed M & Schreckenbach F (2006) Optimization of unequal power coded multiuser DS-CDMA using extrinsic information transfer charts. In: Proceedings of The 48th Annual Conference in Information Sciences and Systems (CISS). Princeton, USA.
51. Brink ST (2001) Convergence behavior of iteratively decoded parallel concatenated codes. IEEE Transactions on Communications 49(10): 1727–1737.
52. Yuan X, Li H, Ping L & Lin X (2008) Precoder design for ISI channels based on iterative LMMMSE equalization. In: Proceedings of International Symposium on Turbo Codes and Related Topics, pp. 198–203. Lausanne, Switzerland.
53. Karjalainen J & Matsumoto T (2008) On the convergence property of an MMSE multiuser MIMO turbo detector with uplink precoding. In: Proceedings of International Conference on Communications. Beijing, China.
54. Karjalainen J, Matsumoto T & Utschick W (2008) Convergence analysis of MMSE based multiuser MIMO turbo detector with linear precoding strategies. In: Proceedings of International Symposium on Turbo Codes and Related Topics. Lausanne, Switzerland.
55. Yuan X, Xu C, Ping L & Lin X (2009) Precoder Design for Multiuser MIMO ISI Channels Based on Iterative LMMSE detection. IEEE Journal of Selected Topics in Signal Processing 3(6): 1118–1128.
56. Karjalainen J, Codreanu M, Tölli A, Juntti M & Matsumoto T (2011) EXIT chart-based power allocation for iterative frequency domain MIMO detector. IEEE Transactions on Signal Processing 59(4): 1624–1641.

57. Berrou C & Glavieux A (1996) Near optimum error correcting coding and decoding: Turbo-codes. IEEE Transactions on Communications 44(10): 1261–1271.
58. Brink ST (1999) Convergence behavior of iterative decoding. IEE Electoric Letters 35(10): 806–808.
59. Ashikhmin A, Kramer G & ten Brink S (2004) Extrinsic information transfer functions: Model and erasure channel properties. IEEE Transactions on Information Theory 50(11): 2657–2673.
60. Brännström F, Rasmussen LK & Grant AJ (2005) Convergence analysis and optimal scheduling for multiple concatenated codes. IEEE Transactions on Information Theory 51(9): 3354–3364.
61. Ten Brink S, Kramer G & Ashikhmin A (2004) Design of low-density parity-check codes for modulation and detection. IEEE Transactions on Communications 52(4): 670–678.
62. Ten Brink S & Kramer G (2003) Design of repeat-accumulate codes for iterative detection and decoding. IEEE Transactions on Signal Processing 51(11): 2764–2772.
63. Tervo V, Tölli A, Karjalainen J & Matsumoto T (2014, (accepted with minor revision), arXiv:1310.8067) Convergence constrained multiuser transmitter-receiver optimization in single carrier FDMA. IEEE Transactions on Signal Processing .
64. Wunder G, Fischer R, Boche H, Litsyn S & No JS (2013) The PAPR problem in OFDM transmission: New directions for a long-lasting problem. IEEE Signal Processing Magazine 30(6): 130–144.
65. Gangwar A & Bhardwaj M (2012) An overview: Peak to average power ratio in OFDM system & its effect. International Journal of Communication and Computer Technologies 1(2): 22–25.
66. Baltar L, Waldhauser D & Nossek J (2007) Out-of-band radiation in multicarrier systems: A comparison. In: Plass S, Dammann A, Kaiser S & Fazel K (eds.) Multi-Carrier Spread Spectrum 2007, volume 1 of *Lecture Notes Electrical Engineering*, pp. 107–116. Springer Netherlands.
67. Bäuml RW, Fischer RF & Huber JB (1996) Reducing the peak-to-average power ratio of multicarrier modulation by selected mapping. Electronics Letters 32(22): 2056–2057.
68. Müller SH & Huber JB (1997) OFDM with reduced peak-to-average power ratio by optimum combination of partial transmit sequences. Electronics letters 33(5): 368–369.
69. Alavi A, Tellambura C & Fair I (2005) PAPR reduction of OFDM signals using partial transmit sequence: an optimal approach using sphere decoding. IEEE Communications Letters 9(11): 982–984.
70. Litsyn S (2007) Peak Power Control in Multicarrier Communications. Cambridge Univ. Press, Cambridge, U.K.
71. Kwok HKC & Jones D (2000) PAR reduction for hadamard transform based OFDM. In: Proceedings of Annual Conference in Information Sciences and Systems (CISS). Princeton, NJ.
72. Mobasher A & Khandani A (2006) Integer-based constellation-shaping method for PAPR reduction in OFDM systems. IEEE Transactions on Communications 54(1): 119–127.
73. Eugen C, Sterian D & Wesolowski K (2010) Reducing the peak and average power for OFDM systems using QAM by constellation shaping. European Transactions on Telecommunications 21(1): 35–49.
74. Peng F & Ryan W (2006) On the capacity of clipped OFDM channels. In: Proceedings of IEEE International Symposium on Information Theory, pp. 1866–1870. Seattle, WA.

75. Fischer R (2010) Capacity of clipped 4-QAM-OFDM. In: Proceedings of ITG Conference on Source and Channel Coding. Siegen, Germany.
76. Al-Safadi E & Al-Naffouri T (2009) On reducing the complexity of tone-reservation based PAPR reduction schemes by compressive sensing. In: Global Telecommunications Conference, 2009. GLOBECOM 2009. IEEE, pp. 1–6.
77. Al-Safadi E & Al-Naffouri T (2012) Peak reduction and clipping mitigation in OFDM by augmented compressive sensing. IEEE Transactions on Signal Processing 60(7): 3834–3839.
78. Tellado J (2000) Peak to average power reduction for multicarrier modulation. Ph.D. thesis, Stanford Univ.
79. Han SH & Lee JH (2005) An overview of peak-to-average power ratio reduction techniques for multicarrier transmission. IEEE Wireless Communications 12(2): 56–65.
80. Slimane S (2007) Reducing the peak-to-average power ratio of OFDM signals through precoding. IEEE Transactions on Vehicular Technology 56(2): 686–695.
81. Falconer D (2011) Linear precoding of OFDMA signals to minimize their instantaneous power variance. IEEE Transactions on Communications 59(4): 1154–1162.
82. Yuen C & Farhang-Boroujeny B (2012) Analysis of the optimum precoder in SC-FDMA. IEEE Transactions on Wireless Communications 11(11): 4096–4107.
83. Bertsekas DP (2005) Nonlinear Programming. Cambridge Univ. Press, Cambridge, U.K.
84. Marks BR & Wright GP (1978) Technical Note-A General Inner Approximation Algorithm for Nonconvex Mathematical Programs. Operations Research 26(4): 681–683.
85. Meyer R (1976) Sufficient conditions for the convergence of monotonic mathematicalprogramming algorithms. Journal of computer and system sciences 12(1): 108–121.
86. Kaleva J, Tölli A, Venkatraman G & Juntti M (2013) Downlink precoder design for coordinated regenerative multi-user relaying. IEEE Transactions on Signal Processing 61(5): 1215–1229.
87. Chiang M, wei Tan C, Palomar D, O'Neill D & Julian D (2007) Power control by geometric programming. IEEE Transactions on Wireless Communications 6(7): 2640–2651.
88. Boyd S & Vandenberghe L (2004) Convex Optimization. Cambridge Univ. Press, Cambridge, U.K.
89. Chiang M (2005) Geometric programming for communication systems. Now Publishers Hanover.
90. Tervo V, Tölli A, Karjalainen J & Matsumoto T (2012) On convergence constraint precoder design for iterative frequency domain multiuser SISO detector. In: Proceedings of the Annual Asilomar Conference on Signals, Systems, and Computers, pp. 473–477. Pacific Grove, CA, USA.
91. Tervo V, Tölli A & Matsumoto T (2014, (submitted)) PAPR constrained power allocation for multicarrier transmission in multiuser SIMO communications. IEEE Transactions on Signal Processing .
92. Wiesel A, Eldar Y & Shamai S (2006) Linear precoding via conic optimization for fixed MIMO receivers. IEEE Transactions on Signal Processing 54(1): 161–176.
93. Tervo V, Tölli A, Karjalainen J & Matsumoto T (2014) Transmission power variance constrained power allocation for iterative frequency domain multiuser SIMO detector. In: Proceedings of IEEE International Conference on Acoustics, Speech, and Signal Processing, pp. 3493–3497.
94. Tervo V, Tölli A, Karjalainen J & Matsumoto T (2014) PAPR constrained power alloca-

tion for iterative frequency domain multiuser SIMO detector. In: Proceedings of IEEE International Conference on Communications. Sydney, Australia.
95. Tervo V, Fukawa K & Matsumoto T (2012) Error resistant lossless data compression with equal length coding using fine tuned multiple label mapping. In: Proceedings of IEEE International Conference on Communications, pp. 4707–4711.
96. Tervo V, Matsumoto T & Karjalainen J (2010) Joint source-channel coding using multiple label mapping. In: Proceedings on IEEE Vehicular Technology Conference, pp. 1–6.
97. Tervo V, Matsumoto T & Lu PS (2013) Distributed joint source-channel coding for correlated sources using non-systematic repeat-accumulate based codes. Wireless Personal Communications 69(1): 387–401.
98. Lu PS, Tervo V, Anwar K & Matsumoto T (2011) Low-complexity strategies for multiple access relaying. In: Proceedings on IEEE Vehicular Technology Conference, pp. 1–6.
99. Tüchler M, Singer AC & Koetter R (2002) Minimum mean squared error equalization using *a priori* information. IEEE Transactions on Signal Processing 50(3): 673–683.
100. Karjalainen J (2011) Broadband single carrier multi-antenna communications with frequency domain turbo equalization. Ph.D. thesis, University of Oulu, Oulu, Finland.
101. Kansanen K & Matsumoto T (2007) An analytical method for MMSE MIMO turbo equalizer EXIT chart computation. IEEE Transactions on Wireless Communications 6(1): 59–63.
102. Brännström F (2004) Convergence analysis and design of multiple concatenated codes. Ph.D. thesis, Chalmers University of Technology, Gothenburg, Sweden.
103. Ramon V, Herzet C & Vandendorpe L (2007) A semi-analytical method for predicting the performance and convergence behavior of a multiuser turbo-equalizer/demapper. IEEE Transactions on Signal Processing 55(3): 1104–1117.
104. Kaleva J, Tölli A & Juntti M (2012) Weighted Sum Rate Maximization for Interfering Broadcast Channel via Successive Convex Approximation. In: Proceedings of IEEE Global Communications Conference.
105. Moore EH (1920) On the reciprocal of the general algebraic matrix. Bulletin of the American Mathematical Society 26(9): 394–395.
106. Golub GH & van Loan CF (1996) Matrix Computations. The Johns Hopkins University Press, Baltimore, 3rd edition.
107. Divsalar D, Jin H & McEliece RJ (1998) Coding theorems for 'turbo-like' codes. In: Proceedings of Annual Allerton Conference on Communication, Control and Computing, pp. 201–210. Urbana, Illinois, USA.
108. Chiang M (2009) Nonconvex optimization for communication networks. In: Gao DY & Sherali HD (eds.) Advances in Applied Mathematics and Global Optimization, volume 17 of *Advances in Mechanics and Mathematics*, pp. 137–196. Springer US.
109. Yuan G, Zhang X, Wang W & Yang Y (2010) Carrier aggregation for lte-advanced mobile communication systems. Communications Magazine, IEEE 48(2): 88–93.

Appendix 1 The average power of the transmitted signal in SC-FDMA

Let

$$\mathbf{G}^u = \mathbf{F}^{-1}\mathbf{P}_u^{\frac{1}{2}}\mathbf{F}. \tag{211}$$

The entry (m,n) of $\mathbf{G}^u$ is obtained as

$$g_{m,n}^u = \frac{1}{N_F}\sum_{q=1}^{N_F}\sqrt{P_{u,q}}a_{qnm}, \tag{212}$$

where

$$a_{qnm} = e^{\frac{j2\pi(q-1)(n-m)}{N_F}}. \tag{213}$$

Thus, the m^{th} output of the transmitted waveform for the u^{th} user is

$$s_m^u = \sum_{n=1}^{N_F} g_{m,n}^u b_n^u. \tag{214}$$

Assuming $\mathbb{E}\{|b_n^u|\} = 1$, $\forall u,n$ and $\mathbb{E}\{b_p^u b_q^{u*}\} = 0$, $\forall p \neq q$, the average can be calculated as

$$\begin{aligned}
&\text{avg}[|s_m^u|^2] = \frac{1}{N_F}\sum_{m=1}^{N_F}\mathbb{E}\Big\{[|s_m^u|^2]\Big\}\\
=&\frac{1}{N_F}\sum_{n=1}^{N_F}\mathbb{E}\Big\{|\sum_{m=1}^{N_F} g_{n,m}^u b_m^u|^2\Big\}\\
=&\frac{1}{N_F}\sum_{n=1}^{N_F}\mathbb{E}\Big\{\sum_{m=1}^{N_F} g_{n,m}^u b_m^u \sum_{m=1}^{N_F} g_{n,m}^{u*} b_m^{u*}\Big\}\\
=&\frac{1}{N_F}\sum_{n=1}^{N_F}\mathbb{E}\Big\{\sum_{m=1}^{N_F}|g_{n,m}^u|^2|b_m^u|^2 + \sum_{\substack{n_1,n_2=1\\ n_1\neq n_2}}^{N_F} g_{n,n_1}^u b_{n_1}^u g_{n,n_2}^{u*} b_{n_2}^{u*}\Big\}\\
=&\frac{1}{N_F}\sum_{n=1}^{N_F}\sum_{m=1}^{N_F}|g_{n,m}^u|^2\\
=&\frac{1}{N_F^3}\sum_{n=1}^{N_F}\sum_{m=1}^{N_F}\sum_{l=1}^{N_F}P_{u,l} + \frac{1}{N_F^3}\sum_{n=1}^{N_F}\sum_{m=1}^{N_F}\sum_{\substack{n_1,n_2=1\\ n_1\neq n_2}}^{N_F}\sqrt{P_{u,n_2}P_{u,n_1}}e^{\frac{j2\pi(m-n)(n_2-n_1)}{N_F}}\\
=&\frac{1}{N_F}\sum_{l=1}^{N_F}P_{u,l}.
\end{aligned} \tag{215}$$

The last step is justified by

$$\sum_{m=1}^{N_F} \sum_{\substack{n_1,n_2=1 \\ n_1 \neq n_2}}^{N_F} \sqrt{P_{u,n_2} P_{u,n_1}} e^{\frac{j2\pi(m-n)(n_2-n_1)}{N_F}} = 0, \ \forall n = 1,2,\ldots,N_F. \tag{216}$$

Appendix 2 The instantaneous power of the transmitted signal in SC-FDMA

The power of the transmitted waveform of user u at time instant m is calculated as

$$
\begin{aligned}
|s_m^u|^2 =& |\sum_{n=1}^{N_F} g_{m,n}^u b_n^u|^2 \\
=& |\sum_{n=1}^{N_F} \frac{1}{N_F} \sum_{l=1}^{N_F} \sqrt{P_{u,l}} a_{lnm} b_n^u|^2 \\
=& \left(\sum_{n=1}^{N_F} \frac{1}{N_F} \sum_{l=1}^{N_F} \sqrt{P_{u,l}} a_{lnm} b_n^u \right) \left(\sum_{n=1}^{N_F} \frac{1}{N_F} \sum_{l=1}^{N_F} \sqrt{P_{u,l}} a_{lnm}^* b_n^{u*} \right) \\
=& \frac{1}{N_F^2} \left(\sum_{n=1}^{N_F} \left(b_n^u b_n^{u*} \Big(\sum_{l=1}^{N_F} \sqrt{P_{u,l}} a_{lnm} \Big)^2 \right) + \sum_{\substack{n_1,n_2=1 \\ n_1 \neq n_2}}^{N_F} \left(b_{n_1}^u b_{n_2}^{u*} \Big(\sum_{l=1}^{N_F} \sqrt{P_{u,l}} a_{ln_1m} \Big) \Big(\sum_{l=1}^{N_F} \sqrt{P_{u,l}} a_{ln_2m} \Big) \right) \right) \\
=& \frac{1}{N_F^2} \left(\sum_{n=1}^{N_F} |b_n^u|^2 \sum_{l=1}^{N_F} P_{u,l} + \sum_{n=1}^{N_F} |b_n^u|^2 \sum_{\substack{n_1,n_2=1 \\ n_1 \neq n_2}}^{N_F} \sqrt{P_{u,n_1} P_{u,n_2}} a_{nn_1n_2} a_{mn_1n_2}^* \right. \\
& \left. + \sum_{\substack{n_1,n_2=1 \\ n_1 \neq n_2}}^{N_F} b_{n_1}^u b_{n_2}^{u*} \sum_{l=1}^{N_F} P_{u,l} a_{ln_1q} + \sum_{\substack{n_1,n_2=1 \\ n_1 \neq n_2}}^{N_F} b_{n_1}^u b_{n_2}^{u*} \sum_{\substack{n_1',n_2'=1 \\ n_1' \neq n_2'}}^{N_F} \sqrt{P_{u,n_1'} P_{u,n_2'}} a_{n_1'n_1m} a_{n_2'n_2m}^* \right)
\end{aligned}
\tag{217}
$$

The order of the summations in the second term of (217) can be changed as

$$
\begin{aligned}
\sum_{n=1}^{N_F} |b_n^u|^2 \sum_{\substack{n_1,n_2=1 \\ n_1 \neq n_2}}^{N_F} \sqrt{P_{u,n_1} P_{u,n_2}} a_{nn_1n_2} a_{mn_1n_2}^* &= \sum_{\substack{n_1,n_2=1 \\ n_1 \neq n_2}}^{N_F} \sqrt{P_{u,n_1} P_{u,n_2}} \sum_{n=1}^{N_F} |b_n^u|^2 a_{nn_1n_2} a_{mn_1n_2}^* \\
&= \sum_{\substack{n_1,n_2=1 \\ n_1 \neq n_2}}^{N_F} \beta_{mn_1n_2}^u \sqrt{P_{u,n_1} P_{u,n_2}},
\end{aligned}
\tag{218}
$$

where

$$
\beta_{mn_1n_2}^u = \sum_{n=1}^{N_F} |b_n^u|^2 \Big(\mathscr{R}[a_{nn_1n_2}] \mathscr{R}[a_{mn_1n_2}] + \mathscr{I}[a_{mn_1n_2}] \mathscr{I}[a_{nn_1n_2}] \Big). \tag{219}
$$

Operators $\mathscr{R}$ and $\mathscr{I}$ in (219) take the real and imaginary part of a complex argument, respectively.

The order of the summations in the third term of (217) can be changed as

$$\frac{1}{N_F^2}\sum_{\substack{n_1,n_2=1\\ n_1\neq n_2}}^{N_F} b_{n_1}^u b_{n_2}^{u*}\sum_{l=1}^{N_F} P_{u,l}a_{ln_1n_2} = \frac{1}{N_F^2}\sum_{l=1}^{N_F} P_{u,l}\sum_{\substack{n_1,n_2=1\\ n_1\neq n_2}}^{N_F} b_{n_1}^u b_{n_2}^{u*}a_{ln_1n_2}, \tag{220}$$

which can be further developed to

$$\frac{1}{N_F^2}\sum_{l=1}^{N_F} P_{u,l}\sum_{\substack{n_1,n_2=1\\ n_1\neq n_2}}^{N_F} b_{n_1}^u b_{n_2}^{u*}a_{ln_1n_2} = \frac{1}{N_F^2}\sum_{l=1}^{N_F} P_{u,l}2d_l^u, \tag{221}$$

where

$$\begin{aligned} d_l^u = \sum_{\substack{n_2,n_1=1\\ n_1>n_2}}^{N_F} \Big(&\mathscr{R}[a_{ln_1n_2}](\mathscr{R}[b_{n_1}^u]\mathscr{R}[b_{n_2}^u]+\\ &\mathscr{I}[b_{n_1}^u]\mathscr{I}[b_{n_2}^u]) + \mathscr{I}[a_{ln_1n_2}](\mathscr{R}[b_{n_1}^u]\mathscr{I}[b_{n_2}^u] - \mathscr{I}[b_{n_1}^u]\mathscr{R}[b_{n_2}^u])\Big). \end{aligned} \tag{222}$$

Denoting

$$\begin{aligned} \eta_{n_1n_2m}^u = \sum_{\substack{n_4,n_3=1\\ n_3>n_4}}^{N_F} \Big((&\mathscr{R}[b_{n_3}^u]\mathscr{R}[b_{n_4}^u] + \mathscr{I}[b_{n_3}^u]\mathscr{I}[b_{n_4}^u])(\mathscr{R}[a_{n_1n_3m}a_{n_2n_4m}^*] + \mathscr{R}[a_{n_1n_4m}a_{n_2n_3m}^*])-\\ &(\mathscr{I}[b_{n_3}^u]\mathscr{R}[b_{n_4}^u] - \mathscr{R}[b_{n_3}^u]\mathscr{I}[b_{n_4}^u])(\mathscr{I}[a_{n_1n_3m}a_{n_2n_4m}^*] - \mathscr{I}[a_{n_1n_4m}a_{n_2n_3m}^*])\Big), \end{aligned} \tag{223}$$

the last term of (217) can be expressed as

$$\frac{1}{N_F^2}\sum_{\substack{n_1,n_2=1\\ n_1\neq n_2}}^{N_F} b_{n_1}^u b_{n_2}^{u*}\sum_{\substack{n_1',n_2'=1\\ n_1'\neq n_2'}}^{N_F} \sqrt{P_{u,n_1'}P_{u,n_2'}}a_{n_1'n_1m}a_{n_2'n_2m}^* = 2\sum_{\substack{n_1,n_2=1\\ n_2>n_1}}^{N_F} \eta_{n_1n_2m}^u\sqrt{P_{u,n_1}P_{u,n_2}}. \tag{224}$$

Substituting (218), (221) and (224) to (217), the signal power is expressed as

$$|s_m^u|^2 = \frac{1}{N_F^2}\sum_{l=1}^{N_F}\Big(\kappa^u + 2d_l^u\Big)P_{u,l} + \frac{2}{N_F^2}\sum_{\substack{n_1,n_2=1\\ n_2>n_1}}^{N_F}\Big(\beta_{mn_1n_2}^u + \eta_{n_1n_2m}^u\Big)\sqrt{P_{u,n_1}P_{u,n_2}}, \tag{225}$$

where

$$\kappa^u = \sum_{n=1}^{N_F}|b_n^u|^2. \tag{226}$$

It is worth noting that $\kappa^u + 2d_l^u$ can be rewritten as

$$\kappa^u + 2d_l^u = \Big(\sum_{n=1}^{N_F} b_n^u a_{ln1}\Big)\Big(\sum_{n=1}^{N_F} b_n^u a_{ln1}\Big)^* \geq 0. \tag{227}$$

The number of summation terms in $\sum_{\substack{n_2,n_1=1 \\ n_1>n_2}}^{N_F}$ is $N_F(N_F-1)-\sum_{n=1}^{N_F} n$. Therefore, the total number of summation terms in (225) increases in the order of $N_F^4 - N_F^2(1+2\sum_{n=1}^{N_F-1} n)+N_F+(\sum_{n=1}^{N_F-1} n)^2$.

Appendix 3 The instantaneous power of the transmitted signal in OFDMA

The power of the transmitted waveform of user u at time instant m is calculated as

$$\begin{aligned}
|s_m^u|^2 =& |\sum_{n=1}^{N_F} g_{m,n}^u b_n^u|^2 \\
=& (\sum_{n=1}^{N_F} g_{m,n}^u b_n^u)(\sum_{n=1}^{N_F} g_{m,n}^u b_n^u)^* \\
=& \sum_{n=1}^{N_F} g_{m,n}^u g_{m,n}^{u*} b_n^u b_n^{u*} + \sum_{\substack{n_1,n_2=1 \\ n1\neq n_2}}^{N_F} g_{m,n_1}^u g_{m,n_2}^{u*} b_{n_1}^u b_{n_2}^{u*} \\
=& \frac{1}{N_F} \sum_{n=1}^{N_F} |b_n^u|^2 P_{u,n} + \frac{1}{N_F} \sum_{\substack{n_1,n_2=1 \\ n1\neq n_2}}^{N_F} a_{mn_2n_1} b_{n_1}^u b_{n_2}^{u*} \sqrt{P_{u,n_1} P_{u,n_2}}.
\end{aligned} \tag{228}$$

Denoting

$$\begin{aligned}
\tilde{d}_{mn_2n_1}^u =& a_{mn_2n_1} b_{n_1}^u b_{n_2}^{u*} + a_{mn_2n_1}^* b_{n_1}^{u*} b_{n_2}^u \\
=& 2\Bigg(\mathscr{R}[a_{mn_2n_1}] \Big(\mathscr{R}[b_{n_2}^u] \mathscr{R}[b_{n_1}^u] + \mathscr{I}[b_{n_2}^u] \mathscr{I}[b_{n_1}^u] \Big) - \\
& \mathscr{I}[a_{mn_2n_1}] \Big(\mathscr{R}[b_{n_2}^u] \mathscr{I}[b_{n_1}^u] - \mathscr{I}[b_{n_2}^u] \mathscr{R}[b_{n_1}^u] \Big) \Bigg),
\end{aligned} \tag{229}$$

(228) can be written as

$$|s_m^u|^2 = \frac{1}{N_F} \sum_{l=1}^{N_F} |b_l^u|^2 P_{u,l} + \frac{1}{N_F} \sum_{\substack{n_1,n_2=1 \\ n_2>n_1}}^{N_F} \tilde{d}_{mn_2n_1}^u \sqrt{P_{u,n_1} P_{u,n_2}}. \tag{230}$$